UNIVERSITÁ DEGLI STUDI DI NAPOLI FEDERICO II

Department of Materials and Production Engineering

Progress in polyesters flame retardancy: new halogen- free formulations

EMANUELA GALLO

Ph.D Dissertation

SUPERVISOR

Ch.mo Prof. Domenico Acierno

2006-2009

UNIVERSITÁ DEGLI STUDI DI NAPOLI FEDERICO II

Department of Materials and Production Engineering

Scuola di dottorato in ingegneria industriale

Progress in polyesters flame retardancy: new halogen- free formulations

Emanuela Gallo

INTRODUCTION

The demand for better, cheaper and safer materials has lead to a rapid proliferation of high-performance and specialty polymers in the building construction, automotive and aerospace industries. As protection is required in all these domains the reduction in flammability is a major concern.

Poly (1, 4-butylene terephthalate) (PBT) is an engineering plastic with a good balance of mechanical and electrical properties, good dimensional stability, thermal resistance and processing advantages. Thanks to its good performance characteristics, the market of PBT is growing quickly in particular it is widely used in automobile components such as connectors. However, it is well known that at the processing temperature (250–280°C) thermal, oxidative and hydrolytic degradation may take place.[1] PBT is progressively degraded, depending on the temperature and the outdoor applications, by thermo- and photo-oxidative reactions that arise during its lifetime. Furthermore, the flammability and the serious dripping during combustion limit its applications; this is the reason why the thermal decomposition of polyesters such as poly (ethylene terephthalate) (PET) and poly (butylene terephthalate) (PBT) has been the centre of continued attention.

Halogen-containing additives were found to be very efficient fire retardants in PBT however they have some negative aspects, in particular the release of toxic and corrosive gases.[2] Environmental problems that have occurred in the past show that polymer blend with halogen compounds are undesirable materials that run the risk of polluting the environment. In particular, the movement to eliminate such pollutants became active in Europe in the 1990s[3] even if there have been many efforts to find non-halogen flame retardants since the 1960s. The growing number of restrictions and recommendations from the European Community has promoted the development of safe and ecological non-halogen containing flame retardant polymers.[4]

In recent years, polymer/inorganic composites have attracted great attention. Inorganic compounds such as aluminium hydroxide,[5] organic phosphates, red phosphorus (red-P), ammonium polyphosphate, silicone compounds and nanocomposites made with clays[6] are typical examples of non-halogenated flame retardants because they are environmentally friendly. Among the most promising flame retardant additives are organoclays. In spite of the good potential of these alternatives, in general higher levels of additions are required, resulting in a worsening of the matrix properties.

Especially promising for their advantages over the traditional fire retardants has been the discovery of polymer nanocomposites. They do not only enhance the fire retardancy but also the mechanical properties, due to a high interphase specific area between nanometric filler and hosting matrix.[7, 8, 9] These materials exhibit enhancements in a variety of physical properties at one tenth the loading required as compared to when micrometer size additives are used. Recent literature reports an interest in the use of oxide particles[10,11,12,1314,15,16] in the nanometric range as synergistic agents in addition to usual fire retardant additives. The synergism between phosphorus-containing additives and inorganic oxides, [11] which provide oxidizing effect was shown early in the Russian literature.[17] Apart from acting mainly as thermal stabilizer, [16] their nanometric size makes them suitable for synergistic effects with organoclays, allowing

combining both fire resistance performances and enhanced mechanical properties.

The flame retardancy of polymers can be achieved according to three major mechanisms: (a) the gas phase mechanism, which is typical for halogen based FR systems, (b) the condensed phase mechanism, which governs treatments based on phosphorus and sulphur derivatives and (c) the mechanism based on physical effects governing the endothermic processes (Mg and Al hydroxides). Synergistic and catalytic phenomena are recently observed in many systems based on all above mechanisms, and constitute at present the subject of intensive study.[18,19] The synergistic effects are diverse. They include chemical and physical interactions between the basic FR agents and one or more synergists, between the polymer and the synergists and between polymers in a blend. Additives that increase the amount of carbonaceous char residue that is formed during the polymer combustion are very effective flame retardants. Char formation reduces the amount of small, volatile polymer pyrolysis fragments or fuel available for burning in the gas phase. The approach of these issues (control of polymer flammability without the use of halogenated additives) in this study is to design new materials, in which the synergism between different halogen-free additives, give the best in reducing the polymer flammability combining a gas phase action with a solid phase action.

This research is focused on reducing polymer flammability by promoting char formation investigating additives which enhance charring. Because of important commercial applications, PBT has been chosen as a standard material. The thermal decomposition of PBT has been studied both in the condensed and in the gas phase, in combination with different nanodispersed inorganic oxides in the nanometric range (TiO_2, Al_2O_3 , Fe_2O_3 and Sb_2O_3) and a promising phosphorous-based flame retardant (aluminium diethlyphosphinate). The effects of these combinations on the flame retardancy and thermal stability of PBT were examined by thermal analysis (TG), FTIR analysis in the gas phase (TG-FTIR) and in the solid state, flammability tests (UL 94, LOI) and monitoring the fire behaviour under forced-flaming conditions (cone calorimeter).

CHAPTER 1

POLYMER COMBUSTION AND FLAME RETARDANCY

1.1. Polymer combustion

Due to their chemical structure, made up mainly of carbon and hydrogen, polymers are highly combustible.[20] The combustion of polymers is a complex physic-chemical process involving chemical reactions of polymer degradation in the condensed phase and heat- and mass transfer processes. Combustion reactions liberate the energy stored in the chemical bonds of the molecules of polymer. The combustion reaction involves two factors: one or more combustibles (reducing agents) and a combustive (oxidizing agent). The combustive is generally the oxygen in the air. The whole process usually starts with an increase in the temperature of the polymeric material due to a heat source, to such an extent that it induces polymer bond scissions. The volatile fraction of the resulting polymer fragments diffuses into the air and creates a combustible gaseous mixture (fuel). This gaseous mixture ignites when the auto-ignition temperature

(defined as the temperature at which the activation energy of the combustion reaction is attained) is reached, thus liberating heat. Alternatively, the fuel can also ignite at a lower temperature (flash point) upon reaction with an external source of intense energy (spark, flame, etc.). The life span of the combustion cycle depends on the quantity of heat liberated during the combustion of the fuel. When the amount of heat liberated reaches a certain level, new decomposition reactions are induced in the solid phase, and therefore more combustibles are produced. The combustion cycle is thus maintained, and can therefore be called fire triangle (Fig. 1).

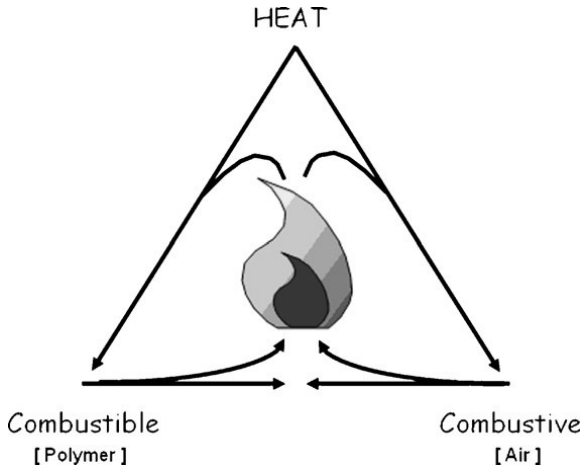

Fig. 1 Fire triangle of combustion.

This global process is complex and involves several reactions and transport phenomena in the solid, gaseous and interfacial phases (Fig. 2). Heating can be caused by a contribution of thermal energy from an external heat source (radiation, convection or conduction), by a chemical process induced inside the material (fermentation, oxidation, etc.) or by the exothermicity of the combustion reaction initiated.

In polymers, the amount of energy required to initiate combustion varies in function of the physical characteristics of the material. For instance, during the heating of semi-crystalline thermoplastics, the polymer softens melts and drips. The energy stored by the polymer during these processes depends on both its heat-storage capacity and its enthalpy of

fusion and degree of crystallinity. Therefore, the increase in polymer temperature and the related rate depend primarily on the heat flow, the difference in temperature due to the exothermicity of the reactions involved, and the specific heat and thermal conductivity of the semi-crystalline thermoplastic. In contrast, in the case of amorphous thermoplastics and most thermosets, due to the absence of a melting point, the heating step leads directly to polymer decomposition.

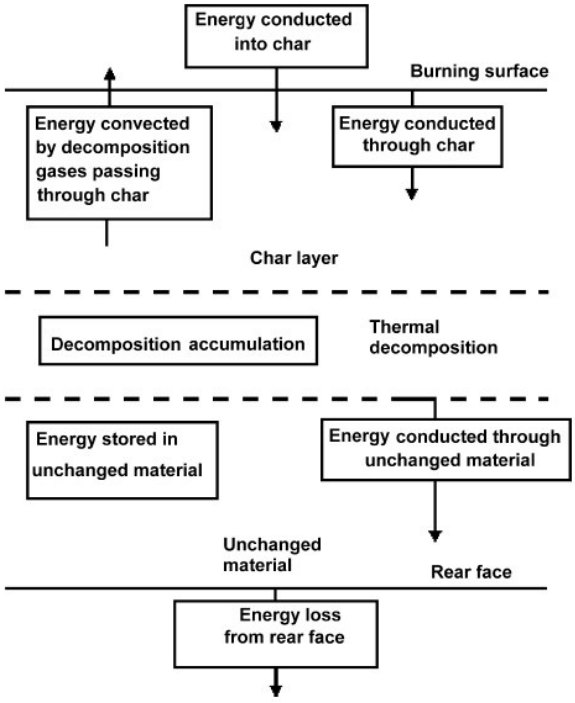

Fig. 2 Thermal transfer during combustion.

The thermal decomposition of a polymer (i.e. covalent bond dissociation) is an endothermic phenomenon, which requires an input of energy. The energy provided to the system must be higher than the binding energy between the covalently linked atoms (200–400 KJ/mol for most C–C polymers). The decomposition mechanism is highly dependent on the weakest bonds and also on the presence or absence of oxygen in the solid and gas phases. Generally, thermal decomposition is the result of a combination of the effects of heat and oxygen. It's possible to distinguish between non-oxidizing thermal degradation and oxidizing thermal degradation.[21] Non-oxidizing thermal degradation is generally initiated by

chain scissions under the simple effect of temperature (pyrolysis). This scission involves varying degrees of material depolymerization. The initial scission depends on several factors: the presence of oxygen atoms in the chain and catalyst residues, former residues of oxidation, chemical defects in polymer chains and the existence, particularly at the end, of weak bonds along the chain, which can initiate unzipping reactions. Chain scission can occur in two ways:

(1) By formation of free-radicals, in this case, the reaction does not stop at this stage because these radicals start a chain/cascade reaction that occurs under both oxidizing and non-oxidizing conditions;

(2) by migration of hydrogen atoms and the formation of two stable molecules one of which has a reactive carbon–carbon double bond.

In oxidizing thermal conditions, the polymer reacts with oxygen in the air and generates a variety of low molecular weight products: carboxylic acids, alcohols, ketones, aldehydes, etc. This degradation also releases very reactive species, i.e. $H^{\bullet}$ and $OH^{\bullet}$, particularly in polyolefins. Oxidation can lead to cross linking through recombination reactions of the macromolecular radicals. However, bond scission usually remains the dominant reaction. The propagation rate of the degradation process is controlled by the wrenching reaction of hydrogen atoms from the polymer chains. The oxidation stability of the polymer thus depends on the C–H bond energy. Some researchers[22] suggest that at combustion temperatures above 300°C polymer degradation takes place via non-oxidizing thermal decomposition. Under these conditions, the rate of pyrolysis is much faster than the diffusion of oxygen in the solid phase. Oxidation therefore only occurs in the gas phase due to the presence of low molecular weight compounds produced by thermal decomposition. The decomposition gases generated by pyrolysis first mix with oxygen by both convection and diffusion into the layer close to the surface, create free radicals, and then ignite. This ignition can be triggered by an external flame (flash ignition) or self-induced (self-ignition) when the temperature is sufficiently high. Ignition depends on several parameters, in particular oxygen concentration. The combustion of the gases increases the polymer temperature and thus

supports the pyrolysis and production of new combustible gases. Combustion thus continues even in the absence of an external heat source.

Flame propagation is also affected by physical factors, more specifically thermal transfers. Conductive and convective transfers are important in the initial phase of fire development when the height of the flame remains limited to a few tenths of centimetres. In a more advanced phase, flame propagation on the surface contributes to a rapid increase in radiative transfer. During these different stages, the development of considerable material heterogeneity can be highlighted, particularly during combustion. A gradient structure tends to form inside the material, arising from the interaction with atmospheric oxygen, coupled with the out-diffusion of reactive species and also concomitant polymer chain breakdown within the material. Several zones inside the material can therefore be identified.[23] The gaseous decomposition products tend firstly to be located in the cavities of this under layer, and afterwards migrate (through this microporous under layer) towards the surface where combustion takes place. The material under layer is in direct contact with the thermal decomposition zone of the polymer and lies on the top of another layer in which the polymer remains intact even if it may undergo phase transitions. In addition, these authors established an energy balance between the heat transfers occurring in the heterogeneous structure.

A variety of physical changes result from pyrolysis, including char development, intumescences, melting, and vaporization.

Char. Char is a black, carbonaceous, porous residue. The char is a thermal degradation (physical change) of the material being pyrolyzed (chemical decomposition). Organic materials such as wood, wood products, thermoset plastics and some thermoplastic polymers form a char layer as they are pyrolyzed. As the char layer develops, it acts as an insulating barrier between the external heat source and the unpyrolyzed fuel under the char. This will slow the pyrolysis rate unless the external heat flux increases to compensate for the insulating char layer. When exposed to heat thermoplastics tend to soften and melt without forming char. For example, polymethylmethacrylate (PMMA) pyrolyzes with very little melt and leaves no

residue. However, rigid polyvinyl chloride (PVC) chars when burned, as do some polyurethane foams.

Intumescence. Intumescence is defined as the process of swelling up or bubbling up. There are many intumescent coatings on the market for fire protection purposes. These coatings, when heated, increase in volume and decrease in density, simulating the development of a char layer. As the intumescent "char" layer is formed, a blowing agent (a substance used to create bubbles in the material) is released, creating a low-density, relatively thick carbonaceous layer. Intumescent reactions are typically endothermic due to chemically bound water in hydrates. As the material expands, the water is released, maintaining the surface temperature. Once the water has been expended, the remaining "char" layer acts as insulation to the material underneath. The "char" can expand 50 to 100 times the original thickness of the intumescent coating.[24]

Melting. When most thermoplastic materials are heated, they melt or soften prior to being vaporized. The rates at which melting occurs compared to the burning rate and the melt viscosity, are important for determining the fire hazard. If initial exposure to a heat flux and subsequent burning produces a copious amount of melt having a low viscosity, then there is the potential for extensive fire spread to the surroundings as this melt comes in contact with new material surfaces. This would be especially dangerous if the melting substance is part of a wall or ceiling lining.

1.2. Flame retardancy

Flame retardant systems are intended to inhibit or to stop the polymer combustion process. In function of their nature, flame retardant systems can either act physically (by cooling, formation of a protective layer or fuel dilution) or chemically reacting in the condensed or gas phase.[25] All flame retardants act either in the vapour phase or the condensed phase through a chemical and/or physical mechanism to interfere with the combustion process during heating, pyrolysis, ignition or flame spread.[26] For example, the incorporation of fillers mainly acts to dilute the polymer

and reduce the concentration of decomposition gases. Hydrated fillers also release non-flammable gases or decompose endothermically to cool the pyrolysis zone at the combustion surface. Halogen, phosphorus and antimony act in the vapour phase by a radical mechanism to interrupt the exothermic processes and to suppress combustion. Phosphorus can also act in the condensed phase promoting char formation on the surface, acting as a barrier to inhibit gaseous products from diffusing to the flame and to shield the polymer surface from heat and air.

There exist two approaches to achieve flame retardancy in polymers generally known as the 'additive' type and the 'reactive' type. Additive type flame retardants, which are widely used, are generally incorporated into polymeric by physical means and do not react at this stage with the polymer but only at higher temperature, at the start of a fire. They are usually mineral fillers, hybrids or organic compounds that can include macromolecules. This obviously provides the most economical and expeditious way of promoting flame retardancy for commercial polymers. Nevertheless, a variety of problems, such as poor compatibility, leaching, and a reduction in mechanical properties, weaken the attraction. Reactive flame retardants are usually introduced into the polymer during synthesis (as monomers or precursor polymers) or in a post-reaction process (e.g. via chemical grafting) thus integrating in the polymer chains. The application of reactive flame retardants involves either the design of new intrinsically flame retarding polymers or modification of existing polymers through copolymerisation with a flame retarding unit either in the chain or as a pendent group. At the present time, new polymer design lacks sufficient versatility in manufacturing, processing and is uneconomical, due to the expense associated with qualifying a new material for use.

The main modes of action of flame retardant systems are reported.

1.2.1. Physical action

The endothermic decomposition of some flame retardant additives induces a temperature decrease by heat consumption. This involves some cooling of the reaction medium to below the polymer combustion

temperature. In this category, we can mention hydrated tri-alumina or magnesium hydroxide, which start liberating water vapour at approximately 200- 300 °C, respectively. Such a marked endothermic reaction is known to act as a "heat sink". When the flame retardants decompose, with the formation of inert gases (H_2O, CO_2, NH_3, etc.), the combustible gas mixture is diluted, which limits the concentration of reagents and the possibility of ignition. In addition, some flame retardant additives lead to the formation of a protective solid or gaseous layer between the gaseous phase where combustion occurs and the solid phase where thermal degradation takes place. Such a protective layer limits the transfer of matter such as combustible volatile gases and oxygen. As a result, the amount of decomposition gases produced is significantly decreased. Moreover, the fuel gases can be physically separated from the oxygen, which prevents the combustion process being sustained.

1.2.2. Chemical action

Flame retardancy through chemical modification of the fire process can occur in either the gaseous or the condensed phase. The free-radical mechanism of the combustion process can be stopped by the incorporation of flame retardant additives that preferentially release specific radicals (e.g. Cl• and Br•) in the gas phase. These radicals can react with highly reactive species (such as H• and OH•) to form less reactive or even inert molecules. This modification of the combustion reaction pathway leads to a marked decrease in the exothermicity of the reaction, leading to a decrease in temperature and therefore a reduction in the fuel produced. In the condensed phase, two types of chemical reactions triggered by flame retardants are possible: first, the flame retardants can accelerate the rupture of the polymer chains. In this case, the polymer drips and thus moves away from the flame action zone. Alternatively, the flame retardant can cause the formation of a carbonized (perhaps also expanded) or vitreous layer at the surface of the polymer by chemical transformation of the degrading polymer chains. This char or vitrified layer acts as a physical insulating layer between the gas phase and the condensed phase.

1.3. Char formation

1.3.1. The role of char in flame retardancy

There's a strong correlation between char yield and fire resistance.[28] The higher the amounts of residual char after combustion, the lower the amount of combustible material available to perpetuate the flame and the greater the degree of flame retardancy of the material. An attractive way of reducing flammability of polymers is reducing the rate of production of combustible gases while increasing the rate of production of char in the solid phase, acting as a thermal barrier. Better solid phase flame retardants are those that cause a layer of carbonaceous char to form on the polymer surface. Besides char formation usually reduces the formation of smoke and other products or incomplete combustion.

According to the widely accepted "two stage theory of polymer combustion", the polymer must be volatilizes before combustion can occur. Once ignited, the polymer will continue to burn as long as energy feedback from the flame is sufficient to maintain volatilization of the polymer. This volatilization requires decomposition of the polymer to lower-molecular-weight fragments. Thus, has been suggested that the flame retardant action may act through three possible mechanisms. First, the flame retardant may act in the gas phase to inhibit exothermic oxidation and reduce energy feedback to the polymer from the flame. Second, the flame retardant may form a thermal barrier between the condensed and gaseous phases. Third, the flame retardant may alter the pathway or rate of pyrolytic decomposition of the polymer. Some additives act as flame retardants lowering the ratio of volatiles to non volatile pyrolysis products. This means that some additives, as phosphate groups, reduce the volatility of the fragments produced by the scission of the polymer chain. Reducing volatility also means increasing the residence time of the fragments on the surface of the polymer. If the rate of the reaction producing small, volatile fragments is slower than the reactions in the solid state resulting in char formation during pyrolysis, volatile fragments will be incorporated into a char before they can volatilize. Red phosphorous in PET was found to reduce the volatility of the oligomers and

thereby increases the chances that oligomers will be cross linked to the char before they leave the surface of the polymer.

Cross-linked polymers remain an area of significant interest for enhancing the flame retardancy of polymeric materials, due to the formation of a network which is expected to increase the difficulty of eliminating small molecules. In principle, chemical cross-linking reduces the molecular mobility and increases the number of bonds which must be broken in order for a material to exhibit mass loss. Cross linking reactions are predominant secondary reactions that occur in the solid phase leading to the formation of polyaromatic char.[27] another way to increase the amount of solid char is removing the side chains and thus generating double bonds in the polymer. Usually aromatic polymers give rise to a greater degree of condensation into aromatic chars and therefore only relatively low levels of flammable gases are available to feed the flame. Of particular importance in this area was the work of Van Krevelen[28] on the linear correlation between char and flammability parameters. The structural morphology and chemical nature of char residues from burning polymers can lead to invaluable information about the mechanism aspects and mode of action of flame retardants.[28]

1.3.2. Correlation between cross-linking and char formation

The resistance to combustion of a polymer is connected to both the number of cross-links and to the strength of the bonds that make up cross-linked structure.[29] If the cross-linked structure is produced by weak bonds that may be easily cleaved thermally, the cross-linked structure is lost and the fire resistance of the resulting polymer is not different from the original one without cross-links. The cross-linking reagent enhances char formation because it causes otherwise volatile fragments to remain in the polymer for longer time. These cross-linking reagents not only accelerate the appearance if char but also reduce the amount of fuel formed.

To cross-link aromatic containing polymers, Friedel-Craft substitution reactions may be used, where the OH group from an alcoholic functionality combines with hydrogen from an aromatic ring to produce water. In the presence of acid catalysts (usually Lewis acids), this kind of reaction

consists in an alkylation or acylation of aromatics. Many examples are reported in literature. In the presence of $ZnCl_2$[30], polyesters like PET or PBT produce a highly aromatic char at a low temperature. A possible mechanism involves a Friedel-Craft reaction. The fire retardant action of iron oxide in the halogen-containing systems has been associated with the condensed phase activity due to Friedel-Craft chemistry.[31]

1.3.3. Formation of char

It is believed that the temperature at the surface of a burning polymer is close to the temperature at which extensive thermal degradation occurs (usually between 300-600°C). The bottom layer of the char, near to the polymer surface, is at the same temperature, whereas the upper surface exposed to the flame, can be as hot as 1500°C. Therefore, fire retardancy chemistry is concerned with chars, which may be produced at temperatures between 300 and 1500°C.

A polymer passes through several steps in the formation of char:

(1) cross-linking
(2) aromatization
(3) fusion of aromatics
(4) turbostratic char formation and
(5) graphitization.

The char formed during polymer combustion is similar to turbostratic char. Turbostratic char refers to an incomplete process of graphitisation, when solid spheroids, precursor of graphite, appear in molten carbonaceous material, typically at 500-700°C. At this point, the graphite layers are arranged in a parallel fashion.

In fire retardant terminology, all polymers are usually classified as non-charrable or charrable, depending on whether or not they produce char under pyrolytic conditions. In term of chemical processes governing the thermal degradation, polymers may be divided into three classes:

(a) polymers that undergo chain scission and volatize with a negligible amount of char formation (e.g. PP, PS, PMMA);

(b) polymers that undergo chain stripping reaction producing insaturation in the main chain with loss of hydrogen atoms and the pendant groups and give rise to a moderate amount of char (e.g. PVC, PVA, PAN);

(c) polymers that contain aromatic rings that can cross-link simultaneously with chain scission reactions and produce relative high amount of char (e.g. aromatic polyamides, PA, polyesters, polycarbonates, PC, polyimide, PI).

Molecular dynamics can provide a realistic description of the thermal degradation of polymers. Molecular simulation of char forming process in polyethylene[32] is shown in Fig. 3. The polymer chains (Fig. 3a), which are too big to move away from each other as long as they remain intact, are coiled into a ball-like structure which brings nascent radical sites from neighbouring chains into close proximity (Fig. 3b). Although this arrangement would be favourable for the formation of cross-links, it is destroyed before a significant number of radical sites can develop as the mobile fragments produced in random scission of the C-C bonds volatilize as fuel (Fig. 3c). During the initial stages of thermal degradation the structure of the solid begins to break down. Computer movies of the trajectories obtained from molecular dynamic simulations indicate that the polymer network, which contains many elongated and highly strained intermolecular bonds at room temperature, responds by forming stronger cross-links (Fig. 3d). The presence of these crosslinks makes fragmentation of the backbone during thermal degradation more difficult. At some point, the rate of C-H bond dissociations will exceed the rate at which mobile fragments are produced and a char should form (Fig. 3e).

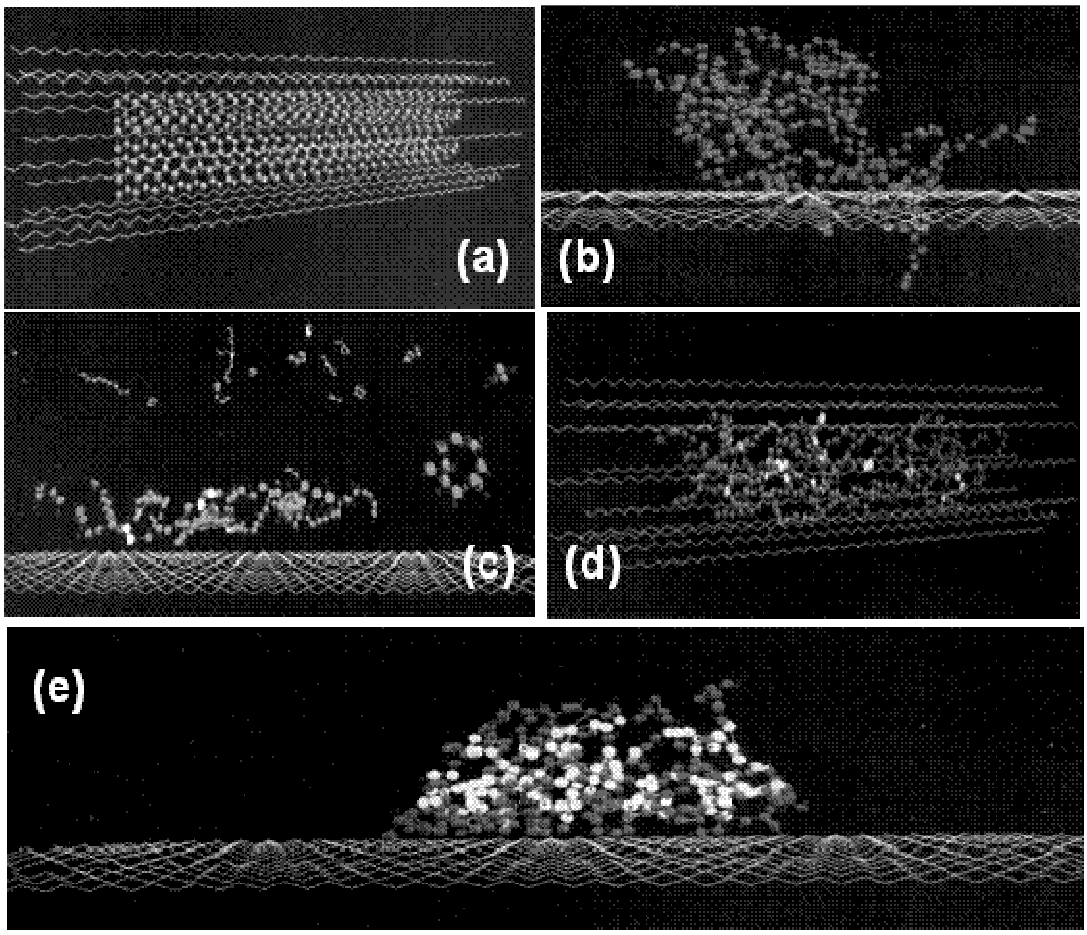

Fig. 3 (a) Dynamic model consisting of different polymer chains; (b) Polymer chains coiled into a ball-like structure during the early stages of the thermal degradation; (c) Mobile fragments which are produced by random scission of the C-C bonds volatilizing as fuel for gas-phase combustion reactions; (d) Intermolecular crosslinks formation (large white spheres) created by random scission of the C-H bonds; (e) High density of white spheres, formed when there are a large number of radical sites in close proximity.

1.3.4. Polymers that naturally produce char

Under certain experimental conditions, even aliphatic polyhydrocarbons can produce some char with a process called carbonization of polyhydrocarbons. The dissociation energy of C-C bonds in hydrocarbons is about 65-90 Kcal/mol, depending on the structure, while C-H bonds have a dissociation energy between 90-105 Kcal/mol. Due the similar energies, dehydrogenation may compete with the chain scission at high temperature.

Vinyl chain ends activate hydrogen in allylic positions. The dissociation energy of the allylic C-H is ~85 Kcal/mol, and this leads to the

formation of conjugate dienes through dehydrogenation reactions. The dienes may react with the activated double bond and lead to aromatization, as shown in Scheme 1.

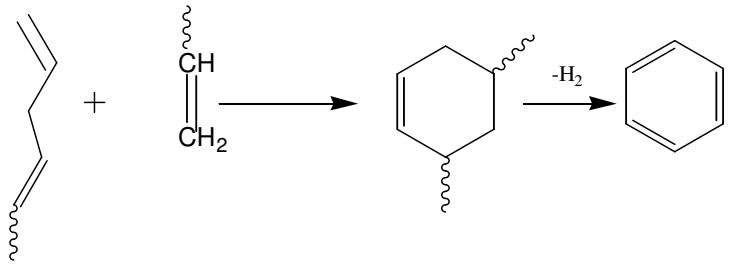

Scheme 1

The formation of char by carbonization of polyhydrocarbons, under the normal degradation conditions in an inert atmosphere, is usually quite limited but one of the goals of fire retardant science is to promote these char-forming mechanisms.

To improve the fire retardancy of polymers with high flammability, special additives that can promote cyclization reactions should be utilized. It is commonly accepted that polymers containg aromatic rings, give a high char yield as the aromatic rings are the building blocks from which char is produced. This is the reason why these aromatic polymers usually show higher thermal stability than vinyl polymers or aliphatic heterochain polymers. The higher is the aromaticity of the polymer, the higher is the char yield is expected to produce. Van Krevelen showed that the char-forming tendency of the aromatic cross-linking polymers is an additive value that can be estimate from the contributions of the structural units.[28] The thermal decomposition of aromatic cross-linking polymers usually begins with the elimination of small molecules (H_2O, CO_2, CO, CH_4, etc.), forming insaturation in the polymer chain, that can lead to cross-linking. Upon further heating, dehydrogenation occurs, giving aromatic radicals that undergo fusion to yield thermally stable polyaromatic structures. At these temperatures, hydrogen and heteroelementes are eliminated from the char which leads to an accumulation of graphitic carbon (carbonization).

The tendency of a polymer to produce char can be increased by chemical additives and/or by altering its molecular structure.

1.3.5. Lewis Acid

When a polymer does not naturally produce char or produces only a small amount of char, the char-forming reactions can be enhanced by the use of additives, as Lewis acids.

Lewis acids represent a wide range of chemical substances that are able to accept an electron pair and create a coordinative bond. Some polymers with strongly electronegative groups can coordinate Lewis acids and this may change the polymer decomposition mechanism. Lewis acids may enhance the char-forming process, decreasing the amount of volatile aromatics and increasing the amount of solid residue left. Thermal degradation of complexes of poly (methyl methacrylate) with metal halides was studied by Wilkie[33]. The conclusion was that the presence of reasonably strong Lewis acid can affect the conversion of the ester into a metal carboxylate salt. In polymers bearing aromatic rings, Lewis acids are effective cross-linking catalysts. To recall this chemistry, it is important to remember that, for examples, aromatics like toluene undergo vigorous polymerization in the presence of $AlCl_3/CuCl_2$. To avoid interaction with the polymer during compounding, precursors of Lewis acids were used.

1.3.6. Promoting char formation: metal and phosphorus-containing additives

It is well- Known in the literature[34,35] that certain metal compounds have a catalytic influence on the rate and degree of graphitization of carbon materials. Catalytic graphitisation refers to formation of graphitic material involving a chemical reaction between the ungraphitized carbon and the metal. A wide variety of metal oxides are reported to show a catalytic activity in graphitization.[34] Among these, iron oxide seems to be the more effective as it also improves the char morphology that appears shiny, continuous and free of cracks.[36,37] These changes will provide better insulating properties to the char layer and thus enhance fire retardancy. Iron compounds show a synergism in both halogen-containing and halogen-free fire retardant systems. Various iron-containing compounds are beneficial for decreasing the flammability and smoke production, reacting with polymeric carbon

containing free-radical sites, that may form smoke particles, and converting them into char. The formation of this char occurs quickly so the concentration of free radicals drops below the level needed to sustain combustion. Fe_2O_3 was the most effective catalyst yielding a graphite of high density.[38] Acheson[39] showed that heating iron compounds with amorphous carbon led to the formation of cementite (Fe_3C) which decomposed on further heating to give graphite. It was also found that heating a non-graphitising carbon in the presence of iron transformed it into a mixture of graphite and graphitisable phase. It was believed that iron acted to form an instable phase which then decomposes to give shell of graphitisable carbon surrounding the iron. Iron oxide acts as a catalyst for dehydrogenation and oxidative dehydrogenation, catalysing the reorganization of pyrolytic carbon to turbostratic graphite at about 600°C. Dehydrogenation and oxidative dehydrogenation catalysts are a generic class of additives that may accelerate char formation. This char will have a value as a barrier to heat and mass transfer. Besides, its carbon material would represent material not contributing to the heat release.

There are several examples in the literature where alkali metals or alkaline earths or other metal salts accelerate the dehydration of polymers containing hydroxyl groups. Cellulose decomposes at low temperature, but with high char yield in the presence of small concentration of sodium or potassium cations[40] and this indicates the catalytic nature if the char promotion by cations.

It is well documented[41] that phosphorus-containing flame retardants exhibit both gas phase and condensed phase activities. If the volatility of the phosphorus-containing additive is low, it remains in the condensed phase and promotes char formation. A more pronounced effect is observed if the additive reacts with products of decomposition of the polymer. Red phosphorus is an active flame retardant additive. It was found that it does not change the composition of evolved volatile products but changes the kinetics of polymer thermal degradation.[42]

1.3.7. Structure and characterization of char

Char is a complex material in term of physical, chemical and mechanical structures. It is composed if the mixture of many chemical aromatic-aliphatic compounds, often with heteroatom (O, N, P, and S). Inorganic substances may be incorporated in the char. Morphologically, char consists of crystalline and amorphous regions. Some physical properties, as well as the mechanical properties, depend on its chemical structure and conditions of preparations.

Infrared and Raman spectroscopy are very attractive for char studies because they reveal information concerning the chemical structure. There are serious difficulties because the char is black and will not transmit infrared radiation. Conventional infrared dispersion techniques usually give poorly defined spectra but if special preparation techniques are used (e.g. finely grounded samples) good results can be achieved. Although infrared is a powerful tool for char investigation at low- medium temperatures (300-550°C), Raman-scattering microprobe spectroscopy can be a useful method for mature char, once graphitization begins.

Nuclear magnetic resonance (NMR) spectroscopy can give further insight into the chemical structure of the char, but, as chars are insoluble, only solid-state NMR techniques can be used.

CHAPTER 2
FLAME RETARDANT ADDITIVES

Flame retardant additives are used to limit the risk of fire and its propagation. They are incorporated in the polymer matrix to increase the time to ignition, improve the self-extinguishability of the polymer, decrease the heat release rate during combustion and prevent the formation of flammable drops.

The growing number of restrictions and recommendations from the European Community promoted the development of safe and ecological non-halogen containing flame retardant polymers.[43] To improve the flame retardant efficiency of halogen-free flame retardant, some techniques such as nanotechnology and catalysis technique can be employed.

2.1. Phosphorus-based flame retardants

Phosphorus flame retardants are the second most widely used class of flame retardants. The range of phosphorus containing flame retardants is

extremely wide and the materials versatile, since the element exists in several oxidation states. Phosphines, phosphine oxides, phosphonium compounds, phosphonates, elemental red phosphorus, phosphites and phosphate are all used as flame retardants. Phosphorous flame retardants can remain in the solid phase and promote charring or volatize into the gas phase, where they act as potent scavengers of H· or OH radicals.

In the condensed phase, the phosphorus-based flame retardants are particularly effective with polymers containing oxygen or nitrogen (polyesters, polyamides, cellulose, etc.)[44,45] If the polymer cannot contribute to charring because of the absence of suitable reactive groups, a highly charring co-additive has to be introduced in combination with the phosphorated flame retardant.[46] With most of them, thermal decomposition leads to the production of phosphoric acid, which condenses readily to produce pyrophosphate structures and liberate water. The water released dilutes the oxidizing gas phase. In addition, phosphoric acid and pyrophosphoric acid can catalyze the dehydration reaction of the terminal alcohols leading to the formation of carbocations and carbon–carbon double bonds. At high temperature, this can subsequently result in the generation of cross linked or carbonized structures. Ortho- and pyrophosphoric acids are turned into metaphosphoric acid and their corresponding polymers. The phosphate anions (pyro- and polyphosphates) then take part, with the carbonized residues, in char formation. This carbonized layer (char) isolates and protects the polymer from the flames and:

(1) limits the volatilization of fuel and prevents the formation of new free-radicals;
(2) limits oxygen diffusion, which reduces combustion;
(3) insulates the polymer underneath from the heat.

There are two char forming mechanisms: (a) redirection of the chemical reactions involved in decomposition in favour of reactions yielding carbon rather than CO or CO_2 and (b) formation of a surface layer of protective char.

Phosphorus-based flame retardants can also volatilize into the gas phase, to form active radicals (PO2•, PO• and HPO•), and act as scavengers of H• and OH• radicals. Volatile phosphorated compounds are among the most effective combustion inhibitors since phosphorus-based radicals are, at the same molar, five times more effective than bromine and 10 times more effective than chlorine radicals.[47] The mechanism of radical scavenging by P was suggested by Hastie and Bonnel.[48] The most abundant P radicals in the flame are HPO_2, PO, PO_2 and HPO. Some examples are:

$HPO_2\bullet + H\bullet = PO + H_2O$

$HPO_2\bullet + H\bullet = PO_2 + H_2$

$HPO_2\bullet + OH\bullet = PO_2 + H_2O$

The phosphorated flame retardant agents can be used as additives or incorporated into the polymer chain during its synthesis. Even though many organic phosphorus derivatives display flame-retardant properties, only a few have commercial potential, due to the processing temperature and the nature of the polymer to be modified.

2.1.1. Red Phosphorus

Red phosphorus is the most concentrated source of phosphorus for flame retardancy. Used in small quantities (less than 10%), it is very effective in polymers such as polyesters, polyamides and polyurethane. A typical example is glass-filled PA-6,6 containing 6–8% red phosphorus, which achieves V-0 classification in the UL 94 test.[49] The first report about the use of red phosphorus as a flame retardant in polyurethane, by Piechota[50], dates back to 1965. However, its action mechanism has not yet been clearly established. Initially, it was believed that red phosphorus exhibited flame retardant properties only in the presence of polymeric materials containing oxygen atoms (polyesters, polyamides, polyurethanes, etc.) It was therefore suggested that its mode of action involved specific scavenging of oxygen containing radicals, acting as chain carriers in the secondary pyrolysis step and leading to the generation of gaseous fuel

species.[51] However, it was later found that red phosphorus is also active in polyethylene and other non-oxygenated polymers.[52] Consequently, a different mode of action of red phosphorus was proposed[53] where red phosphorus depolymerises into white phosphorus (P4). P4 can volatilize at high temperature and act in the gaseous phase, or it can diffuse from the bulk of the polymer to the burning surface, where it is oxidized to phosphoric acid derivatives that can eventually come into close contact with the flame and form phosphoric acid. This phosphoric acid could act as a char forming agent, thus physically limiting oxygen access and fuel volatilization. Furthermore, Peters[52] found that, in polyethylene, red phosphorus is active both in the gas and the condensed phase. In the gas phase, PO• species produced from the combustion of red phosphorus quench the free-radical processes. In the condensed phase, red phosphorus substantially lowers the heat of oxidation and also traps free-radicals. This improved thermal stability results in a decrease in fuel production during the burning of the material. However, red phosphorus has a major disadvantage. Throughout the melting process, it can release highly toxic phosphine (PH3) through reaction with moisture as a direct result of its poor thermo stability. Interestingly enough, phosphine formation can be avoided by prior polymeric encapsulation of the red phosphorus.

2.1.2. Organic phosphorus-based compounds

Organic phosphorus derivatives (Fig. 4) can act as additives or as reactive (co)monomers/ oligomers. The main groups of organophosphorus compounds are phosphate esters, phosphonates and phosphinates[54]. The use of (alkyl-substituted) triaryl phosphates such as triphenyl phosphate (TPP), cresyl diphenyl phosphate, isopropylphenyl diphenyl phosphate, tert-butylphenyl diphenyl phosphate or tricresyl phosphate is very limited in plastics engineering because of their high volatility and relatively low fire retardant efficiency. For instance, the incorporation of TPP in polycarbonate/ acrylonitrile butadiene styrene (PC/ABS) blends[55] does not affect the thermal decomposition behaviour of the blend. In fact, TPP volatilizes before decomposition of the polymer blend. In similar

experiments, V-0 ratings for poly(phenylene oxide) (PPO)/high impact polystyrene (HIPS)- based formulations were obtained at 2 wt% of phosphorus.

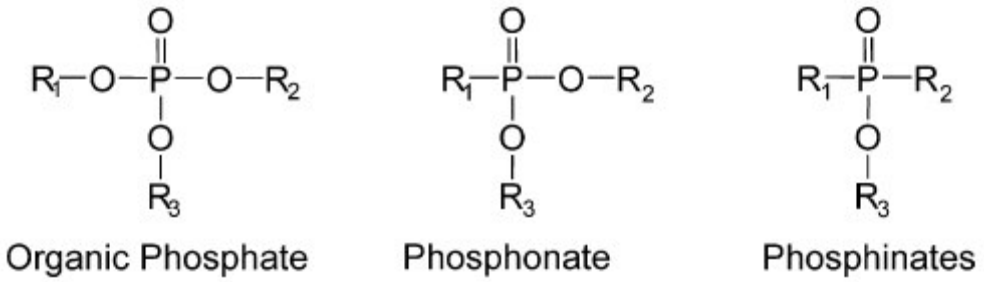

Fig. 4 Chemical structures of some phosphorus flame retardant additives.

BDP and RDP react with PC phenolic functions, thus promoting crosslinking of the polymer chains and consecutive charring.[56] During thermal degradation, the "P–O–C" bonds of BDP react via transesterification with phenolic groups originating from PC, which leads to cross-linking.

2.2. Mineral flame retardants

The most commonly used mineral flame retardants are metal hydroxides, hydroxycarbonates and zinc borates. Besides the mentioned general effects, these inorganic fillers have a direct physical flame retardant action. As the temperature rises, these fillers decompose endothermically and therefore absorb energy. Moreover, they release non-flammable molecules (H_2O, CO_2), which dilute combustible gases, and can also promote the formation of a protective ceramic or vitreous layer.

The major materials that are used as fire retardant mineral fillers for polymers are alumina trihydrate (ATH), ($Al_2O_3 \cdot 3H_2O$) and magnesium hydroxide (MH), ($Mg(OH)_2$).[57,58] These two materials account for more than 50% by weight of the world-wide sales of fire retardants. Most of this is low cost ATH that is used in thermosetting resins. The use of ATH is limited to those polymers processed below about 200°C while MH is stable above 300°C and thus can be used in polymers that must be processed at higher

temperatures. Their effectiveness comes from the fact that they both decompose endothermically and consume a large amount of heat, while also liberating water, which can dilute any volatiles and thus decrease the possibility of fire. For ATH, decomposition begins near 300°C and consumes 1270 J/g of ATH; for MH, decomposition begins at higher temperature, near 400°C, and consumes 1244 J/g of MH. There is some tendency for MH to catalyze the degradation of some polymers; in unsaturated polyester resins it can act as a chain extender, affecting resin rheology. A major use of both ATH and MH is in low smoke, halogen-free wire and cable applications, where there is significant commercial activity.

Oxide particles are emerging fillers for many applications. TiO_2 has received a great amount of applications due to its strong oxidizing power of the photogenerated holes, chemical inertness, non-toxicity, low cost, high refractive index and other advantageous surface properties. Any type of inorganic filler, even inert, can influence the reaction of polymers to fire for several reasons:

(1) reduces the content of combustible products;
(2) modifies the thermal conductibility of the resulting material and all its thermo-physical properties;
(3) changes the viscosity of the resulting material.

All these actions have an indirect incidence on the polymer's fire performance. Nevertheless, some minerals are more specifically used as flame retardants owing to their behaviour at high temperature. Metal oxide nanoparticles may interact with the acidic functionalities of the polymer giving interaction. In Fig. 5, three possible structures of carboxylate coordinated to a titania surface are reported. The first structure, carboxylate is bound to one Ti (IV) centred in a chelating bidentate mode (a). The carboxylate could also be bound to one Ti (IV) in a monodentate (ester-like linkage) mode (b), and finally, the carboxyl group could bind with each of its oxygen atoms to two Ti (IV) atoms yielding the bridging bidentate mode (c).

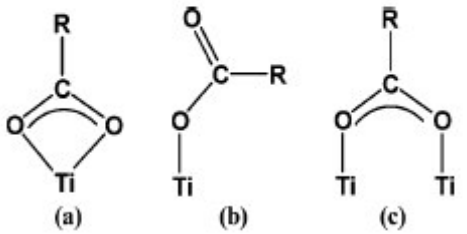

Fig. 5 Binding modes of RCOO-with Titania surface. (a) Chelating bidentate, (b) monodentate (c) bridging bidentate.

2.3. Nanometric particles

2.3.1. Nanoscale approach

Nanocomposites constitute a new development in the area of flame retardancy.[59] Although first reported by Blumstein in 1961, the real exploitation of this technology started in the 1990s. Polymer nanocomposites are already part of an important worldwide business: automotive (molten part in cars), electronics and electrical engineering, household products, packaging industry, aircraft interiors, appliance components, security equipments.

Nanocomposites are formed when phase mixing occurs at a nanometres dimensional scale and as a result, show superior properties over their micro counterparts or conventionally filled polymer. As the interfacial area between the polymer and the nanofiller is greatly increased, a considerable reduction of the loading rate is possible. Moreover, when they are properly dispersed in polymer matrices, they are Known to contribute to the enhancement of properties such as thermal, mechanical or fire resistance. [60]

The improvement in thermal stability and flammability properties of polymer nanocomposites has been reported by several research groups.[61, 62] Obviously, the contribution of each type of nanoparticle to flame retardancy varies and strictly depends on its chemical structure and geometry. According to Gilman[61],the nanocomposites flame retardant mechanism is a consequence of high performance carbonaceous char build-up on the surface during burning, which insulates the underlying material and slow

down the mass loss rate of decomposition products (Fig. 6). The incorporation of nanoparticles such as organoclay, carbon nanotubes or POSS reduces polymer flammability by several mechanisms (limiting fuel transfer to the flame, formation of a protective char layer, etc.). However, these polymer nanocomposites still burn with very little, if any, reduction in total heat release, and time to ignition is generally not improved and can even decrease for some nanocomposites. In other words, nanoparticles have to be used in combination with other flame retardant agents in order to achieve the required fire performance levels. Nanocomposites may be produced using several different materials for the nano-dimensional material, including clays, graphite, carbon nanotubes, and polyhedral oligosilsesquioxanes, POSS. Most work to date has been with clays, particularly with montmorillonite clay, an alumina-silicate material.

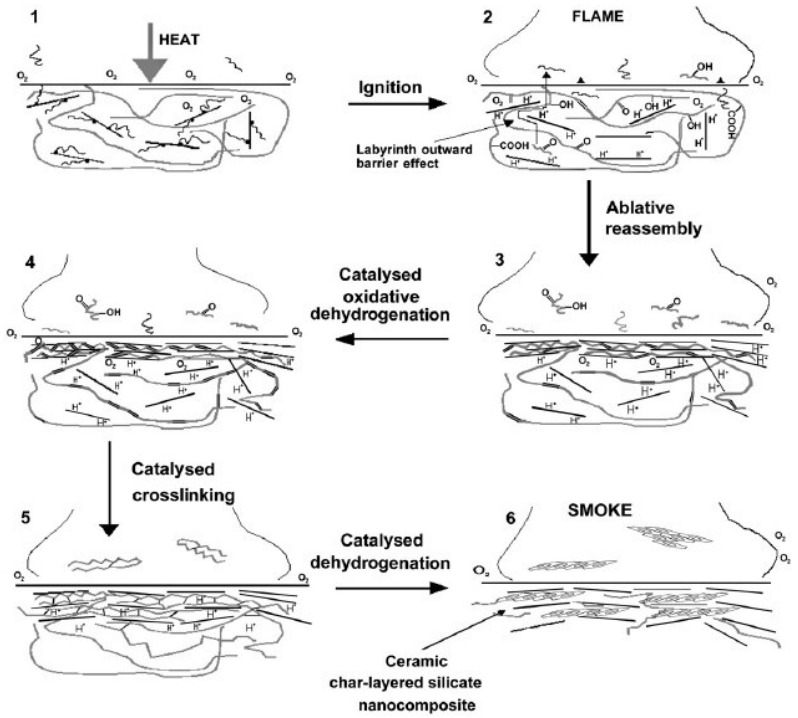

Fig. 6 Schematic representation of the combustion mechanism and ablative assembly of a nanocomposite during the cone calorimeter test.

The thermal stability of the clay based polymer nanocomposites have been extensively studied by several research groups. Cone-calorimeter analysis of different polymer nanocomposites reveals significant

improvements in flammability properties due to a char-layered formation in the solid phase. To prepare polymer nanocomposites, the unmodified layered silicate clay is first modified with suitable organic species (commonly various organic amines) containing positively charged functional groups to replace the small cations in the interlayer region. This organically modified clay is then incorporated into polymer matrix using different methods, like solution intercalation, melt-compounding to obtain the nanocomposites. The morphology of the dispersed clay particles in these polymer nanocomposites may vary from an intercalated structure (where the polymer chains remains intercalated within the clay layers) to a completely exfoliated structure (where individual clay layers remain completely separated from each other and dispersed homogeneously throughout the matrix). One of the challenges for preparing nanocomposite materials is the agglomeration of the nanofillers in the polymer matrix that leads to poor performance of the composite. One approach to address this problem has been the use of ultrasonic irradiation for dispersion of SiO2, TiO_2, and Al_2O_3 nanoparticles during the synthesis of inorganic-polymer nanocomposites materials. However, without any chemical bonding, optimized interaction between the matrix and filler is not achieved.

2.3.2. Nanoscale oxide-based nanocomposites

The catalytic effect of divalent and multivalent metal compounds on the flame retardancy of intumescent systems has been well studied by Lewin and Endo.[63] Laachachi[64] investigated the effect of the incorporation of nanometric titanium oxide (TiO_2) and ferric oxide (Fe_2O_3) particles on the thermal stability and fire reaction of poly(methyl methacrylate) (PMMA). The incorporation of a small amount (5 wt%) of nanometric TiO_2 or Fe_2O_3 enhanced the thermal stability of PMMA nanocomposites. HRR values, as determined by the cone calorimetry test (irradiance of 30 Kw/m^2), were found to depend on the filler content and to decrease at higher loadings (Fig. 7). Even though the Fe_2O_3 nanoparticles had a similar particle size (23 nm) and surface area (48 m^2/g) to the TiO_2 (21 nm and 50 m^2/g), their incorporation led to a different behaviour in the cone calorimeter test. The

combustion of PMMA/Fe_2O_3 nanocomposite produced more smoke than virgin PMMA. The pea K HRR was reduced by about 50% in the presence of 20 wt% TiO_2 while it decreased by only 37% when the same quantity of Fe_2O_3 was used. Time to ignition increased significantly (more than 20 s) in the presence of TiO_2 and remained largely unchanged at higher TiO_2 loading rate. By contrast, no significant change was observed with Fe_2O_3, which has tentatively been explained by the lower thermal diffusivity of iron oxide compared to TiO_2, leading to a more rapid rise in temperature at the surface of the samples filled with iron oxide. The improved flame retardancy of PMMA-TiO_2 and PMMA- Fe_2O_3 nanocomposites was attributed to a restriction of the mobility of polymer chains resulting from strong interactions between PMMA and the nanoparticle surface. In fact, it was demonstrated that both the glass transition temperature (Tg) and LOI increased with metal oxide content. Furthermore, it was shown that the flame retardant effect of both TiO_2 and Fe_2O_3 depends on their particle size and surface area. By comparison with virgin PMMA, the pHRR value was reduced approximately by 45% when 15 wt% of nanometric TiO_2 was used and only by 39% when the same amount of micrometric TiO_2 was introduced. In both cases the time to ignition increased by about 20 s.

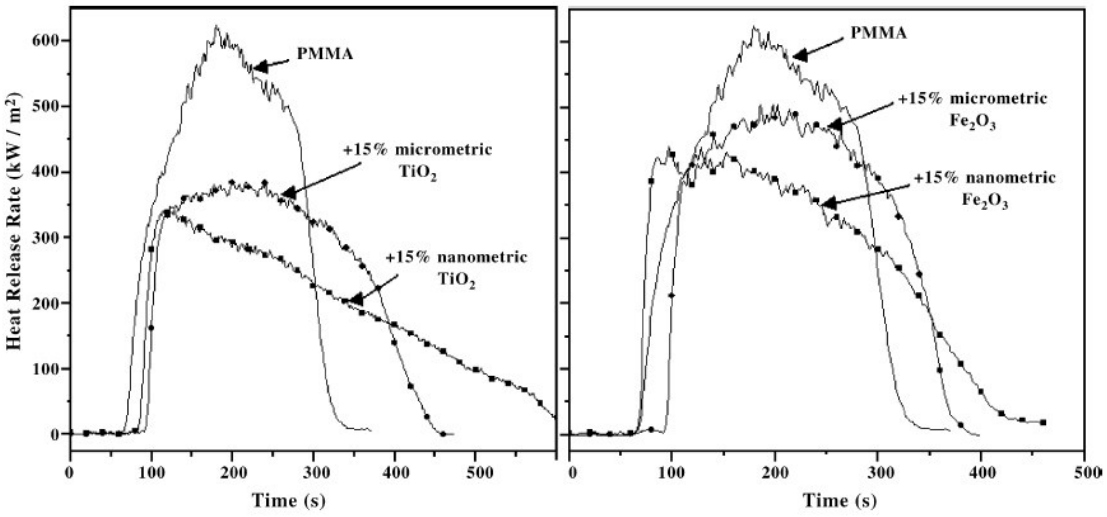

Fig. 7 HRR values for PMMA containing 15 wt% nanometric and micrometric TiO_2 and Fe_2O_3 (35 KW/m²).

With regard to iron oxide-filled PMMA, a 30% reduction in pHRR was recorded in the presence of 15 wt% nanometric Fe_2O_3. This reduction was limited to 20% with the same quantity of micrometric Fe_2O_3. The TTI value increased from 69 s for the nanometric filler to 99 s for the micrometric one. The TTI reduction, recorded when nanometric fillers are used, was attributed to heat transfer between the metal oxide nanoparticles and the polymer chains, which is enhanced by the increased metal oxide/polymer contact interface at lower particle size. The polymer temperature therefore increases more rapidly, particularly at the surface, decreasing the time to ignition

2.4. Synergism and catalysis in flame retardancy

The concept of synergism is very often used in the optimization of flame retardant formulations. The term synergism refers to the combined effect of two or more additives, which is greater than that predicted on the basis of the additivity of the effect of the components.[65] In other words, synergism is achieved when the performance level due to a mixture of additives xA + yB (x + y = 1) for a given property (P) is greater than that predicted for the linear combination (xPA + yPB) of the single effects of each additive (PA and PB). Conversely, antagonistic effects can be detected.

As discussed above, polymer flame retardancy can be achieved through one or more chemical and/or physical mechanisms taking place in either the gas or the condensed phase. Synergistic phenomena can be obtained either by a combination of flame retardancy mechanisms, such as char formation by a phosphorated flame retardant combined with a gas phase action by a halogenated flame retardant or by a combination of flame retardant agents reinforcing the same mechanism, e.g. nanoclays and phosphorated flame retardant agents, both acting in the condensed phase. The two mostly common examples are halogen with antimony and P with N.[66] The gas-phase flame retardant action of halogenated additives can be improved by the incorporation of antimony oxide (Sb_2O_3). Antimony oxide

reacts with the hydracids (HCl or HBr) generated by the halogenated flame retardants to form antimony oxyhalides, that are much heavier than the native hydracids, thus prolonging their residence time in the flame.[67]

Regarding the P-N synergism, the formation of phosphorus–nitrogen intermediates can accelerate the *in situ* production of phosphoric acid and therefore polymer phosphorylation. P-N bonds are more reactive than P–O bonds in the phosphorylation process. They maintain phosphorus in the condensed phase, yielding cross linked networks that promote more intensive char formation Synergistic effects can also be obtained by combining the gas phase action of halogen species with the condensed phase action of phosphorus-based compounds. A very sharp synergistic effect between ammonium polyphosphate (APP) and some inorganic mineral salts and oxides was discovered by Levchik.[68] The principal mechanism appears to be the interaction of polyphosphoric acid and metal-containing compounds. Since only divalent or higher-valence metals show this effect, it is reasonable to assume that metal cations help to cross-link and thus to create a more thermally insulative char structure. If the mineral compound is added in large quantities, solid crystalline phosphates are formed resulting in cracking of the char and the loss of insulative properties. This indicates how synergistic effects are observed only in a very narrow concentration range.

The action in the polymer of nanoparticles alone proves to be insufficient for ensuring adequate fire resistance to meet the required standards. However, their association with other flame retardant systems such as phosphorated compounds could potentially be a very interesting approach. Several recent works have focused on such methods. For example, Laachachi[64] combined the flame retardant action of nanometric metallic oxides (TiO_2, Al_2O_3) with the char formation induced by phosphorated flame retardant systems (ammonium polyphosphates and phosphinates) in PMMA. In the case of aluminium phosphinate supplied by Clariant under the trade name Exolit OP930 (hereafter noted phosphinate), cone calorimeter results showed that partial substitution of phosphinate by alumina nanoparticles promoted synergistic effects, with a marked decrease

in pHRR. However, no significant effect could be achieved with TiO_2 nanoparticles. Although Al_2O_3 and TiO_2 promote positive flame retardant effects in PMMA, their combination with phosphinate does not automatically lead to a synergistic effect. Observation of residues involving alumina nanoparticles essentially shows a continuous solid layer. However, with TiO_2– phosphinate combinations, the char residues do not cover the entire sample surface, leading to a poor barrier effect, which explains the limited performances displayed by these compositions. It has been shown that there is no chemical reaction between Al_2O_3 (or TiO_2) and phosphinate but only the formation of a vitreous layer, promoted by the phosphorated compound and reinforced by alumina particles. It appears that, in addition to their role in char reinforcement, alumina particles also have a positive catalytic effect on the formation of the protective layer with phosphinate (not provided by titanium oxide particles).

CHAPTER 3

EXPERIMENTAL: COMPOUNDING AND CHARACTERIZATION

3.1. Materials

PBT (Pocan B 1505), supplied by LANXESS, was used in this study. Different kinds of nanometric metal oxides were used. Aluminium oxide, iron oxide, Fe_2O_3 and Sb_2O_3 were purchased from Sigma Aldrich. Nanometric titanium dioxide, TiO_2 (P-25 99.5%) from Degussa with a mean particle size of 21 nm was used. Al-phosphinate Exolit OP 1240 (AlPi), a fine-grained white powder with a phosphorus content of about 23.5 %, was purchased from Clariant (Fig. 8).

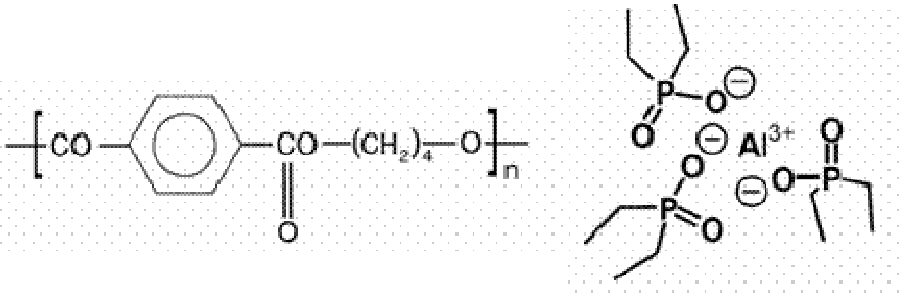

Fig. 8 PBT and Al-phosphinate flame retardant.

3.2. Melt processing

Extrusion is the process of producing and shaping specific products from raw materials by forcing material through a die under controlled conditions. Extrusion technology has been used by industry since the 18th century. However, it was not until the 1930s that the manufacturing industry attempted to significantly improve extrusion processes. Nowadays, applications of extrusion processes include the production of foodstuffs, plastics and many other manufactured goods.[69]

Melt processing technique is the most popular and economic method for thermoplastics and the composites based on them. In the present case, melt processing was carried out both in small scale using a batch mixture and in kilogram size scale using a twin-screw extruder. There are several parameters associated with melt processing technique that control the quality of the processed materials. For example, temperature, mixing time, shear rate applied (speed of screw elements), design of the mixing equipments, etc all critically control the extrudate quality of thermoplastics.

Before blending, PBT and metal oxides were dried in a vacuum oven at 363 K overnight. AlPi was used as received. The materials were prepared by melt blending using an HAAKE PolyLab Twin-Screw Extruder with 10 zones. The first zone was fed by the polymer pellets together with the nanofillers and AlPi, previously mechanically mixed. 473-508 K was the temperature profile from the feed to the die section of the extruder barrel; a screw speed of 120 rpm was used. The different formulations were prepared as showed in Table 1.

Resulting composites were water cooled, pelletized with a rotary cutter mill and dried at 333 K for two hours. Successively they were pressed at 523 K in a hot press in order to obtain a 3 mm thick plaque before being machine-sectioned.

The distribution of the nanoparticles inside the matrix was optimised changing the processing-conditions of the blends inside the extruder. The morphology of the samples was investigated by electron scanning microscope (SEM). Changing the screw speeds changes the morphology as

well. SEM micrographs of the fractured surfaces of the same PBT/AlPi/Al formulation prepared at different screw speeds are compared in Fig. 9.

Table 1 Formulations

PBT	AlPi	TiO_2	Al_2O_3	Fe_2O_3	Sb_2O_3	Sample identification
100	-	-	-	-	-	PBT
95	5	-	-	-	-	PBT/5AlPi
92	8	-	-	-	-	PBT/8AlPi
90	10	-	-	-	-	PBT/10AlPi
93	5	-	-	2	-	PBT/5AlPi/Fe
93	5	-	-	-	2	PBT/5AlPi/Sb
90	8	-	-	2	-	PBT/8AlPi/Fe
90	8	-	-	-	2	PBT/8AlPi/Sb
90	8	2		-	-	PBT/8AlPi/Ti
89	10		1	-	-	PBT/10AlPi/Al
98	-	2	-	-	-	PBT/Ti
99	-	1	-	-	-	PBT/Al
98	-	2	-	-	-	PBT/Fe
99	-	2	-	-	-	PBT/Sb

The morphology at 70 rpm is clearly characterized by uneven distribution of different agglomerates of the nano-powder that means a non homogeneous distribution of the filler inside the hosting matrix.

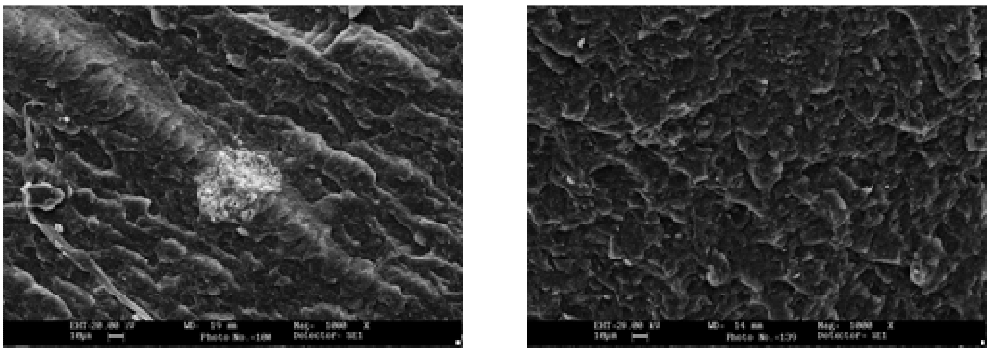

Fig. 9. SEM micrographs of cryogenic-fractured PBT/ 8AlPi/ Fe extruded at 70 rpm (left) and at 120 rpm (right).

Sample extruded at 120 rpm do not show any agglomerate formation inside the hosting matrix. For that reason, all the materials investigated in this work, been extruded at 120 rpm.

3.3. Characterizations

3.3.1. Thermal analysis

Thermal analysis of all the additives and the formulations was performed using a TGA/SDTA 851 (Mettler/Toledo, Gießen, Germany). Samples of 8 mg were heated in alumina pans from room temperature to 1175 K at a heating rate of 10 $K \cdot min^{-1}$, under a constant nitrogen flow of 30 ml min^{-1}. The apparatus-specific deviations (buoyant force) were estimated by blanck measurements.

The TG was coupled with a FTIR infrared spectrometer Nexus 470 (Nicolet Instruments, Offenbach, Germany). The purge gas flow was completely transferred to the FTIR gas analysis cell through a transfer tube. This coupling element has an inner diameter of 1 mm and connects the TG and the infrared cell. The IR-spectrometer was equipped with a DTGS KBr detector, operating with an optical resolution of 4 cm^{-1}.

3.3.2. FTIR Analysis

FTIR data were recorded over the wavenumber range 400-4000 cm^{-1} and evaluated by the characteristic absorption bands; the decomposition products were identified using reference spectra from a database. The product release rate was performed using the height of product specific pea Ks as a function of time.

The IR investigations of solid residues were recorded at room temperature using attenuated total reflection (ATR, Smart Orbit Accessory) in Nicolet 6700 FT-IR spectrometer (Thermo Scientific) with a DTGS KBr detector. The residues were collected from TG experiments (ca. 20 mg samples), cone calorimeter and LOI experiments, 32 scans were taken for a spectrum and an optical resolution of 4 cm^{-1} was used.

3.3.3. Fire Properties

The fire behaviour of all the formulations were determined by the UL94 protocol, according to IEC 60695-11-10 by the oxygen index test (LOI), according to ISO 4589 and by the cone calorimeter test.

3.3.4. Underwriters Laboratory Standard: UL94

The set of UL94 tests has been approved by the "Underwriters Laboratories" as tests of the flammability of plastic materials for parts in devices and appliances. It includes a range of flammability tests (small and large flame vertical tests, horizontal tests for bulk and foamed materials, radiant panel flame-spread test). In terms of practice and usage, the most commonly used test is UL94 V for measuring the ignitability and flame-spread of vertical bulk materials exposed to a small flame. The corresponding experimental device is shown in

Fig. 10. The burner is controlled to produce a blue flame with a 20 mm high central cone and a power of 50 W. The flame is applied to the bottom of the specimen (125 x 13 x 3 mm) and the top of the burner has to be located at 10 mm from the bottom edge of the specimen. The flame is applied for 10 s and removed. The after flame time t_1 (the time required for the flame to extinguish) is noted. After extinction, the flame is applied for another 10 s. The after flame time t_2 is noted, together with the afterglow time t_3 (the time required for the fire glow to disappear). During the application of the flame, the distance between burner and specimen must remain constant. During the test, the presence of burning drops, causing a piece of cotton located under the sample to ignite, must be noted. The standard specifies that five specimens must be tested. The specimen is classified as V0, V1 or V2 according to the criteria listed in Table 2.

Table 2 UL94 Vertical and Horizontal Test Criteria

	V-0	V-1	V-2
t_1	≤ 10 s	≤ 30 s	≤ 30 s
t_2	≤ 30 s	≤ 60 s	≤ 60 s
$\Sigma(t_1+t_2)$	≤ 50 s	≤ 250 s	≤ 250 s
Dripping	no	no	yes

The three vertical ratings V-2, V-1 and V-0 indicate that the material was tested in a vertical position and self-extinguished within a specified time after the ignition source was removed. To achieve the top rating of V-0, the bottom of a vertically mounted test strip was exposed to a flame twice, each time for 10 s duration, after which the sample must self-extinguish in less than 10 s. No flaming drips are permitted. The material tested is UL 94 V-1 classified if none of the test specimen burn for over 30 s at any time when the burner flame is removed. The V-2 rating is less stringent, some flaming drips are allowed and burn times may be up to 30 s.

In the horizontal test the material is classified as UL 94 HB if, after the removal of the flame:

a) The speed of burning does not exceed 38.1mm/minute when the test specimen thickness is 3.05-12.7 mm or

b) The speed of burning does not exceed 76.2 mm/minute when the thickness of the specimen is less than 3.05 mm or

c) Burning finishes before the flame reaches the 25.0 mm. HB rated materials are considered "self-extinguishing".

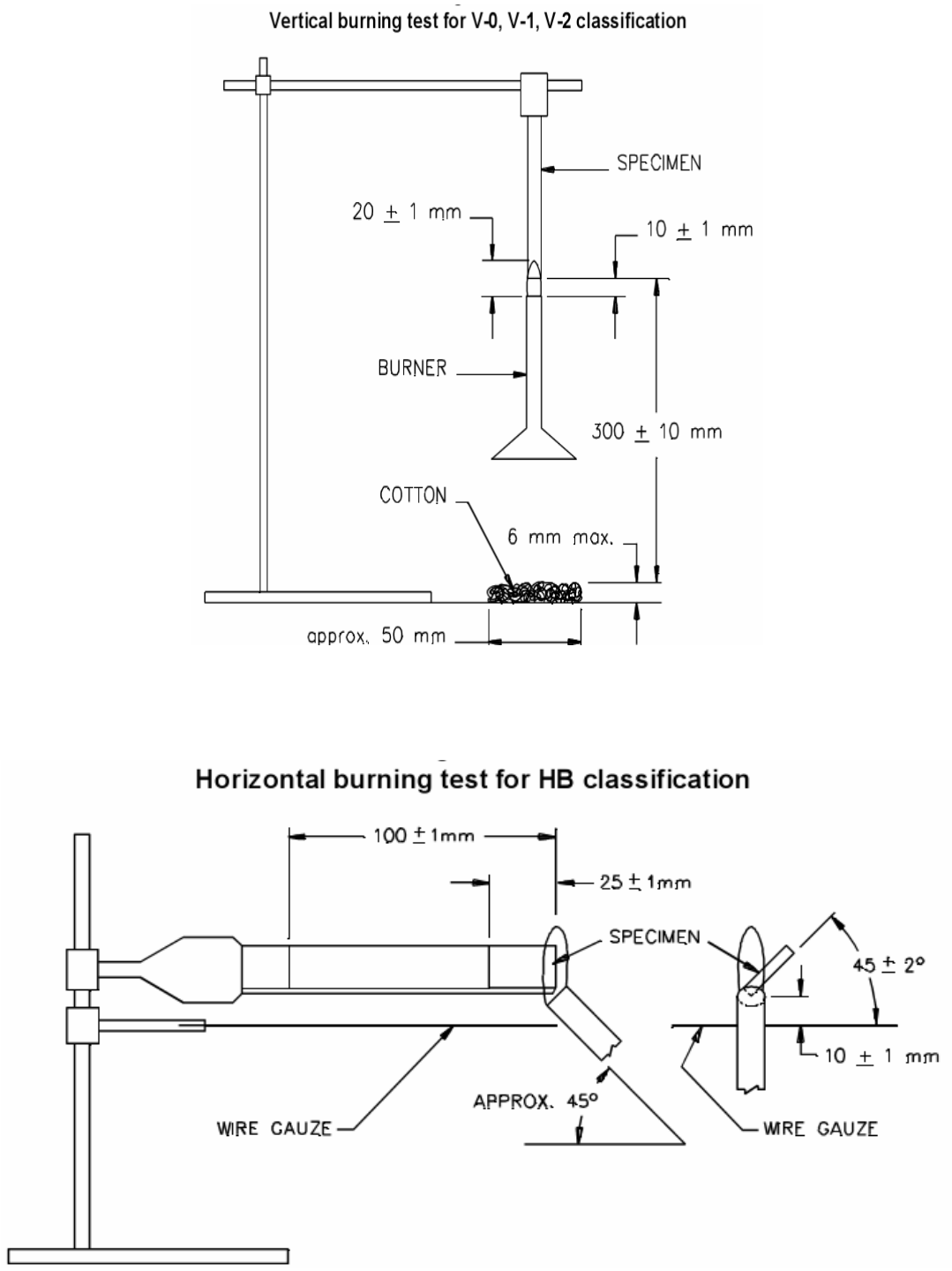

Fig. 10 Set of UL 94 test in a vertical (above) and horizontal (below) configuration.

3.3.5. LOI

Limiting Oxygen Index (LOI) is widely used for the determination of the relative flammability of polymeric materials. This test was first proposed in 1966 by Fenimore and Martin and is used to indicate the relative flammability of materials. The value of the LOI is defined as the minimal oxygen concentration in the oxygen/nitrogen mixture [O2/N2] that either maintains flame combustion of the material for 3 min or consumes a length of 5 cm of the sample, with the sample placed in a vertical position (the top of the test sample is inflamed with a burner).

The LOI is expressed as:

$$LOI = 100\frac{[O_2]}{[O_2] + [N_2]}$$

According to ISO 4589, the LOI is measured on specimens placed vertically at the centre of a glass chimney (Fig. 11). As air contains 21% oxygen, materials with an LOI below 21 are classified as "combustible" whereas those with an LOI above 21 are classified as "self-extinguishing", because their combustion cannot be sustained at ambient temperature without an external energy contribution.

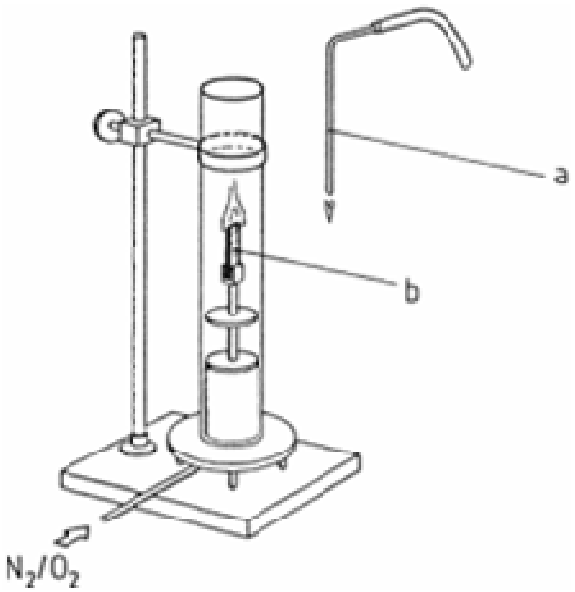

Fig. 11 LOI apparatus.

The higher the LOI the better is the flame retardant property. Although this test is nowadays considered to be relatively unsophisticated due to the development and standardization of more elaborate methods, it remains one of the most important screening and quality control methods used in the plastics industry.

3.3.6. Cone calorimeter test

Cone calorimeter (**Fig. 13**) is one of the most effective medium-sized polymer fire behaviour tests. It was developed at NIST in the 1980s [70] and is presently the most commonly used bench-scale rate of heat release apparatus based on oxygen consumption method. The cone calorimeter has been adopted as ASTM E1354, Test Method for Heat and Visible Smoke Release Rate.

The behaviour of materials in fire can be divided into three stages.

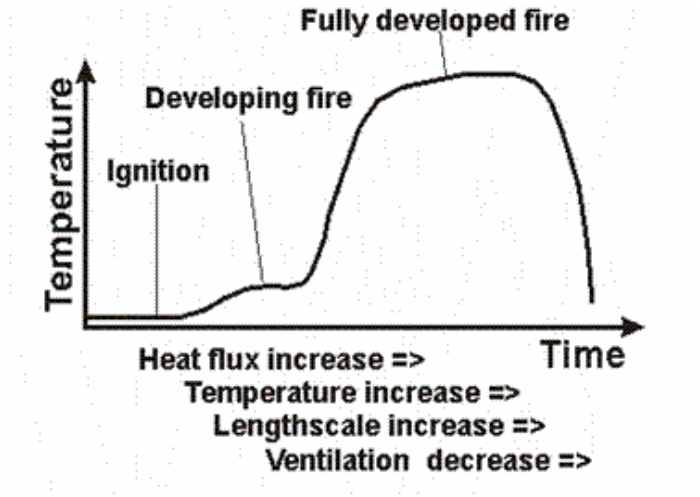

Fig. 12 Different stages of a fire during a combustion process.

1. Ignition: is the onset of flaming combustion, characterized by an ignition source (flame, cigarette, glow wire, etc.), small length scale (cm), ambient temperatures in the range of ignition temperatures (600–700 K), and high ventilation.

2. Developing fire: beginning of the combustion.

3. Fully developed fire: The penultimate stage of fire growth is characterized by a large length scales >m and low ventilation.

The principle of cone calorimeter experiments is based on the measurement of the decreasing oxygen concentration in the combustion gases of a sample subjected to a given heat flux (in general from 10 to 100 KW/m^2). The sample is placed on a load cell in order to evaluate the evolution of mass loss during the experiment. Conical radiant electrical heater uniformly irradiates the sample from above. The combustion is triggered by an electric spar K. The combustion gases produced pass through the heating cone and are captured by means of an exhaust duct system with a centrifugal fan and a hood. The gas flow, oxygen, CO and CO_2 concentrations and smoke density are measured in the exhaust duct. The measurements of the gas flow and oxygen concentration are used to calculate the quantity of heat released per unit of time and surface area: HRR (heat release rate) expressed in KW/m^2. The evolution of the HRR over time, in particular the value of its pea K/ maximum (pHRR or HRR_{max}), is usually taken into account in order to evaluate the fire properties. The calculation is based on Huggett's observation that most organic materials release a quantity of heat practically proportional to the quantity of oxygen consumed while burning. Integration of the HRR vs. time curve gives the total heat released (THR) expressed in KJ/m^2. In addition, the cone calorimeter test also enables characterization of the time to ignition (TTI), time of combustion or extinction (TOF), mass loss during combustion, quantities of CO and CO_2, and total smoke released (TSR).

Smoke has long been identified as the most significant hazard to people during fire. Smoke and the toxic gases contained in it are the primary cause of fatalities in fires. Smoke can also impair visibility and prevent escape from threatened areas. The rate of production of smoke and other products of combustion is very dependent on the fire scenario (type and configuration of material burning, flaming or non-flaming combustion, level of external heat flux) as well as the scale of the fire. In addition, the ventilation air supply and stage of the fire (pre- or post-flashover) will also significantly influence the production of smoke and other species. Smoke

production is measured by weighing the particulates collected on a filter, by determining the optical density of a quantity of smoke collected in a Known volume, or measuring the optical density as an assumed plug flow of smoke moves through an exhaust duct.

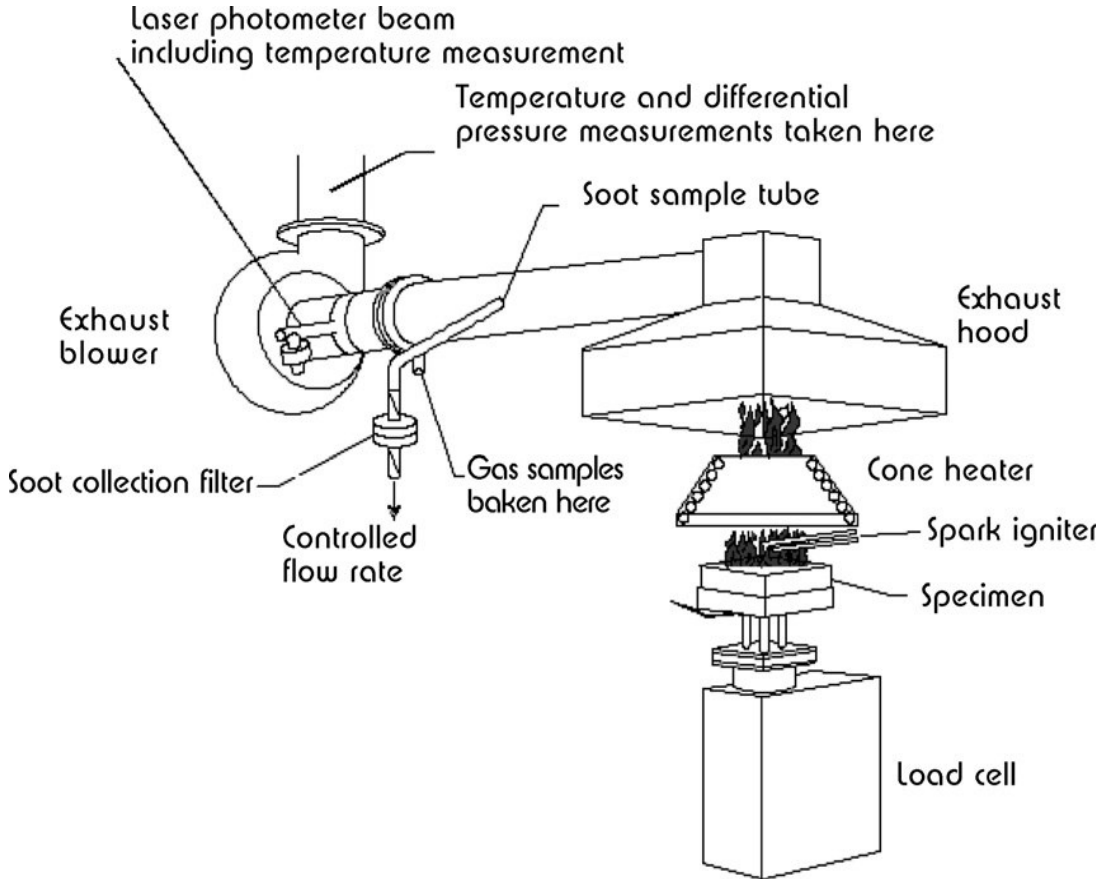

Fig. 13 Cone Calorimeter apparatus.

Typically, the smoke produced during a test is reported as a smoke yield, which is a mass of smoke per unit mass of material burned, with a higher smoke yield representing a greater flammability hazard for two reasons: (1) a higher yield implies that combustion products from a fire will produce more direct damage to life and property for each unit of material that burns and (2) a higher yield implies that there may be more soot in the flame to enhance radiant flame heat transfer, leading to higher heat release rates, more extensive flame spread, and higher burning rates. The cone calorimeter can also be used to obtain smoke obscuration data. The attenuation of light from a He-Ne laser beam passing through the exhaust

duct is measured as a function of time. An extinction coefficient is calculated from the data and used to determine a specific extinction area in the cone test methods whereas a smoke yield is calculated from a smoke generation rate in the fire propagation apparatus test methods. These equivalent quantities can be regarded as an effective material property and measure of flammability hazard.

During the cone calorimeter experiment the HRR is determined by oxygen consumption calorimetry. Different types of typical burning behaviour give rise to characteristic curves of HRR versus the time as shown in Fig. 14.[71]

(a) Thermally thick non-charring (and non-residue forming) samples show a strong initial increase after ignition up to a quasi-static HRR value, corresponding to the 'averaged or steady HRR'.

(b) For intermediate thickness non-charring samples the plateau vanishes. The averaged or steady HRR is only marked by a shoulder.

(c) Thermally thick charring (residue forming) samples show an initial increase in HRR until an efficient char layer is formed. As the char layer thickens, this results in a decrease in HRR. The maximum reached at the beginning equals both the average or steady HRR, and the PHRR.

(d) Some thermally thick charring materials, such as but not only, wood, tend to show a HRR pea K at the beginning, prior to charring, and a second HRR pea K at the end of the measurements. The second pea K may be caused by cracking char or increase in the effective pyrolysis, as observed with the thick non-charring materials.

(e) Thermally thin samples are characterized by a sharp pea K in HRR, since the whole sample is pyrolysed at the same time. In this case, the PHRR becomes dependent on their total fire load.

(f) Some samples show HRR curves characterized by a kind of unsteady development of combustion. Reasons for that can be flashing (ignition and self-extinction) before a sustained flame or during the whole measurement or deformation during burning changing the surface area and/or distance to the cone heater.

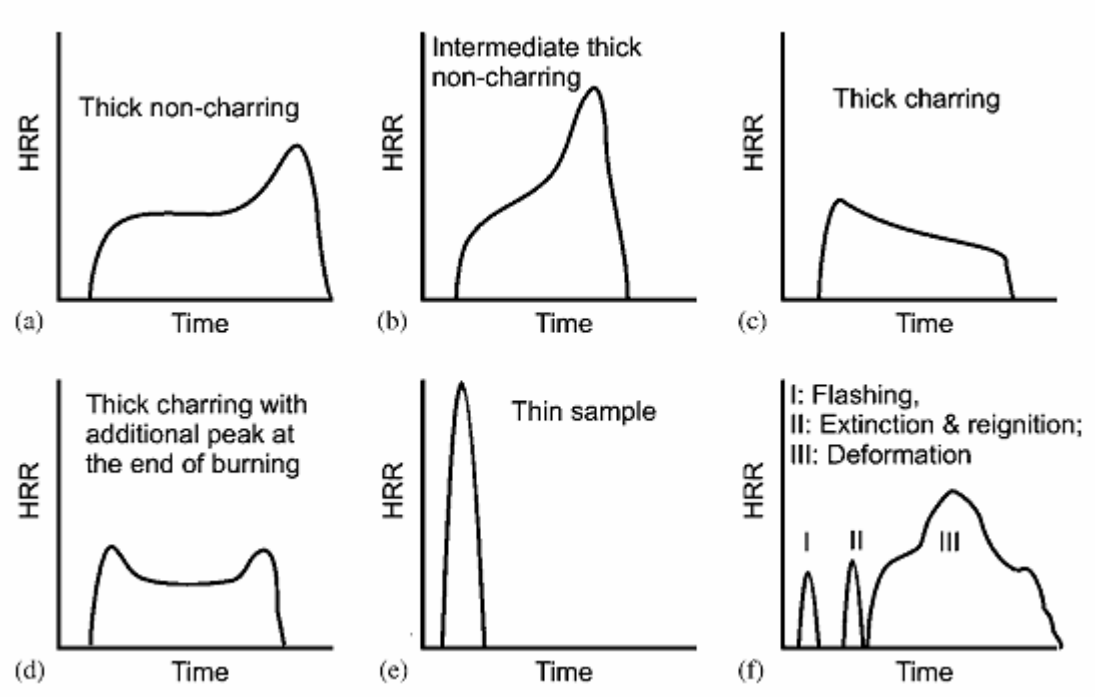

Fig. 14 Different burning behaviour with characteristic curves of HRR versus the time as shown

In this work, the determination of the fire risks (heat release rate, HHR, total heat release, THR and time to ignition, t_{ign}) and the fire hazards (rate of smoke release and CO release) were determined by the cone calorimeter test (Fire Test Technology, East Grinstead, U K), according to ISO 5660. All the samples were preconditioned for 24 h at 23°C and 50% relative humidity. Specimen sheets (100 mm x 100mm x 3.0 mm) were placed in an aluminium tray and exposed to an external heat flux of 50 KWm^{-2}. A spar K ignition was used. For the determination of the flame out, the extinction of the yellow flame was considered. All measurements were repeated: the cone results, reported in the tables, correspond to mean values obtained from two or three experiments. Residue analysis was conducted using attenuated total reflection (ATR, Smart Orbit Accessory) in Nicolet 6700 FT-IR spectrometer (Thermo Scientific) with a DTGS KBr detector.

3.4. Rheological Analysis

3.4.1. Introduction

Rheological analysis of polymeric melts involves the study of the mechanical response of the melt under the action of external mechanical stress or strain. In case of filled polymeric systems, rheological behaviour can be drastically different from that of the unfilled melts, depending on the nature of filler particles (structure, size, shape, surface characteristics, etc.) and the state of their dispersion in the polymer matrix.[72] In fact, rheological analysis is an important tool to investigate the state of filler particle dispersion in filled systems and their response under external force. Though an indirect method, rheological analysis can be treated as a complementary to the direct methods for morphological analysis, like XRD and electron microscopy, which altogether provide a complete picture of the state of filler particle dispersion in polymer matrix. The major advantages of rheological analysis are that it reflects the bulk properties of the matrix and also provides flow behaviour of the melt that are often useful in deciding the optimum processing conditions required for the melt processing of polymer composites.

Polymeric melts are viscoelastic systems and their response to shearing depends on the ratio between the time scales of shear experiments and the characteristic relaxation time of microstructures present within such systems. The term microstructure means molecular entanglements in a high molecular weight unfilled melt. Principally, such microstructures signify structural feature that acts as a physical barrier against flowability of the polymer chains under stress. When the experimental time scale is far below the characteristic relaxation time, the microstructure (experienced at high frequencies or shear rates) shows preferably elastic response characterized by high value of storage modulus. Whereas, at large experimental time scale (experienced at low frequencies or shear rates), the system shows viscous response. Again, shearing actions, if sufficiently high, can change and even destroy these microstructures resulting in an entirely different material response compared to that observed when shearing does

not affect the microstructures. From the scientific point of view, investigations in both these regions are important as they highlight the different mechanism of material's response toward external stress. The polymeric melts are characterized by a critical strain below which stress bears linear relationship with the applied strain and their ratio (Known as relaxation modulus) shows a constant value independent of strain. Thus, the rheological behaviour of polymeric melts below this critical strain is a linear viscoelastic one. Above the critical strain, due to changes in the microstructures, the relaxation modulus decreases with strain and the stress becomes a non-linear function of strain resulting in a non-linear viscoelastic material response. Therefore, the primary task before carrying intensive rheological analysis is to determine the transition point between linear and non-linear viscoelastic regime. One simple way to determine this critical strain or a range about it is to subject the polymeric melt to dynamic oscillatory shear using sinusoidal strain at constant frequency and varying strain amplitude. The strain input functions looks like:

$$\gamma(t) = \gamma_0 \sin(\omega t)$$

where oscillatory strain γ(t) is applied at constant frequency ω with varying strain amplitude γ_0. The storage modulus, G', is then monitored against strain amplitude. In the log G' versus log γ plot, the transition from linear to non-linear regime is indicated by the change of the storage modulus from low strain plateau value to strain dependent values.[73]

3.4.2. Relation between viscoelastic and flammability properties

The effect of nanoscale fillers on the mechanical properties of polymers has been extensively studied,[74] with special attention to the mechanical reinforcement that is afforded when nanoparticles are added to polymers. The cumulative knowledge in this field points to two primary mechanisms responsible for mechanical reinforcement. The first mechanism, which is essentially particle-driven, occurs at relatively high particle volume fraction, beyond the particle percolation threshold, and may

be referred to as “jamming”. The second, termed the “network reinforcement” mechanism, occurs due to the formation of a long-lived percolating polymer network within the particles as the “network nodes”.

Recent experiments on pure entangled polymer melts, polymers filled within platelet fillers and spherical nanoparticles show that, regardless of reinforcing mechanism, the start-up of shear flow is accompanied by stress overshoots. After a certain time, which appears to be related to the “aging” time of the system and the applied strain rate, the stress recovers to a well-defined plateau value. The viscosities derived from these long term stress plateaus suggest that these materials shear thin over the whole range of accessible frequencies. Both of these results have been empirically attributed to network structures which exist in the quiescent state, but which are disrupted on the application of shear.

In the previous chapters, nanoparticle fillers were presented as an attractive method to reduce polymer flammability. The burning process of a polymeric material typically begins with heating to a temperature at which thermal degradation initiates. The boiling temperatures of most of the thermal degradation products of polymers are much higher than the thermal degradation temperatures of thermoplastic, and the degradation products are then superheated and nucleated to form bubbles. These bubbles are formed at and below the heated surface, where thermal degradation occurs, and they grow with the supply of more degradation products by diffusion from the surrounding molten plastic. The bubbles burst at the heated surface evolving their contents into the gas phase as a fuel vapour. One flame retardant approach is to suppress the bubbling rates, so as to reduce the supply rate of fuel by forming a protective and heat shielding char layer. This approach, of forming a solid jammed network structure, has been demonstrated with carbon nanotubes[75]: they form a jammed network structure into the polymer matrix, such that the material as whole behaves rheologically like a gel.

The rheological analysis for the present thesis work was carried out in ARES rheometer using the parallel plate geometry of the sample holding unit. Both dynamic oscillatory and steady shear experiments were

performed. The instrument was used under shear strain controlled mode. The general outlook of the instrument and the sample holding unit are shown in Fig. A1. The sample holding unit in the rheometer chamber consists of two similar plates of radius R fitted parallel in vertical position. The lower plate is connected to a motor via a cylindrical shaft and the upper plate is connoted to a torque-balance transducer. The lower plate is driven by the motor and rotates about its axis maintaining a constant separation with the upper plate during experiment. The upper plate remains fixed, but the transducer connected to it measures the torque experienced by it. The transducer works according to torque-balance principle. This means during experiment, when the sample melt within the parallel plate is sheared by the rotating lower plate, the melt also exerts a force on the upper plate. But, to Keep the upper plate in zero position the transducer applies a torque on the upper plate, which balances the force exerted by the sample. During both steady and dynamic measurement, the motor applies angular displacement to the upper plate.

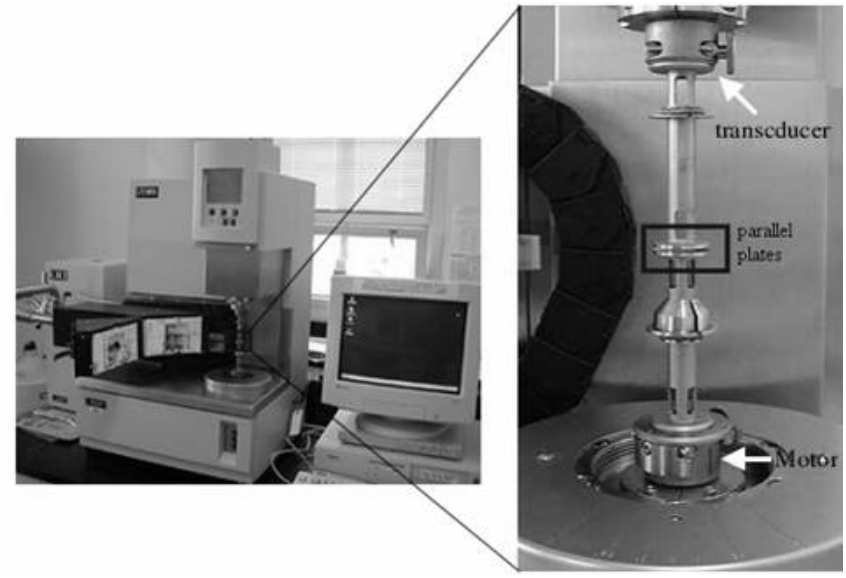

Fig. A1 Rheomether with parallel plate geometry

In case of dynamic oscillatory measurements, rheological responses are interpreted in terms of parameters, like storage modulus (G'), loss modulus (G") and loss tangent (tanδ).

CHAPTER 4
RESULTS AND DISCUSSION

4.1. Pyrolysis: Mass Loss

4.1.1. PBT

The decomposition of PBT is characterised by a single step degradation, in a temperature range between 625 K and 700 K, a maximal mass loss rate at 653 K. It loses about 99 wt% of its mass, leaving only a negligible amount of solid residue at 1000 K. The main decomposition step of PBT is characterised by a DTG maximum at about 653 K.

4.1.2. PBT/AlPi formulations

The TG results for the different formulations under nitrogen are summarised in Table 3, for a heating rate of 10 $Kmin^{-1}$. In Fig. 15, the thermal decompositions of all PBT/AlPi formulations were compared. The combination of AlPi in PBT does not essentially change the decomposition temperature and the decomposition rate of the main decomposition process.

All PBT/AlPi formulations present a main mass loss step (DTG maximum between 651-655 K) and an additional small decomposition steps (between 1-3 wt%) that appears in the DTG signal as a broad shoulder at

682 K (see Table 3). As shown in Fig. 15, the addition of AlPi results in a slight shift in the onset temperature in the DTG curve (T5%) and in the end temperature (T85%) of the decomposition (ΔT= 8-10 K), depending on the amount of AlPi. In comparison to PBT, an additional amount of residue, corresponding roughly to the initial AlPi content, is found. The addition of 5 wt% of AlPi in PBT/5AlPi causes an increase in the inorganic char residue of about 3.3 wt%, in PBT/8AlPi 5.3 wt% and in PBT/5AlPi only 3.3 wt%.

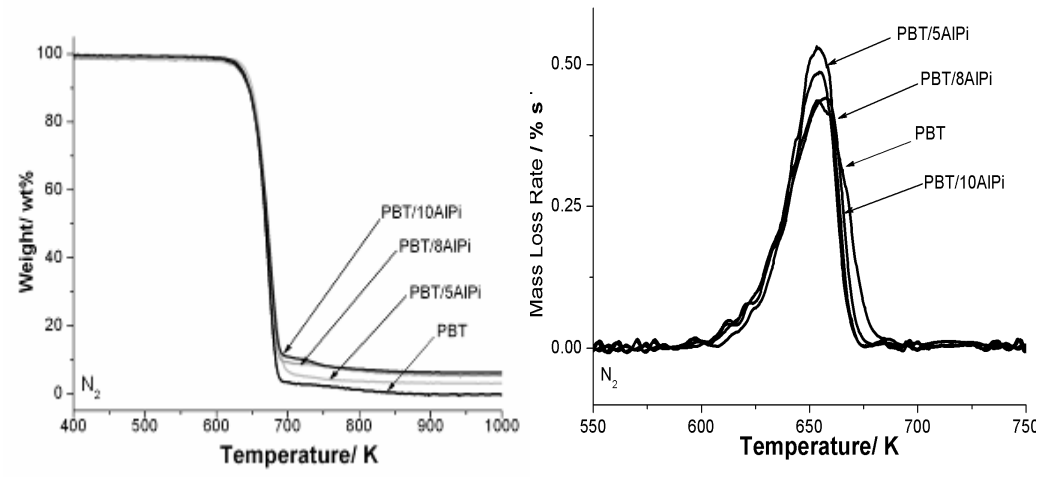

Fig. 15 TG and Mass Loss Rate (MLR) curves of all the formulations containing AlPi (heating rate 10 K·min^{-1}, N_2 atmosphere).

Table 3 Table Thermal decomposition of all the formulations containing different percentage of AlPi (10 Kmin-1, 8 mg, error ±1 wt.-%, ±2 K).

		1st Stage		2nd Stage		
	$T_{2\%}$	Mass Loss	T_{DTG} max	Mass Loss	T_{DTG} max	$Residue_{1000K}$
	K	wt.%	K	wt.%	K	wt.%
PBT	638	99.9	653			/
PBT/5AlPi	644	95.5	651	1.2	682	3.3
PBT/ 8AlPi	637	93.7	653	3.3	682	5.3
PBT/ 10AlPi	641	88.0	655	3.1	682	9.5

4.1.3. PBT/AlPi/TiO_2 formulations

TiO_2 in combination with PBT shows a similar one-step decomposition occurring at 655 K in the DTG maximum (Fig. 16). The addition of only 2

wt% of TiO_2 to PBT leaves a residual weight of 13.6 wt% in comparison with PBT, clearly higher than predicted. With the addition of TiO_2 in PBT/8AlPi/Ti a slightly decreased of the starting decomposition temperature ($T_{2\%}$) to 630 K is observed (Table 4) and only 11.7 wt% of residue is found.

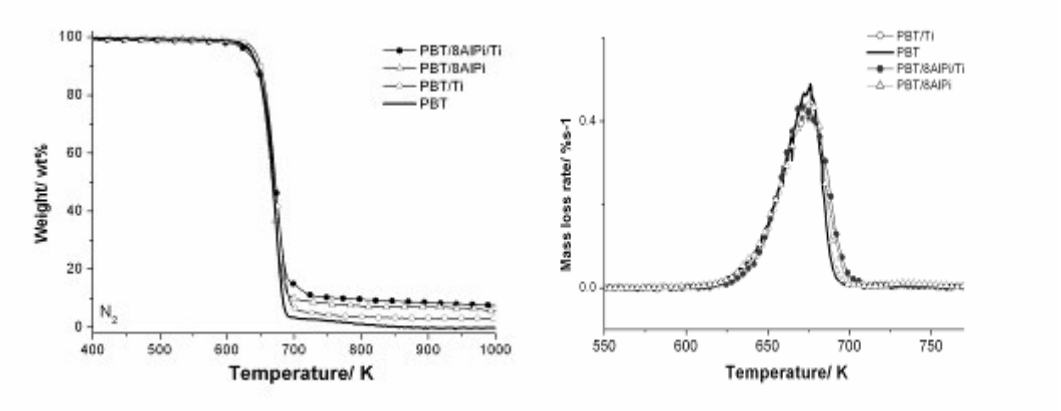

Fig. 16 TG and Mass Loss Rate (MLR) curves of PBT/AlPi/TiO_2 formulations (heating rate 10 K·min^{-1}, N2 atmosphere).

Table 4 Thermal decomposition of all the formulations containing TiO_2 (10 Kmin^{-1}, 8 mg, error ±1 wt.-%, ± 2 K).

		1st Stage		2nd Stage		
	$T_{2\%}$	Mass Loss	T_{DTG} max	Mass Loss	T_{DTG} max	$Residue_{1000K}$
	K	wt.%	K	wt.%	K	wt.%
PBT	638	99.9	653			/
PBT/8AlPi	636	93.7	653	3.3	685	5.3
PBT/ TiO2	638	85.1	655			13.6
PBT/ 8AlPi/ TiO2	630	86	654	3.7	756	11.7

The higher residue amount found indicates an interaction between the polymer and the metal-oxide resulting in an increasing stability of the char.[76] The combination of AlPi and metal oxides damps down this effect (antagonism). Each additive, TiO_2 and AlPi, produces positive effects if used separately but when they are added together the effect is less than expected.[77]

4.1.4. PBT/AlPi/Al_2O_3 formulations

Besides the main decomposition step at about 638 K in PBT/10AlPi curves, in the DTG curve, a small additional shoulder is detected in PBT/10AlPi/Al.

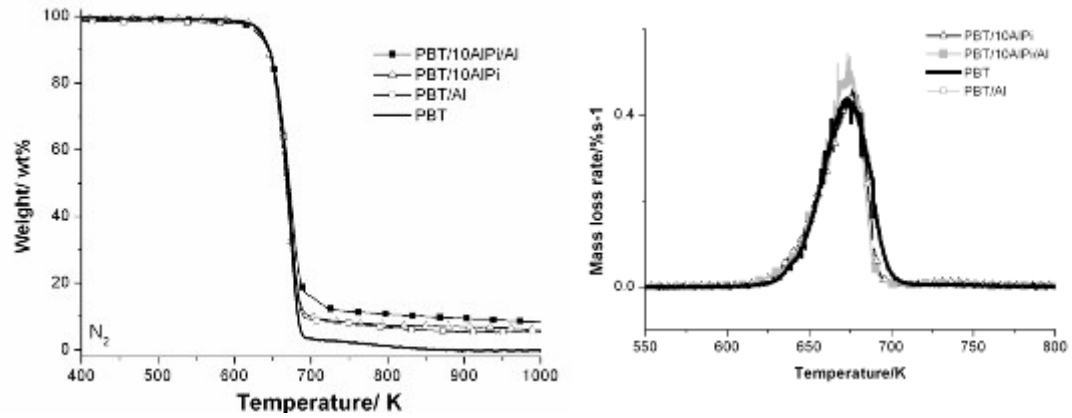

Fig. 17 TG and Mass Loss Rate (MLR) curves of PBT/AlPi/ Al_2O_3 formulations (heating rate 10 K·min^{-1}, N2 atmosphere).

Table 5 Thermal decomposition of all the formulations containing Al_2O_3 (10 Kmin^{-1}, 8 mg, error ±1 wt.-%, ± 2 K).

		1st Stage		2nd Stage		
	$T_{2\%}$	Mass Loss	T_{DTG} max	Mass Loss	T_{DTG} max	$Residue_{1000K}$
	K	wt.%	K	wt.%	K	wt.%
PBT	638	99.9	653			/
PBT/10AlPi	631	88	655	3.1	735	9.5
PBT/ Al	639	89.2	650			10.7
PBT/10AlPi/ Al	633	89.5	653	2.1	724	9.8

In comparison to PBT/10AlPi (Fig. 17), the temperature of this second decomposition step is shifted to lower temperature, from 735 K to 724 K (Table 5). The addition of only 1 wt% of Al_2O_3 in PBT/Al leaves an additional amount of residue at the end of the decomposition of about 10.7 wt%. This effect is damping down in the combination P BT/AlPi/Al, which leaves only 9.8 wt% of solid residue. Again, the positive effect due to the single additives

in increasing the amount of solid residue is reduced when they are added together.

4.1.5. PBT/AlPi/Fe_2O_3 formulations

The addition of Fe_2O_3 in PBT does not lead to any significant change in the TG and DTG curves (Fig. 18). The addition of Fe_2O_3 in PBT/Fe slightly increases the starting decomposition temperature ($T_{2\%}$) up to 640 K. The decomposition temperature of the maximal mass loss (DTG_{max}) is increased by adding Fe_2O_3 to PBT. As observed for the other PBT/AlPi formulations, an additional small decomposition process is observed at 685 K for PBT/5AlPi/Fe and at 688 K for PBT/8AlPi/Fe, slightly shifted to higher temperatures in comparison to the correspondent PBT/AlPi without metal oxide. 2 wt% of iron oxide in PBT leave 7.3 wt% of solid residue. In both the formulations containing AlPi and Fe_2O_3, the amount of solid char at the end of decomposition is clearly less than the sum of the effects of the additives alone.

Table 6 Thermal decomposition of all the formulations containing Fe_2O_3 (10 Kmin^{-1}, 8 mg, error ±1 wt.-%, ± 2 K).

		1st Stage		2nd Stage		
	$T_{2\%}$	Mass Loss	T_{DTG} max	Mass Loss	T_{DTG} max	$Residue_{1000K}$
	K	wt.%	K	wt.%	K	wt.%
PBT	638	99.9	653			/
PBT/5AlPi	644	95.5	651	1.2	682	3.3
PBT/8AlPi	636	87.3	653	3.3	682	5.3
PBT/ Fe	640	92.7	667			7.3
PBT/5AlPi/ Fe	638	87.8	654	3.3	685	8.9
PBT/8AlPi/ Fe	633	87.3	659	3	688	9.7

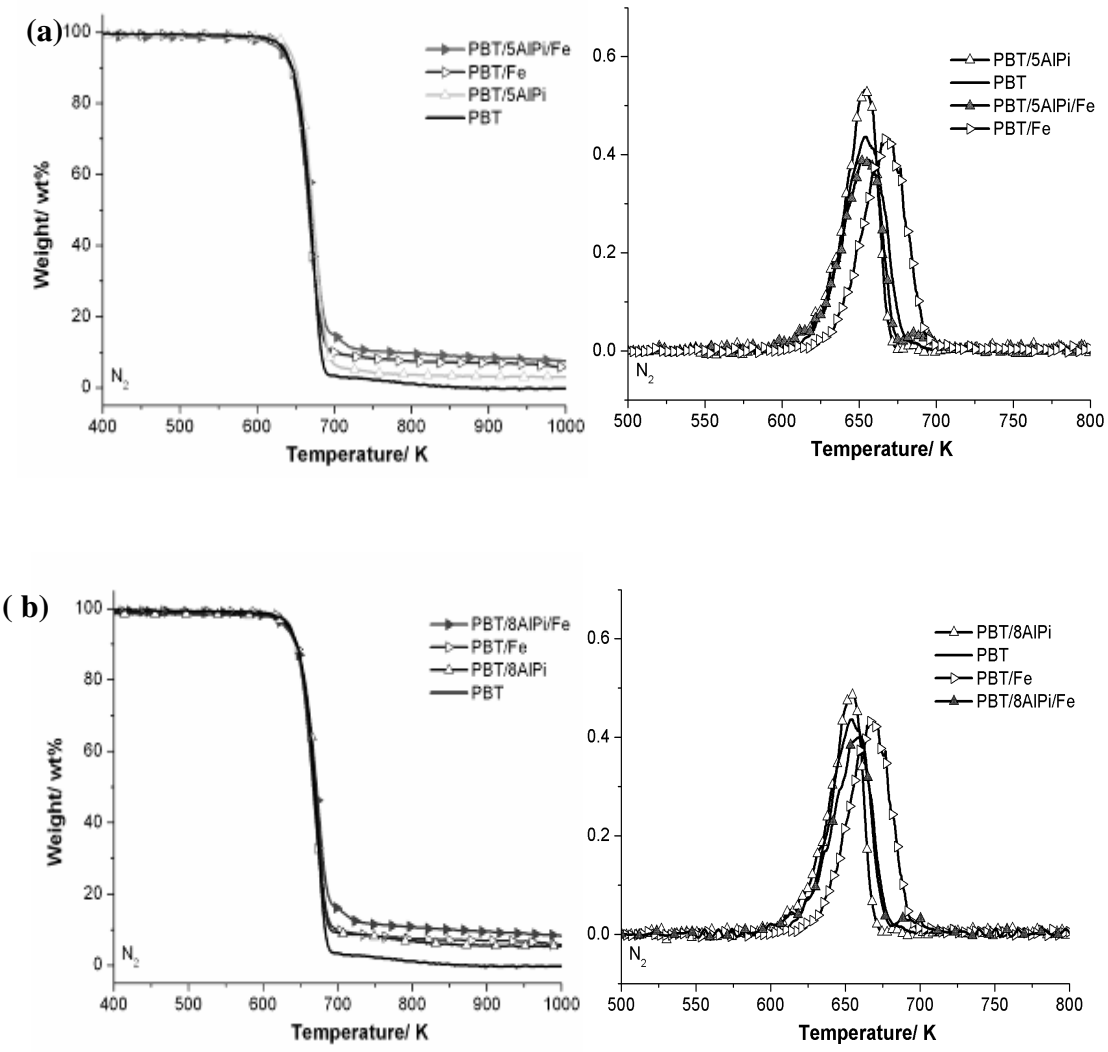

Fig. 18 TG and Mass Loss Rate (MLR) curves of PBT/AlPi/Fe_2O_3 formulations (heating rate 10 K·min^{-1}, N2 atmosphere).

4.1.6. PBT/AlPi/ Sb_2O_3 formulations

The thermal behaviour of all Sb_2O_3 formulations is shown in Fig. 19. The comparison between al the materials (Table 7) shows that Sb_2O_3 is not as efficient as the other investigated metal oxides in increasing the amount of residue at the end of decomposition. This is related to the main gas phase action of this additive. 2 wt% of Sb_2O_3 in PBT/Sb only leaves 1.3 wt% of solid residue. The comparison between PBT/5AlPi/Sb and PBT/5AlPi shows

that the amount of char at the end corresponds roughly to the same amount due to the AlPi.

Table 7 Thermal decomposition of all the formulations containing Sb_2O_3 (10 Kmin^{-1}, 8 mg, error ±1 wt.-%, ± 2 K).

		1st Stage		2nd Stage		
	$T_{2\%}$	Mass Loss	T_{DTG} max	Mass Loss	T_{DTG} max	$Residue_{1000K}$
	K	wt.%	K	wt.%	K	wt.%
PBT	638	99.9	653			/
PBT/5AlPi	644	95.5	651	1.2	682	3.3
PBT/8AlPi	636	87.3	653	3.3	682	5.3
PBT/ Sb2O3	642	98.3	655			1.3
PBT/5AlPi/ Sb2O3	638	87.8	660	2.3	685	5.1
PBT/8AlPi/ Sb2O3	634	87.3	663	2.8	685	6.1

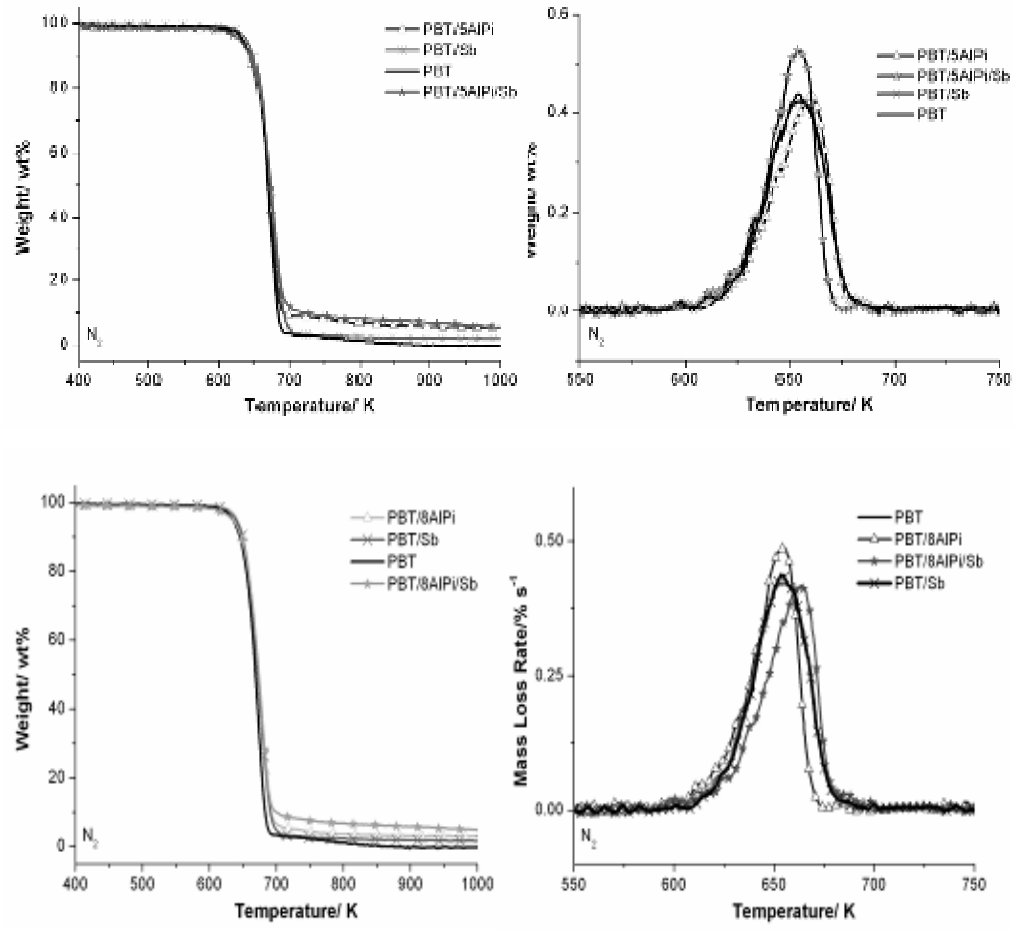

Fig. 19 TG and Mass Loss Rate (MLR) curves of PBT/AlPi/Sb_2O_3 formulations (heating rate 10 K·min^{-1}, N2 atmosphere.

4.1.7. Pyrolysis Conclusions

No significant changes in the thermogravimetry results have been found. The addition of AlPi, TiO_2, Al_2O_3, Fe_2O_3 and Sb_2O_3 did not fundamentally change the decomposition temperature and the decomposition rate of the main decomposition process.

The addition of AlPi in PBT produces an increase in the char yield that roughly corresponds to the initial content of flame retardant.

When metal oxides nanoparticles are added to PBT, a higher residue amount is found, indicating an interaction between the polymer and the metal-oxide and resulting in an increasing stability of the char. The amount of char decreases in the order TiO_2 > Al_2O_3> Fe_2O_3 >Sb_2O_3.

In combination with AlPi the positive effect due to the metal oxides is damped by a pronounced antagonism: each additive produced a positive effect on residue yield when used separately, but in the combination of both additives, the effect was clearly less than is expected for a corresponding superposition.

4.2. Pyrolysis: volatile decomposition products

4.2.1. PBT

All the main decomposition bands in the gas phase spectra are assigned and summarized in Table 8. The evolved gas analysis for PBT exhibited characteristic bands of butadiene (905 cm^{-1}), CO_2 (2354 and 669 cm^{-1}) and tetrahydrofuran, THF (2980 cm^{-1}) in the first stage of decomposition. During the maximum pea K of decomposition (38 min), benzoic acid (3580 cm^{-1}) and esters (1265 cm^{-1}) are released. All decomposition products are in accordance with data reported in literature. The main evolved gases are shown in Fig. 20. Due to its high sublimation point (675 K), terephthalic acid condenses into the heated transfer line preventing its detection in the gas phase. Volatilization of CO, as well as more complex aromatic species, is observed during the latter stages of

polymer decomposition (50 min). Ethene release is also detected with a characteristic sharp band at 950 cm^{-1}.

Table 8 Assignment of IR absorption bands

Band position (cm^{-1})	Assignment
905	butadiene
1737, 1265, 1100	esters
3580, 1760, 1177	benzoic acid
2354, 669	CO_2
2980, 1083	THF
672	benzene
950	ethene
3650, 855, 773	diethylphosphinic aci

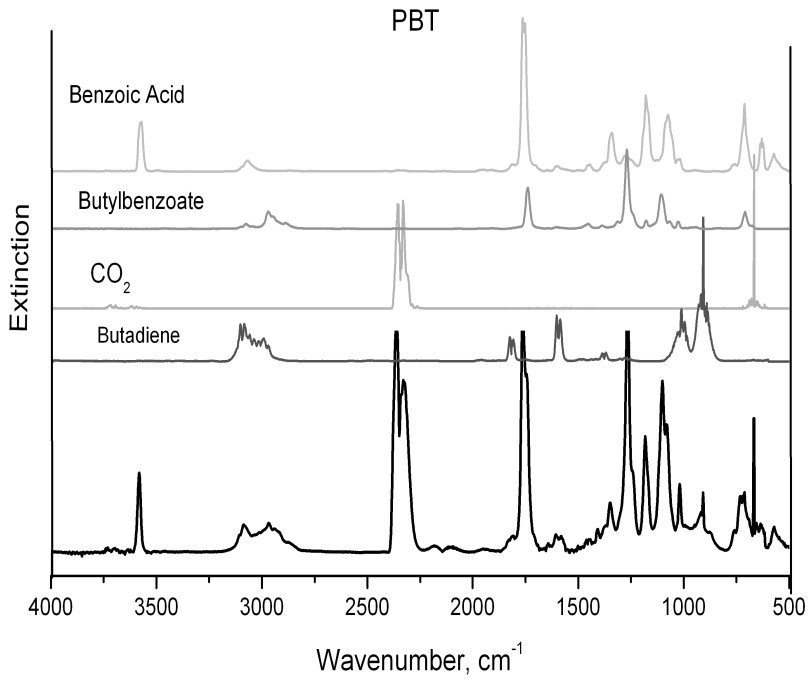

Fig. 20 Evolved gas for PBT during the main decomposition step.

The signal at 670 cm^{-1} is attributed to carbon dioxide but can also be derived from benzene. Benzene has a very intensive band at 672 cm^{-1}.[78] This involves that determination of benzene is not easy by means of FTIR when also CO_2 is released. The comparison between the products release rate of

the characteristic CO_2 signals at 2354 cm^{-1} and 669 cm^{-1}, is a helpful tool to predict if there is additional benzene release to the gas phase. When both signals are in agreement with each other no benzene is released. If the product release rate of both CO_2 signals shows a different behaviour then, during the second mass loss, additional benzene is released. In PBT, the aromatic species such as benzene are detected only at trace levels.

4.2.2. PBT/AlPi

For formulations containing AlPi, the main decomposition products do not change in comparison to PBT. As shown in Fig. 21a, CO_2, butadiene and THF are still detected in the first stage of decomposition. After 38 min (Fig. 21b) benzoic acid and esters were released. Due to the presence of AlPi, additional diethylphosphinic acid was detected during the maximum pea K of decomposition by the characteristic bands at 3650 cm^{-1} (PO-H), 855 cm^{-1} and 773 cm^{-1} (P-O). In the latter part of decomposition (Fig. 21c) benzene, ethene and CO were released.

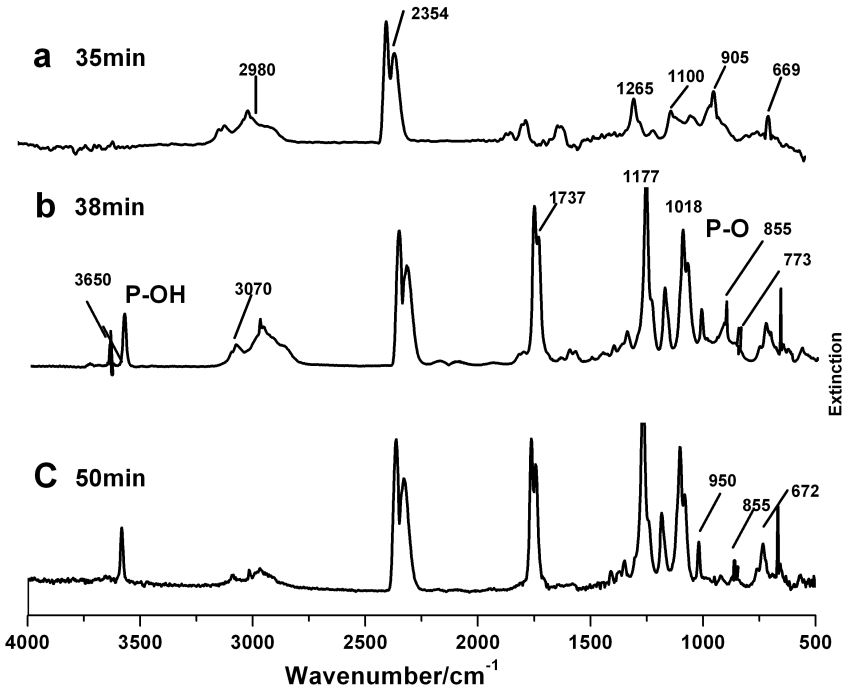

Fig. 21 Identification products of PBT/8AlPi formulation during different stages of decomposition.

The evolved gas release rate analysis for PBT/8AlPi is reported in Fig. as an example. As confirmed by the gas phase spectra, butadiene and CO_2 occurred at the beginning of the decomposition. Unlike PBT, that shows only one pea K in the CO_2 release rate, for all the materials containing AlPi, two maximum in the CO_2 release rate occur, the first one is related to the main mass loss step (38 min) while the second one (43 min) corresponds to the small second decomposition step found in TG curve. This second max in the CO_2 release occurs after the main mass loss of polymer. THF is produced by the hydrolytic ad thermal scission of polyester bonds. The products containing acid and esters dominated the products during the maximum of mass loss rate. Simultaneously diethylphosphinic acid was released. During the second decomposition process ethene and benzene was produced and an increase in CO_2 release was observed.

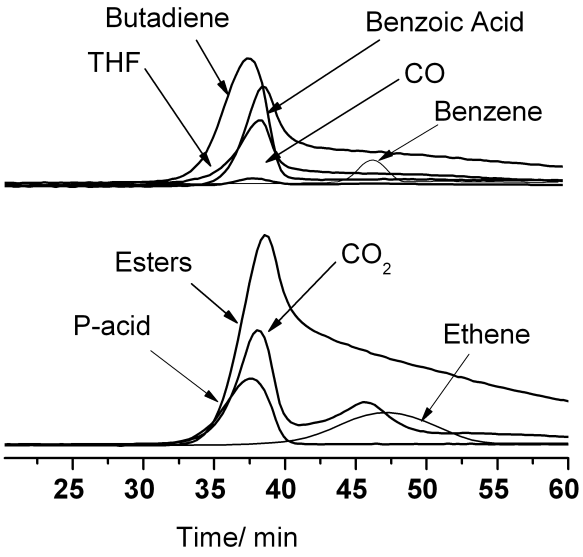

Fig. 22 Release rate analysis for PBT/8AlPi formulation.

The comparison between the FTIR analyses of the different evolved gas release rates is helpful to understand the different decomposition routes among all the materials. In Fig. 23(a) the amount of P-acid released in the different AlPi formulations is shown. With the increasing initial loading of AlPi, the P-acid release increases in the order PBT/10AlPi > PBT/8AlPi>

PBT/5AlPi. In all the AlPi formulations, aromatics functionalities are detected at a higher amount in respect to PBT: the product release rate of the two characteristic signals of CO_2 deviates from each other. The amount of aromatics is related to the initial loading of AlPi, as shown in Fig. 23(b).

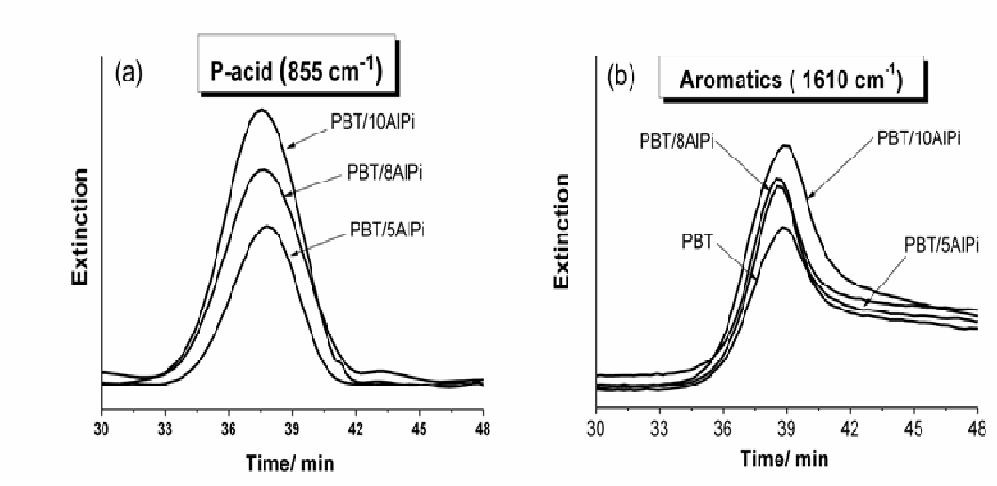

Fig. 23 Products release rates of P-acid and aromatics measured by FTIR for AlPi formulations.

4.2.3. PBT/AlPi/TiO_2 formulations

The pyrolysis of TiO_2 nanocomposites essentially results in the formation of the same products as the pyrolysis of PBT does. No change in the evolved products in the gas phase is detected when TiO_2 is added to PBT/Ti but there is a clear influence on the product release rate. As PBT, also PBT/Ti shows only one pea K in the CO_2 release rate but slightly shifted to later time (39min). PBT/8AlPi/Ti exhibits two pea Ks in the CO_2 release rate (Fig. 24), one corresponding to the main mass loss of the polymer and the second one related to AlPi decomposition. In comparison to PBT/8AlPi (43 min), the second pea K in PBT/8AlPi/Ti occurs at later time (45 min) due to the interaction of the phosphinate anion with TiO_2. The presence of the metal oxide also influences the release of volatiles like butadiene, aromatics and P-acid. As shown in Fig. 24b, the release of butadiene slightly

decreases in PBT/Ti but essentially does not change in all the other formulations.

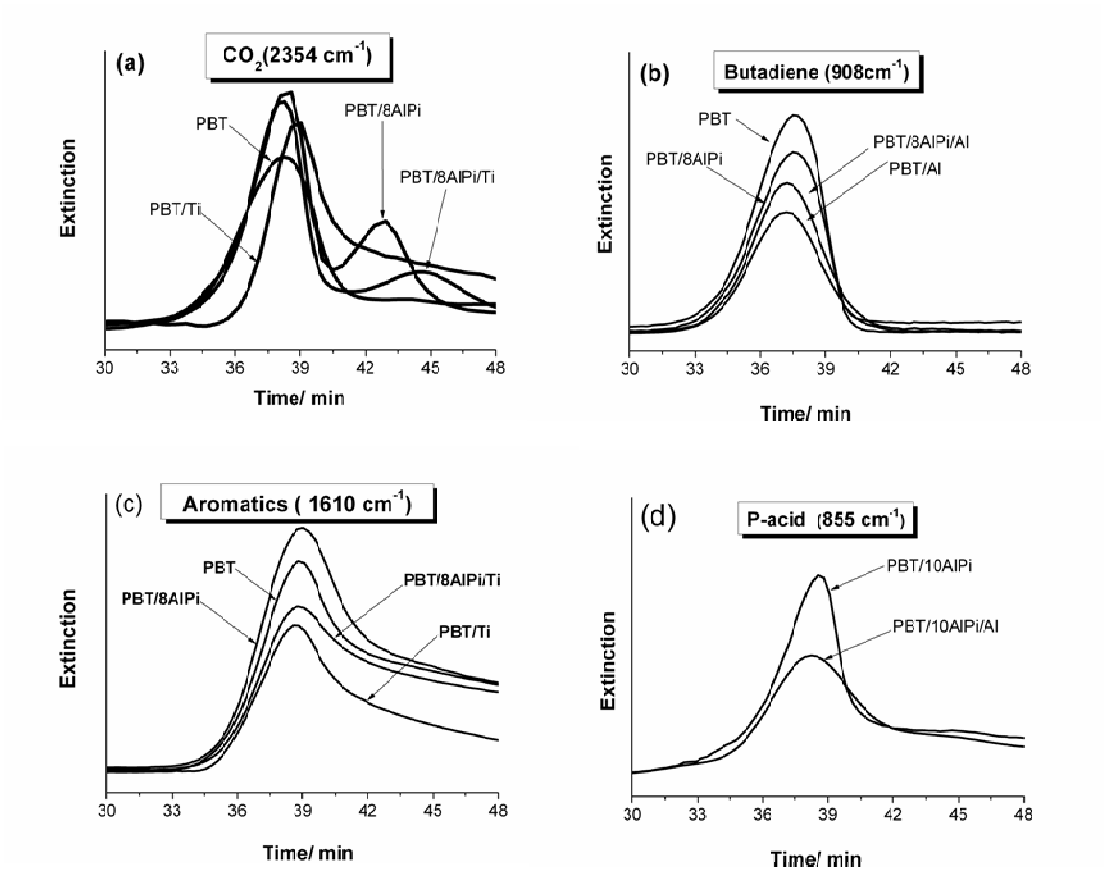

Fig. 24 Products release rates measured by FTIR for TiO_2 formulations.

Aromatic release rate (Fig. 24c) clearly shows a decrease when TiO_2 is added in PBT/Ti but this effect is damped down in the combination with AlPi, as PBT/8AlPi shows a higher amount of benzene released in the gas phase. The comparison between the P-acid release in the gas phase in the presence of TIO_2 shows that nanoparticles of metal oxide are able to prevent the release of P-moieties in the gas phase. In other words, part of the P is retained in the solid phase (Fig. 24d).

4.2.4. PBT/AlPi/ Al_2O_3 formulations

As the addition of Al_2O_3 to PBT does not essentially change the evolved products in the gas phase, the FTIR spectra will not be presented. Only the differences in the product release rate are shown. The CO_2 release rate

(Fig.25a) exhibits only one pea K centred at 38 min for PBT/Al, while the combination with AlPi in PBT/10AlPi/Al shows two peaks, one with a maximum at 38 min and the second one with a maximum at about 43 min.

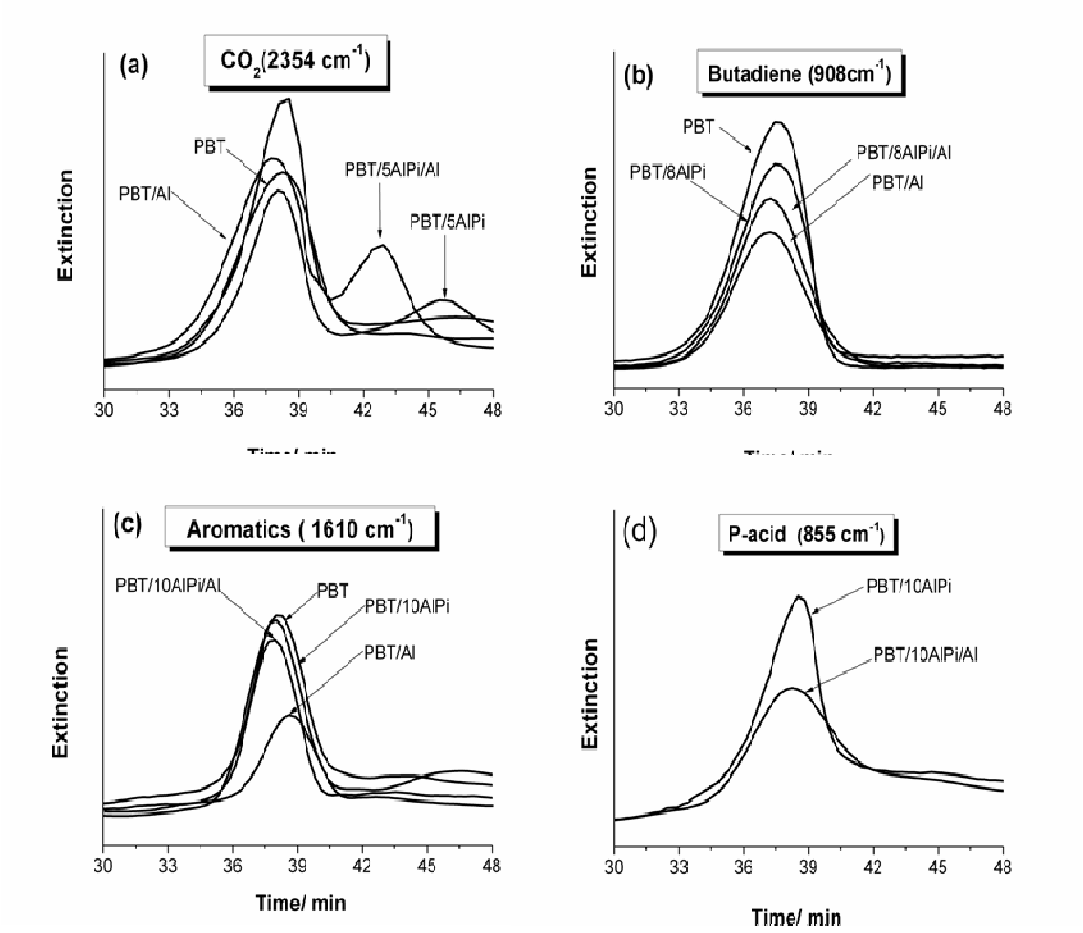

Fig. 25 Products release rate of Al_2O_3 formulations during decomposition between 600- 750 K.

The release of small volatile fragments like butadiene shows that Al_2O_3 is efficient in decreasing the amount of volatiles in comparison to PBT and also delays the volatilization process. Also PBT/10AlPi and PBT/10AlPi/Al exhibit the same effect but with a lower decrease (Fig.25b). In Fig. 25c the release of butadiene is presented. Again, in the presence of metal oxide, the amount of benzene released to the gas phase is clearly lower in comparison to all the other formulations. The metal oxide promotes the retention of aromatic functionalities in the solid phase. The formation of P-acid during combustion seems to be inhibited when the metal oxide is

present: in comparison to PBT/10AlPi, PBT/10AlPi/Al shows a lower production of P-acid (Fig.25d).

4.2.5. PBT/AlPi/ Fe_2O_3 formulations

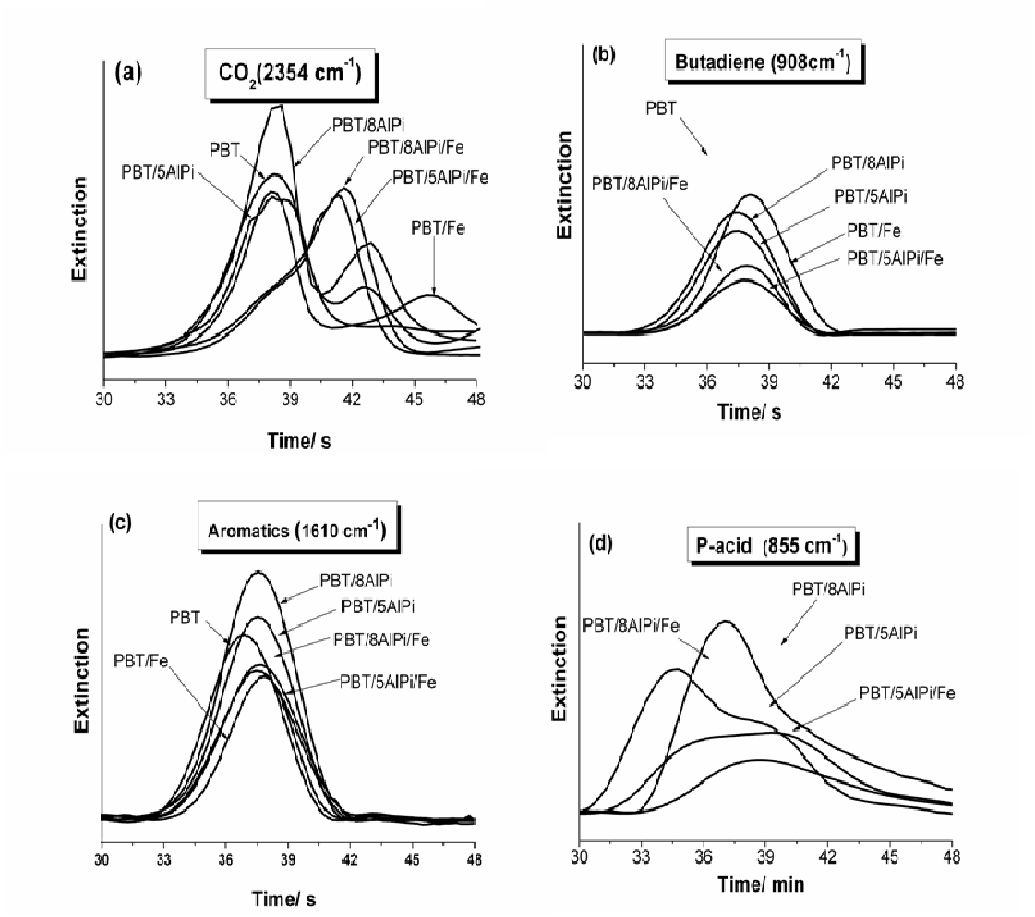

Fig. 26 Products release rate of Fe_2O_3 formulations during decomposition between 600- 750 K.

CO_2 release rate (Fig. 26a) for PBT/Fe shows two pea Ks one occurring during the main mass loss of PBT (38 min) and the second small one occurring at 46 min. The combination of AlPi with Fe_2O_3 in both PBT/8AlPi/Fe and PBT/5AlPi/Fe, seems to exhibits only one pea K centred at around 40 min but, under detailed analysis, it's possible to identify two peaks, as in all the AlPi formulations. One peak appears like a shoulder centred at about 38 min, during the main mass loss decomposition step of the polymer, while the additional one is located at 41-42 min. The decreased release and the delay in the volatilization of small fragments like butadiene (Fig. 26b) in all the Fe_2O_3 formulations (in comparison to PBT) indicates that

Fe_2O_3 acts as a char-enhancing additive, acting as a mass transport barrier. The bigger decrease is shown in PBT/8AlPi/Fe and PBT/5AlPi/Fe. Aromatic release (Fig. 26c), as well as the P-acid release (Fig. 26d) in the gas phase, follow the same trend found in the other metal oxide-formulation: Fe_2O_3 prevents the volatilisation of P-moieties and aromatic, Keeping them in the solid phase.

4.2.6. PBT/AlPi/ Sb_2O_3 formulations

The combination of Sb_2O_3 in PBT does not change the CO_2 release rate in comparison to PBT, as both exhibited one maximum in the curve (a). As presented elsewhere, all the formulations containing the flame retardant showed two maxima in the CO_2 release rate. In this case, with the addition of Sb_2O_3, the curve showed two shoulders, the first one correlates with the main mass loss step at about 39 min while the second pea K is related to the second mass loss decomposition step at about 42 min. The butadiene release rate (Fig.27b) shows that, in general and in comparison to PBT, all the formulations exhibit a lower butadiene release. PBT/5AlPi/Sb and PBT/8AlPi/Sb are the most efficient in reducing the amount of volatile. In comparison to PBT, all the formulations show an increase release of aromatic functionalities in the gas phase. This means that, in contrast with other metal oxides, Sb_2O_3 is not able to retain aromatic in the solid phase (Fig. 27c). Even the P-acid release rate disagrees with the previous results related to the other metal oxides (Fig. 27d). The addition of Sb_2O_3 promotes the release of P-acid in the gas phase.

4.2.7. Conclusions

All materials follow the same decomposition route of PBT, in such a way that they release the same decomposition products but in different amount. In all the AlPi formulation, with and without metal oxide, additional diethylphosphinic acid was detected during the maximum of mass loss rate.

The amount of diethylphosphinic acid released was correlated to the initial loading of flame retardant. The CO_2 release rate exhibits two peaks

only in the formulations containing AlPi. The second peak in the CO_2 release rate is related to the second decomposition step also detected in TG experiment.

According to the char-enhancing approach, Me-oxide in PBT decrease the amount of small volatile polymer pyrolysis fragments like butadiene, in comparison to PBT and also preventing the release of benzene that is accumulating in the solid phase. The char also function as a mass transport barrier, by physically delaying the volatilization of decomposition products and/or chemically reacting with decomposition products.

The inclusion of metal oxides in PBT/AlPi/Me-oxide prevents P-acid volatilization, maintaining part of the phosphorus in the solid phase that can undergo charring.

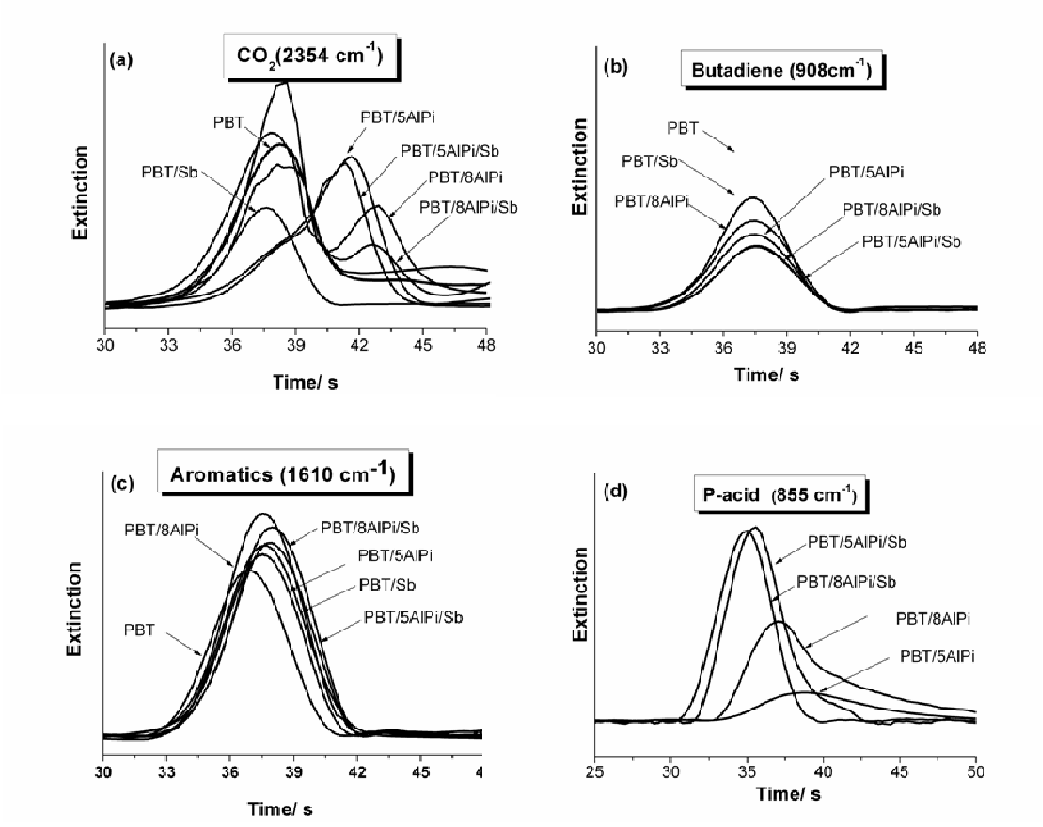

Fig. 27 Products release rate of Fe_2O_3 formulations during decomposition between 600- 750 K

4.3. Pyrolysis: solid residue

Table 9 Assignment of IR absorption bands in the solid phase.

Band location (cm^{-1})	Structure assignment
3080-3064	C-H stretch aromatic
2969-2962	C-H stretch aliphatic
1796-1688	C=O acid , anhydride
1729-1714	C=O stretch ester
1640-1600	C=C polyaromatic
1560-1500	aromatic
1410-1409	Aromatic ring
1393-1380	$(P=O)_{sym}$ stretch
1270-1265	CO-O aromatic esters
1100-1004	O-CH2
1293-1235	$(P=O)_{asym}$ stretch
1100-1000	PO_4^{3-}, $P_2O_7^{4-}$
940-860	$(P-O-P)_{sym}$ stretch
774-766	$(P-O-P)a_{sym}$ stretch
730-726	C-H ring + C=O out of plane
560-532	O-P-O bending

4.3.1. PBT

PBT decomposes in one single step, with a maximum at about 650 K. After the main mass loss, all the evolved bands disappeared and no residue is left in the solid phase as shown in Fig. 28. The most intense bands of the spectra of PBT at room temperature are located at 3063 cm^{-1} (aromatic C-H stretching vibrations), 2962 cm^{-1} and 2876 cm^{-1} (aliphatic C-H asymmetric and symmetric stretching vibrations), 1709 cm^{-1} (C=O stretching vibration), 1268 cm^{-1} and 1104 cm^{-1} (ester C–O–C, asymmetric and symmetric stretching vibrations), 1210 cm^{-1} (ether stretching vibration), 728 cm^{-1} (C–H deformation vibration from aromatic ring) (Fig. 29a).[79]

Pyrolysis of PBT reveals the steady increase of acidic and anhydride structures in the solid residue. Heating to 5% weight loss (640 K) (spectrum b) brings about a decrease in intensity of the aliphatic C–H, ester and ether C–O–C absorption bands, associated with the decomposition of the ester

and ether bonds followed by the volatilization of the aliphatic moieties from the macromolecules. This process is likely to be finished at 50 wt% weight loss as the corresponding IR spectrum (spectrum c) does not exhibit the absorption bands caused by aliphatic structures.

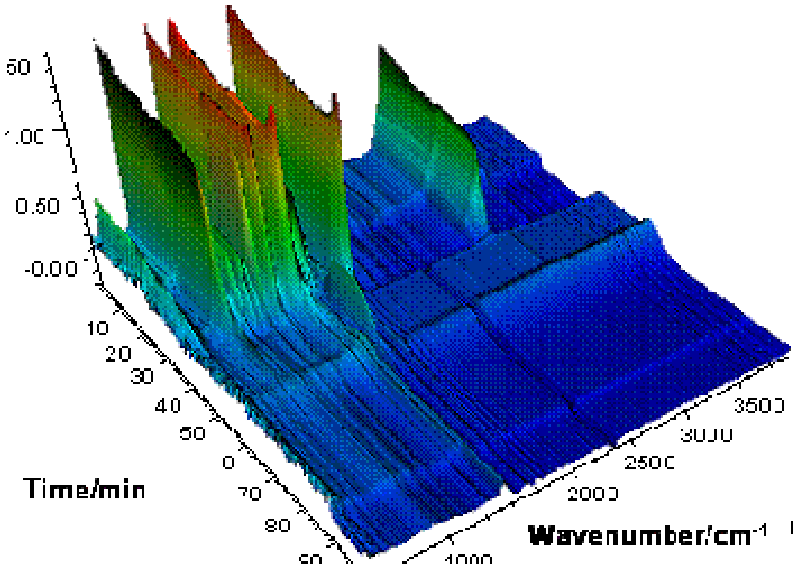

Fig. 28 3D-spectra of PBT pyrolysis in the solid phase.

However, in the course of pyrolysis, the C-O stretching vibration does not vanish, however it moves to 1733 cm^{-1}, indicating the appearance of a new group at the ester oxygen.

Further decomposition, up to 50 wt% (675 K), led to an increase in the characteristic absorption bands of anhydride groups at 1795 and 1208 cm^{-1} and new bands (shoulder at 1640 cm^{-1} and small band at 3077 cm^{-1}) develop indicating the formation of aromatic vinyl groups (C=C). At the same time aliphatic bands disappear. At about 50 wt% (Fig. 29c), new bands at 1694, 1427 and 934 cm^{-1} were formed, characteristic of aromatic carboxylic acid groups.

During decomposition, PBT scarcely undergoes aromatization and, at the end residue is not found, apart from terephthalic acid that condenses into the heated transfer line.[80]

4.3.2. PBT/AlPi formulations

The spectra of pure AlPi at room temperature shows strong bands at 1250 (P=O), 1150 (C-P-O), 1066 (P-O) and 774 cm^{-1}. The addition of AlPi in PBT slightly changes the decomposition route of PBT, starting from the main mass loss step. The decomposition process when AlPi is added in PBT/AlPi involves a more pronounced aromatization: during decomposition the pea Ks corresponding to the absorption of the aromatic functionalities (1640 cm^{-1}) and to the anhydride groups (1795 cm^{-1}) steady increase (Fig. 30b).

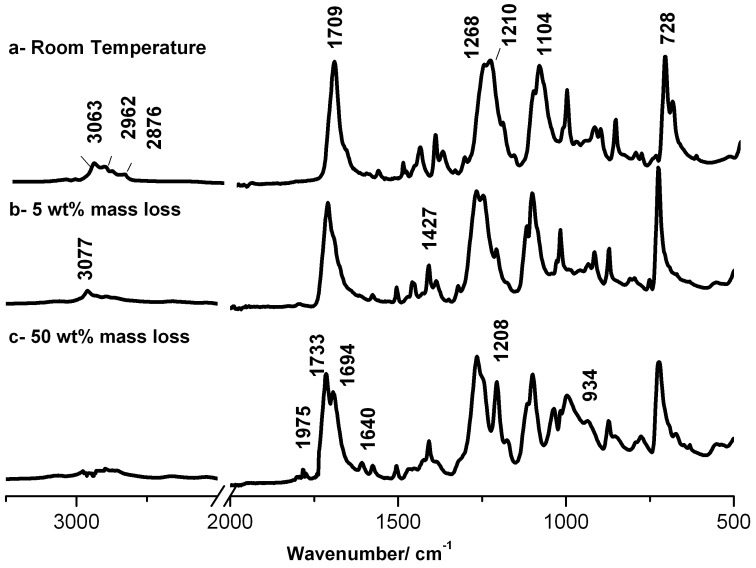

Fig. 29 Thermal decomposition of PBT at different stages of decomposition.

The series at 711, 734 and 784 cm^{-1} suggested that substitution on the benzene ring has changed during pyrolysis.[81] Through the combination of the phosphinate anion and the terephthalic anion coming from polymer's decomposition, Al-phosphinate terephthalate salts are detected in the condensed phase of all the PBT/AlPi formulations (Fig. 30a).[82]

According to the literature [95] the bands at 3064, 1719, 1561, 1380, 1250, 540 cm^{-1} were assigned to the Al-phosphinate salts.[83]

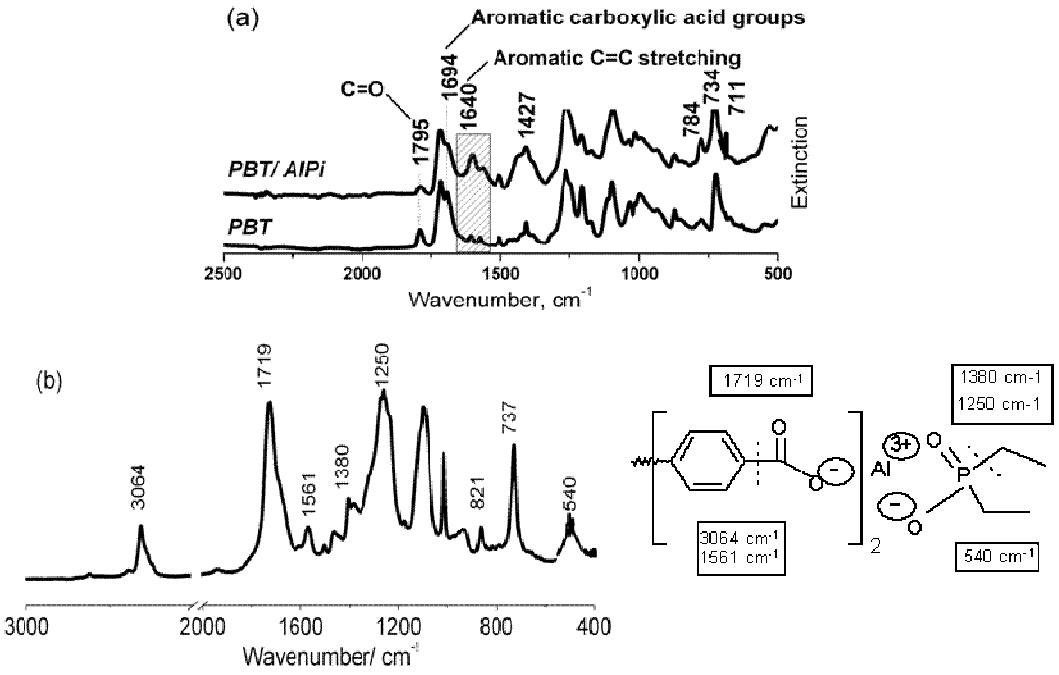

Fig. 30 (a) Comparison between aromatic bands formation in PBT and PBT/8AlPi at 50 wt% mass loss; (b) Formation of AlPi salts in the solid phase after 50 wt% mass loss.

4.3.3. PBT/AlPi/TiO_2 formulations

The thermal decomposition of PBT/Ti is reported in Fig. 31. The initial room temperature spectrum of PBT/Ti shows that there are no clear differences between PBT and PBT/Ti with respect to the additive TiO_2. When the decomposition was stopped at 640 K (5 wt% mass loss) the carboxilic signal at 1712 cm^{-1} and the aliphatic CH stretching at 2960 cm^{-1} decreased, indicating the decomposition of polyester structure.

New bands appear in the region between 1456 and 1407 cm^{-1}, due to the primary chain scission in the aliphatic chain. Increasing the temperature up to 675 K (spectrum c) the IR spectrum is dominated by new signals at 1795 and 1208cm^{-1}, attributed to anhydride formation and new broad bands around 1600 cm^{-1}, attributed to polyaromatic char.[77] At the same time a change in substitution of the aromatic rings is observed, as suggested by the change in the signals between 724 and 760 cm^{-1}.

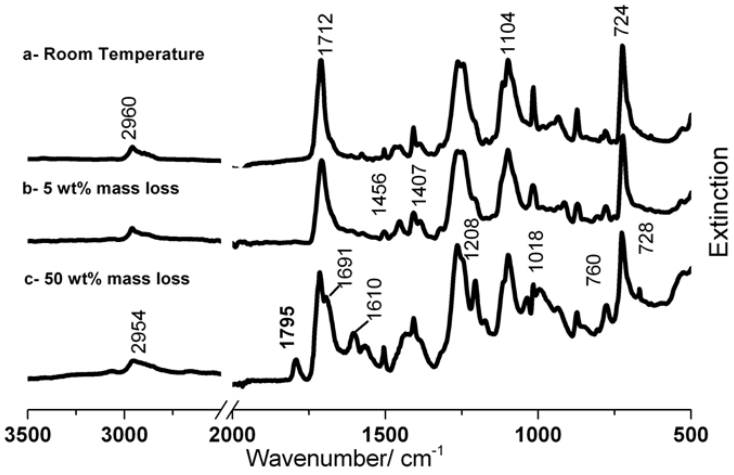

Fig. 31 Thermal decomposition of PBT/Ti at different stages of decomposition.

The comparison between the same 675 K temperature spectra of PBT/Ti and PBT/8AlPi/Ti (Fig. 31) showed that the aromatic functionalities and the anhydride groups are detected in both formulations. In PBT/Ti, the anhydride group's signals are still clearly detected at 1795, 1208 and 996 cm^{-1}. On the other side, in PBT/8AlPi/Ti the anhydride decomposition already started and is followed by a polyaromatization process that results in a graphite-like structure that remains in the condensed phase as detected by the broad band centred at 1610 cm^{-1}.[79 , 94]

4.3.4. PBT/AlPi/ Al_2O_3 formulations

No significant changes in the IR spectra of PBT/Al in comparison to PBT at the beginning of decomposition are detected. Different signals are detected after the main decomposition step in comparison to PBT/10AlPi/Al as shown in Fig. 32. The inclusion of Al_2O_3 alone in PBT/Al leads to an increase of the polyaromatic content of the char in comparison to PBT/10AlPi/Al, as highlighted by the broader pea K of PBT/Al in comparison to PBT/10AlPI/Al at 1610 cm^{-1}. The change in the region around 700-833 cm^{-1} showed that substitution on the aromatic rings occurred. This is clearly evident in PBT/Al where a more complex path of aromatic substitution is detected, a sign that Al_2O_3 catalysis cross-linking reactions between aromatic, promoting char formation. In the region around

1350, 1250, 540 cm^{-1}, the phosphorous signals related to aluminium-phosphinate terephthalate salts formation are detected.

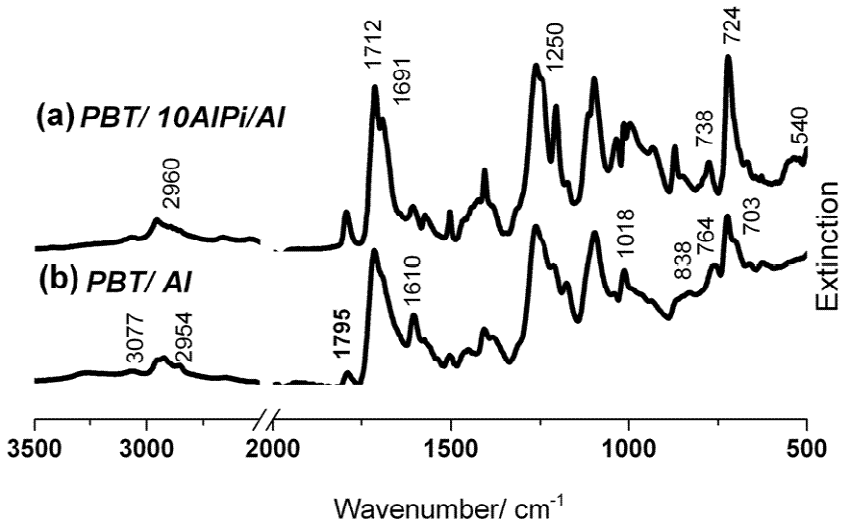

Fig. 32 Comparison between solid residue at 50 wt% mass loss of PBT/10AlPi/Al (a) and PBT/Al (b).

4.3.5. PBT/AlPi/Fe_2O_3 formulations

The PBT/Fe spectrum at 50 wt% mass loss clearly shows that Fe_2O_3 is a very efficient catalyst in promoting charring and cross-linking.

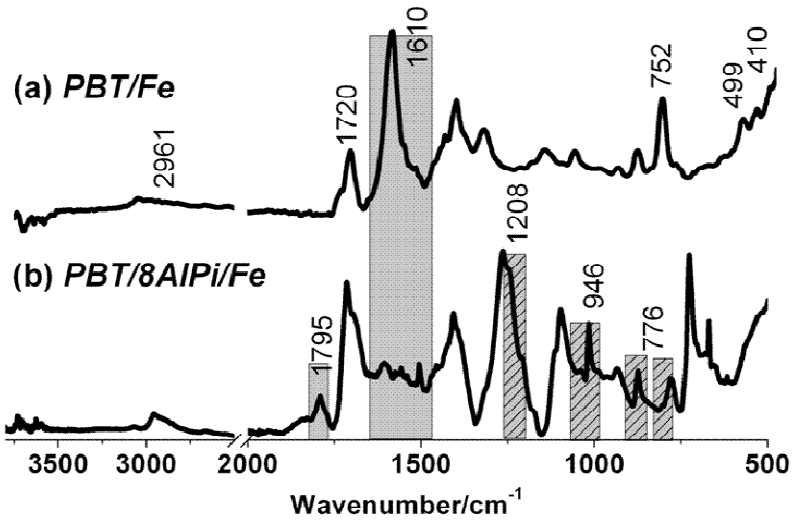

Fig. 33 Comparison between solid residue at 50 wt% mass loss of PBT/Fe (a) and PBT/8AlPi/Fe (b).

The sharp signal at 1610 cm^{-1} highlights the presence of a high content of polyaromatic char. In combination with AlPi this ability is reduced as the pea K located at 1610 cm^{-1} and only appears as a broad band. The anhydride group is still detected in high amount while its formation in PBT/Fe is not evidenced at this stage. Aluminium-phosphinate terephthalate salts are detected in PBT/8AlPi/Fe.

4.3.6. PBT/AlPi/Sb_2O_3 formulations

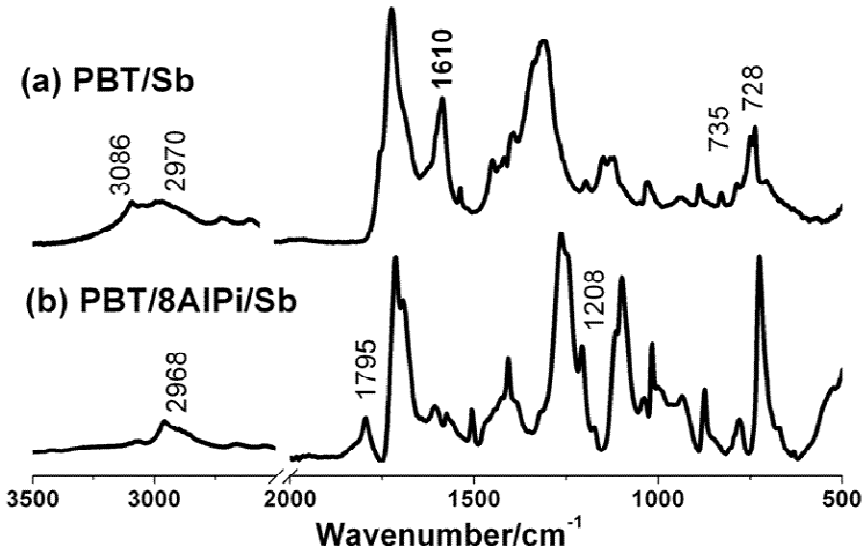

Fig. 34 Comparison between solid residue at 50 wt% mass loss of PBT/Sb (a) and PBT/8AlPi/Sb (b).

The solid phase spectrum of PBT/Sb (Fig. 34a) at 50 wt% mass loss shows a high aromatic content in the char, as highlighted by the strong pea K at 1610 cm^{-1} (polyaromatic), the broad band at 3068 cm^{-1} (CH aromatic) and the peaks in the region between 735 and 728 cm^{-1}, that indicate the substitution on the aromatic rings. No sign of anhydride formation is found at this stage as it has already decomposed to give a polyaromatic char. On the contrary, in PBT/8AlPi/Sb (Fig. 34b), anhydride pea Ks are still detected at 1795 and 1208 cm^{-1}.

4.4. Decomposition model

4.4.1. Thermal decomposition of Poly(1,4-butylene terephthalate)

The chemistry of thermal, thermo- and photo-oxidation reactions that occur in aromatic polyesters has been studied extensively in the past by UV, IR and wet chemistry methods, to follow the process and to identify the products formed,[84] frequently with the support of model compounds. Bothelo et al.[85,86] carried out a comparative study on thermal- and thermo oxidative degradation of PET and PBT with their respective model compounds. On the basis of the products identified by GC–MS, they accomplished that the thermo-oxidation mechanism involves oxidation at the α-methylene carbon with the formation of peroxides. The consecutive chain scission produces aromatic and aliphatic acids, anhydrides and alcohols.

Rivaton et al.[87] studied photolysis and photo-oxidation mechanisms of PBT by using UV and FT-IR, coupled with chemical derivatization reactions. According to the photo-oxidation products identified, they deduced that photolytic reactions have a dominant effect with respect to the photo-oxidative degradation occurring in α-methylene carbon.

The initiation of the thermal decomposition of PBT is similar to that of PET, however the products of decomposition are somewhat different because of longer aliphatic fragments in the chain. Several authors[88] report initial polymer scission occurring via the six-member cyclic transition state (Scheme 2).

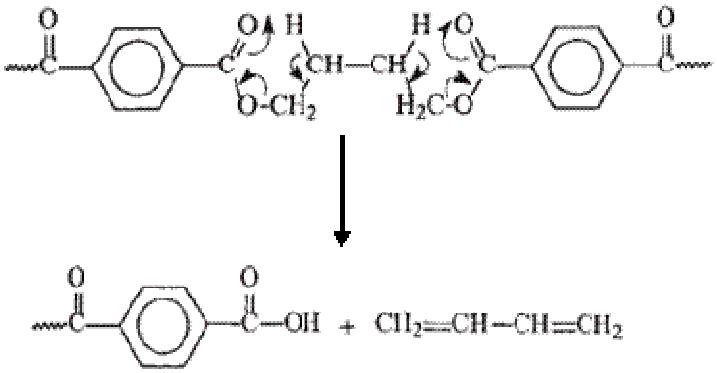

Scheme 2

The β-CH hydrogen transfer involved in the thermal degradation process, leading to the formation of oligomers with carboxylic and olefin end groups, is well established in the literature. According to the actual geometry of the chains, the major degradation route in PBT would lead to the formation of butadiene. Apart from butadiene, a considerable amount of tetrahydrofuran (THF) is also obtained in the degradation products of PBT. When the well- Known acyl-oxygen cleavage of the ester linkages proceeds in the PBT chains, intra- or intermolecular H shifts can occur, leading to the formation of hydroxyl-terminated units, which in turn undergo further degradation to yield THF and the carboxylic acid-terminated chain (Scheme 3). Another less feasible mechanism for the formation of THF and butadiene from PBT by the intra- or intermolecular H shift can form a diol which eliminates a molecule of water to form THF and two molecules of water to form butadiene.

Because of the presence of water in the decomposition products, acid-catalyzed hydrolysis of the butylene ester chain end-groups may also be important in THF production may also be important in THF production (Scheme 4).[89]

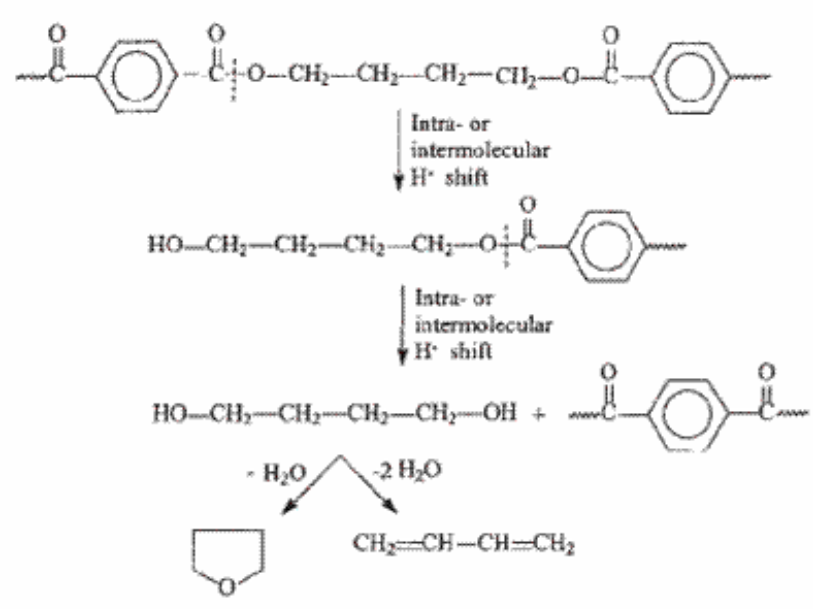

Scheme 3

Regarding the cross-linking, there are three possible mechanisms involving polyesters. First, random scission of polyester chains may take place, forming carboxylic acids, vinyl esters, aldehydes and carbon dioxide. After the vinyl esters accumulate to some concentration, they react with the polymer chain and network structures are formed. In Scheme 5 cross-linking formation in PET is reported as an example.

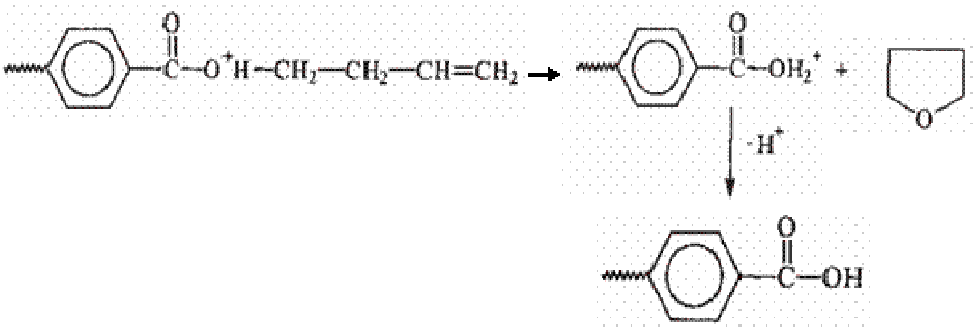

Scheme 4

In contrast, Nearly[90] and Spanniger[91] believed that aromatic fragments are mostly responsible for the cross linking. They suggested a mechanism in which a phenyl radical is formed after the chain scission and this radical may arylate an adjacent benzene ring to form a cross-link between two phenyl radicals.

Thermal decomposition of polyesters could be affected either by acidic or basic species present in the polymer. Therefore flame retardant additives normally modify the mechanism of thermal decomposition of polyesters and this effect is a part of the flame retardant action of these additives. Sato[92] studied the thermal degradation of a flame retarded PBT containing a synergistic flame-retardant system based on brominates polycarbonate and antimony trioxide (Sb_2O_3) using various temperature-programmed analytical pyrolysis techniques. It was found that in this flame-retardant system, brominates phenols are evolved at slightly lower temperatures than those of the flammable product evolution from the substrate polymer, thus causing

the initial flame-retarding effect. Balabanovich and Engelmann[93] flame retarded PBT by addition of poly (sulfonyldiphenylene phenylphosphonate).

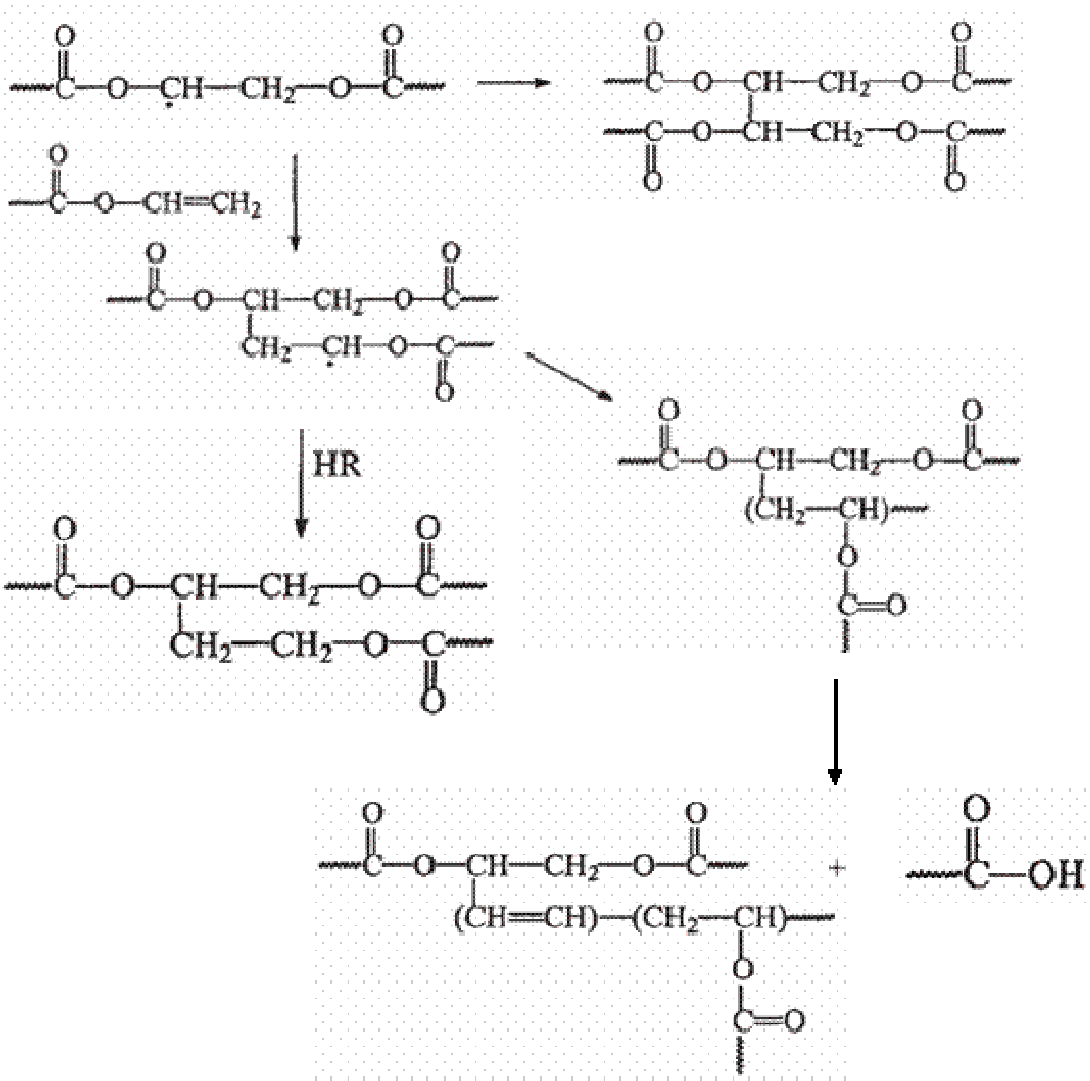

Scheme 5

Using infrared, it was shown that the polyphosphonate changes the degradation pathways of PBT resulting in formation of polyarylates (Scheme 6). It was believed that polyarylates are formed due to recombination of carboxyphenylene and phenylene radicals appearing from thermolysis of PBT.

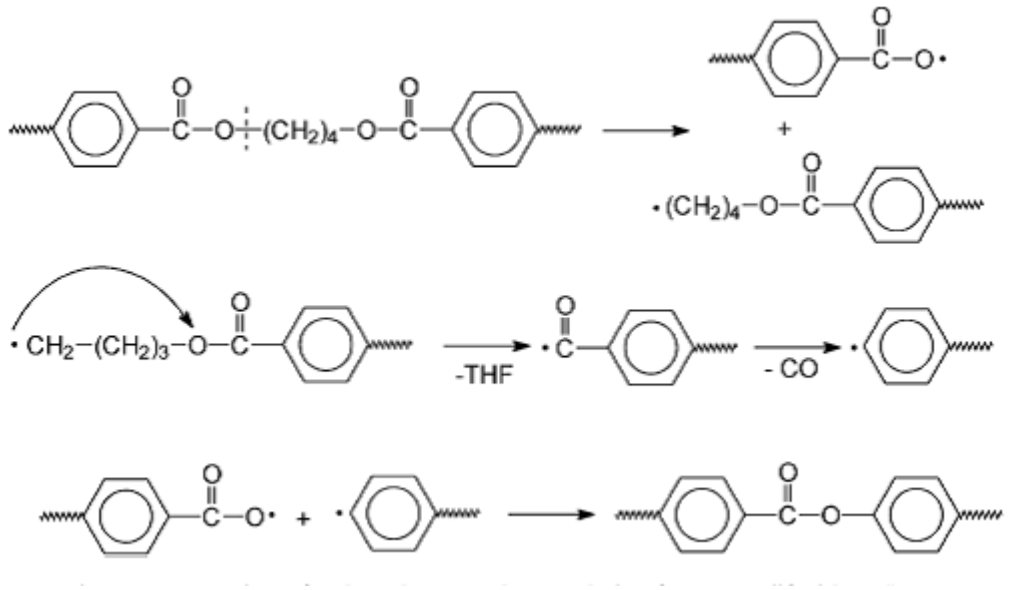

Scheme 6

4.4.2. Decomposition model for PBT/AlPi formulations

All the proposed decomposition models are based on TG experiments, evolved gas analysis and on change in the condensed residue. The possible interactions between the polymer and all the additives are taken into account.

The thermal decomposition of PBT is well established[94,95,96,97] and does not involve solid residue formation. The decomposition of PBT changes slightly when AlPi is added in PBT/AlPi, because it influences the ester scission. Most of the AlPi goes to the gas phase as diethylphosphinic acid.

The interaction of phosphinate anions with terephthalic acid leads to the formation of Al-phosphinate terephthalate salts in the solid phase.[98] This derivate decomposes during the second small decomposition step, between 730-750 K, releasing CO_2, benzene and ethene. The missing hydrogen atoms for benzene formation are taken from the cleavage of the P-ethyl bond from the phosphinate anion. At higher temperatures only Al-orthophosphate ($AlPO_4$) is detected in the solid phase (Scheme 7).

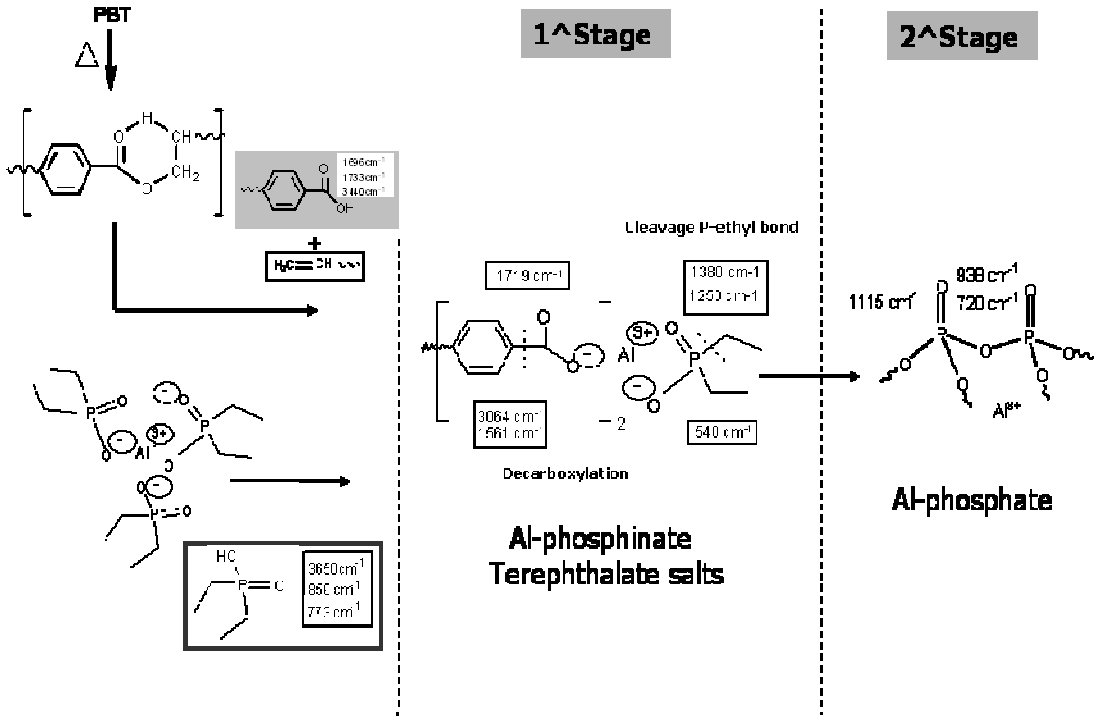

Scheme 7 Decomposition pathway of PBT/AlPi formulations.

The inclusion of metal oxides changes the decomposition of PBT. The route and the type of solid residue are significantly different. Lewis acid-base interaction and charring process is assumed as reported in the literature (

Scheme 8).[99] All the metal cations like Ti^{4+}, Fe^{3+}, Sb^{3+} and Al^{3+} used in this work, may interact with the electron pairs of the carbonyl groups, creating coordinative bond in polymer like PBT, with strongly electronegative groups.

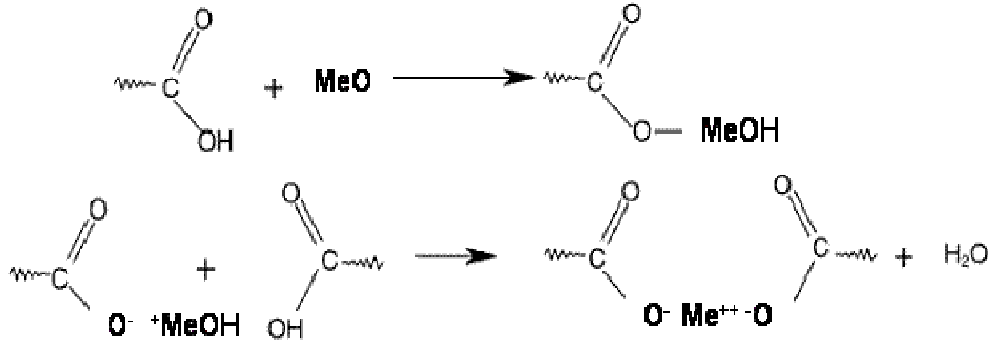

Scheme 8 Ionic interaction between a Me-oxide (MeO) and the acidic functions of PBT.

According to TG-ATR experiments, the addition of Me-oxides in PBT leads to the formation and the stabilization of anhydride groups in the solid phase. Mechanisms visualizing anhydride formation are presented in Scheme 9. Both anhydride formation via condensation of carboxyl groups and ester carboxyl exchange are feasible processes. Water released by the condensation reaction can hydrolyze ester groups, a reaction resulting in the formation of carboxyl and terminal hydroxyl groups.

The addition of metal oxides in PBT stabilize the anhydride formation than Ks to the interaction between the strong Lewis activity of the metal cation and the carboxylic groups of the anhydride, resulting in a stabilization of this intermediate that accumulates in the solid phase (Fig.35).

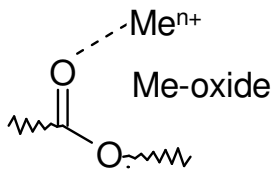

Fig. 35 Interaction and stabilization of anhydride moiety and the metal cation.

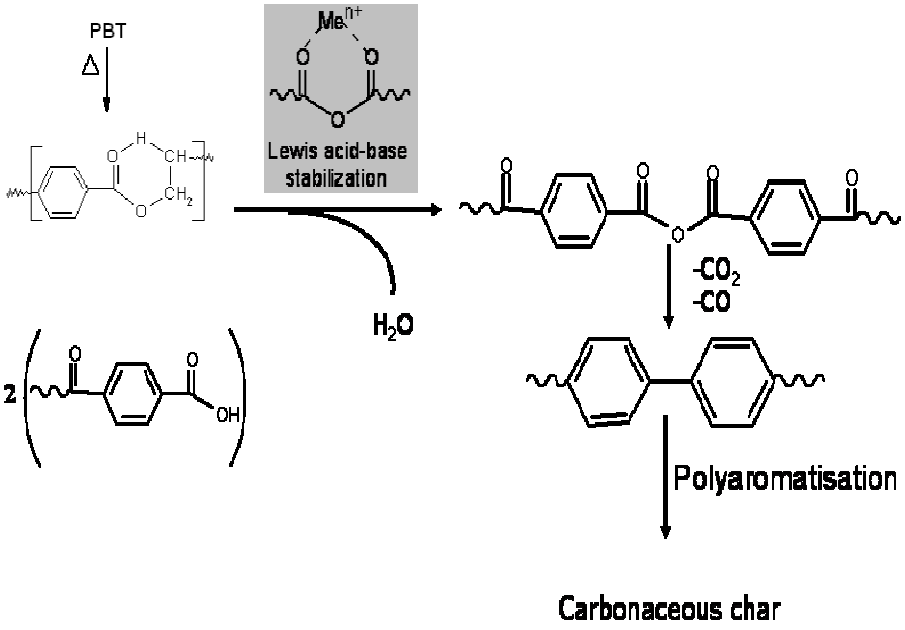

Scheme 9

Further decomposition leads to the decarboxylation of the anhydride species giving a carbonaceous char (Scheme 10). On the contrary to AlPi´s formulations, there are no hydrogen atoms coming from the decomposition of AlPi, providing the formation of benzene in the gas phase, as confirmed in the product release rate analysis in the gas phase. This involves that aromatic species are retained in the solid phase instead than volatilize.

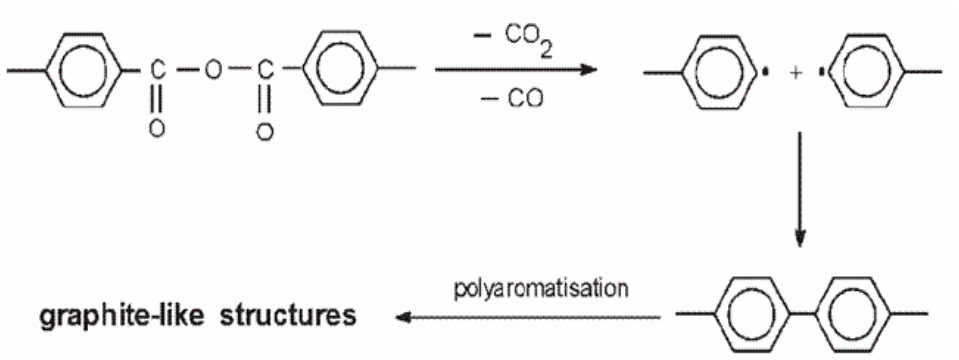

Scheme 10

Among the different metal oxides investigated, TiO_2 and Al_2O_3 show a similar behaviour regarding the anhydride stabilization in the solid phase. The analysis of the thermal decomposition of PBT in presence of Fe_2O_3 suggests that iron oxide may have a different behaviour. As shown in Fig. 33 and on the contrary of other PBT/Me-oxide formulations, at 50 wt% mass loss PBT/Fe does not show anhydride formation but rather a polyaromatic char formations (Scheme 11) as detected by the signals at 1610 and 773 cm^{-1}. Acting as a dehydrogenation catalyst, iron also promotes double bonds formation that may give cross-linking as reported as an example in Scheme 12. The study of the condensed-phase products demonstrates a chain of transformations of the initial aliphatic–aromatic polyester to a polyarylate in the first stage and then to polyaromatic-containing structures.

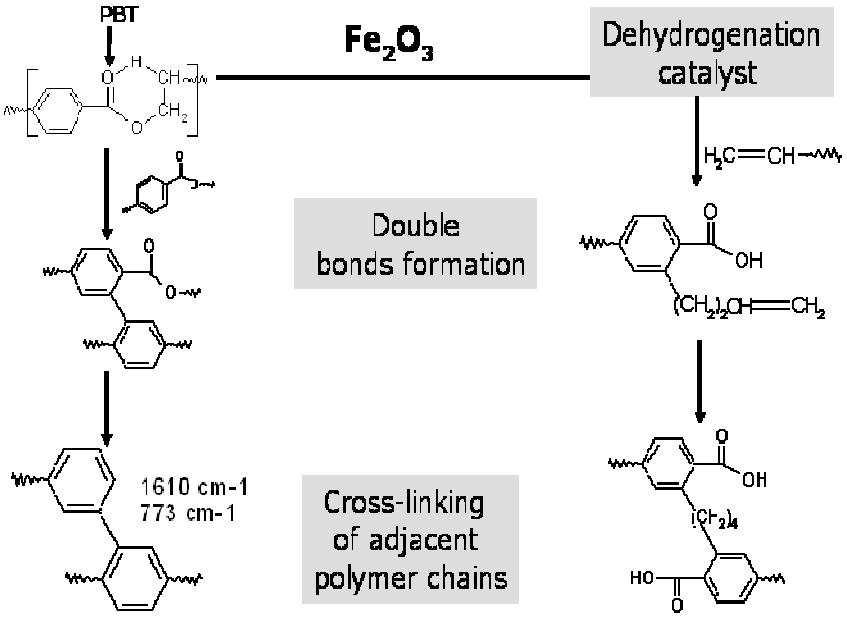

Scheme 11

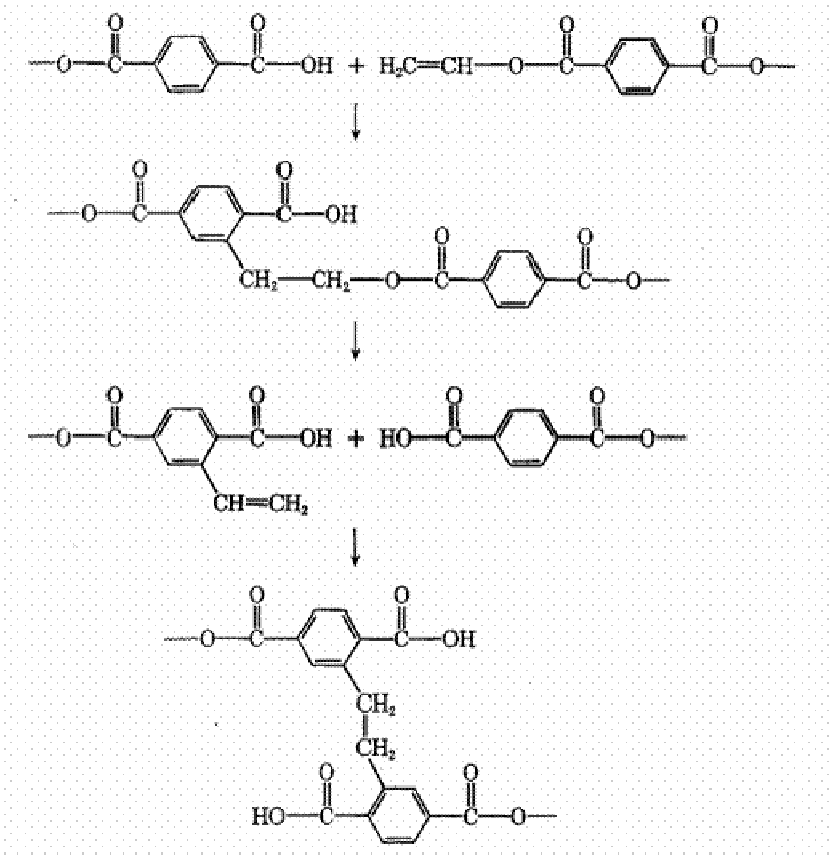

Scheme 12

4.4.3. Proposed decomposition model for PBT/AlPi/Me-oxide formulations

Combining TiO_2, Al_2O_3 and Sb_2O_3 and AlPi in PBT, the Lewis acid activity of the metal ion is suppressed by the stronger phosphinate interaction with the polymer and therefore plays a minor role.

The intermediate Al-phosphinate terephthalate salt is preferred formed than the anhydride group. Therefore the formation of Al-orthophosphate in the solid phase is preferred in respect to the graphite-like structure. With iron oxide, an interaction between phosphorous and metal oxide is observed. As a Lewis acid, iron oxide may help in linking polyphosphoric acid chains, reducing the loss of phosphoric acid in the gas phase and forming a more impenetrable barrier layer. The formation of a phosphorous- carbonaceous char is postulated (Scheme 13). The analysis of the solid phase spectra of PBT/8AlPi/Fe in the region between 850-1350 cm^{-1} present broad band between 1150-1300 cm^{-1}, assigned to P-O-C bonds and a pea K at about 1000 cm^{-1}, assigned to the P-O bonds in a chain P-O-P. The spectral region between 2500-3700 cm^{-1} is also important as it is the absorption range of aliphatic groups.

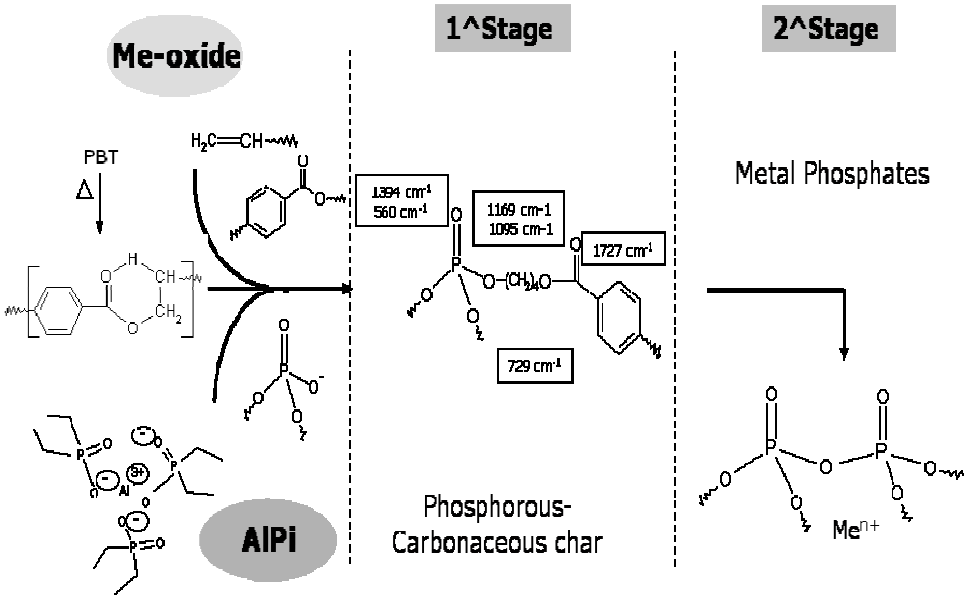

Scheme 13

4.4.4. Conclusions

The use of mineral oxides in combination with PBT leads to synergistic effects on the char formation. However, the mechanisms of action of TiO2, Al_2O_3, Sb_2O_3 and Fe_2O_3 are not similar. All the metal cations, as Lewis acid species, can interact with the acidic groups of PBT, creating a three dimensional network. With TiO_2, Sb_2O_3 and Al_2O_3, this interaction promote the formation and the stabilization of an anhydride group that further decomposes to a graphite-like char.

The decomposition mechanism with iron oxide is slightly different. Iron oxide, as a strong dehydrogenation catalyst, promotes double bond formations, producing a highly cross-linked char.

4.5. Flammability and ignitability

All the results for flammability (LOI, UL94 and time to ignition, t_{ign}) are summarized in Table 10. PBT is a highly combustible material burning with flammable dripping. Therefore it does not pass the V-classification in the UL94 and only gets an HB classification. The LOI value of PBT is only 21.7 % (Table 10a).

Table 10 Flammability results for (a) PBT and PBT/AlPi formulations; (b) PBT/metal oxides formulations; (c) PBT/AlPi/ metal oxides formulations. (LOI error ±1, t_{ign} ±1).

(a)

PBT/	t_{ign}	LOI	UL94
	s	%	
-	50	21.7	HB
5AlPi	46	25.0	V-2
8AlPi	54	29.1	V-2
10AlPi	37	31.3	V-1

(b)

PBT/	t_{ign}	LOI	UL94
	s	%	
Ti	33	19.0	HB
Al	38	22.0	HB
Fe	32	22.0	HB
Sb	45	21.5	HB

(c)

PBT/	t_{ign}	LOI	UL94
	s	%	
5AlPi/Fe	26	29.4	V-0
5AlPi/Sb	34	27.8	V-0
8AlPi/Ti	51	28.1	V-0
8AlPi/Fe	38	26.0	V-0
8AlPi/Sb	32	31.1	V-0
10AlPi/Al	48	29.4	V-0

4.5.1. PBT/AlPi formulations

The combination of AlPi into PBT considerably increases both the LOI value and the UL94 classification because of anti-dripping effects. Time to ignition shows differences among all of the materials. The result and the improvement in the fire resistance are correlated to the original amount of flame retardant: increasing the wt% of AlPi helps in getting better flame retardant properties. As shown in Table 10(a), PBT/5AlPi only get a V-2 classification in the UL94 test and an increase of 13% in the LOI value (25.0%) in comparison to PBT. In PBT/5AlPi, the time to ignition is decreased in comparison to PBT of about 6 s. Increasing the AlPi content up to 8 wt% in PBT/8AlPi does not support improving the UL94 classification but increases the LOI value to 29.1%, approximately 25% more in comparison to PBT. Time to ignition is slightly increased by 4 s. PBT/10AlPi gets the best classification in the UL94 test, with a V-1 ran King and a LOI value of 31.3% but t_{ign} is decreased again to 37 s. In Fig. **36** the amount of AlPi (wt %) *vs* LOI (%) is reported: an average increase in the AlPi content of 1wt % increases the LOI value by 3.0%.

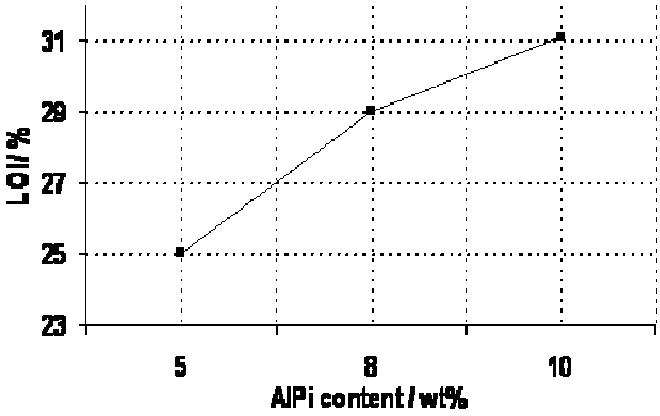

Fig. 36 Correlation between LOI results and the amount of flame retardant in PBT.

4.5.2. PBT/AlPi/TiO_2 formulations

TiO_2 metal oxides blended into PBT/Ti is not active in UL94 test: it burns with flammable dripping and passes the UL94 test with an HB classification [Table 10(b)]. With a LOI value of 19%, below the oxygen concentration in the air (21.0%), material burns easier than PBT. The t_{ign} is

decreased to 33 s. Only in combination with AlPi, the metal oxide exhibits a synergistic effect in PBT/8AlPi/Ti: thanks to the lack of dripping it reaches a V-0 classification and a LOI value of 28.1% [Table 10(c)] while t_{ign} remains similar to PBT.

4.5.3. PBT/AlPi/ Al_2O_3 formulations

Al_2O_3 in combination with PBT in PBT/Al slightly increases the LOI value to 22.0% in comparison to PBT but does not reduce PBT serious dripping during the UL94 test. Therefore the material only gets a HB classification [Table 10(b)]. Time of ignition is reduced in comparison to PBT to 38 s. Addition of 10 wt% of AlPi in PBT/10AlPi/Al is able to pass the UL94 test without flammable dripping and a V-0 ranking. Time to ignition reaches 48 s, similar to PBT. The LOI value of PBT/10AlPi/Al increases in comparison to PBT to 29.4% [Table 10(c)]. However this is less than the LOI value of PBT/10AlPi: Al_2O_3 only acts as a synergist in the UL94 test but as an antagonism in the LOI test.

4.5.4. PBT/AlPi/Fe_2O_3 formulations

Fe_2O_3 blended into PBT in PBT/Fe, as the others PBT/metal oxide formulations, is not sufficient to increase the UL94 ranking in comparison to PBT: both materials burn easily with serious melting and dripping problems. The LOI value of PBT/Fe is only slightly higher than PBT (22.0%) [Table 10(b)]. Time to ignition is strongly decreased in all the Fe_2O_3 formulations up to 32 s in PBT/Fe. The situation changes completely with the addition of AlPi. PBT/5AlPi has a LOI value of 25% and only gets a V-2 in the UL94 test [Table 10(a)]. In Table 10(c) it becomes clear that the addition of Fe_2O_3 in PBT/5AlPi/Fe increases both the UL94 ranking, with a V-0 classification and no dripping, and the LOI value that reaches 29.4%. Only 1 wt% of Fe_2O_3 in PBT/5AlPi/Fe increases the LOI value of PBT/5AlPi by 15%. In this case, the addition of mineral inorganic filler is able to increase the flame retardancy properties of a material, without increasing the amount of flame retardant. Unfortunately, increasing the amount of AlPi up to 8 wt% in PBT/8AlPi/Fe, the same beneficial effect in the LOI value

cannot be found: PBT/8AlPi/Fe has a LOI of 26.0%, which is lower than PBT/8AlPi (29.1%). Only an improvement in the UL94 test (V-0) can be observed.

4.5.5. PBT/AlPi/ Sb_2O_3 formulations

Sb_2O_3 in PBT is not active in reducing the combustion of PBT, both in the UL94 test and in the LOI test. PBT/Sb does not pass the UL94 V-classification, only gets a HB ranking, and shows a LOI value (21.5%) that corresponds roughly to PBT [Table 10(b)]. Time to ignition in PBT/Sb only decreased to 45 s. In Table 10(c) the combination of both Sb_2O_3 and AlPi in PBT is reported. PBT/5AlPi/Sb increases the LOI value to 27.8% in comparison to PBT/5AlPi and gets a V-o classification in the UL94 test. Increasing the amount of AlPi in PBT/8AlPi/Sb, it shows the same V-0 ranking and a further increase in the LOI value is reached. PBT/8AlPi has an LOI value of 29.1 %. Adding 1 wt% of Sb_2O_3 in PBT/8AlPi the LOI reaches a value of 31.1%, almost the same value obtained with 10 wt% of flame retardant in PBT/10AlPi. Times to ignition are decreased in both formulation containing AlPi and Sb_2O_3.

4.5.6. Flammability conclusions

There was no real correlation between the LOI and UL 94 test as reported previously, [100,101] in particular when different flame retardancy mechanisms competed with each other.

Addition of metal oxides alone in PBT is not enough to improve the fire properties of PBT in both LOI and UL94 test. All the PBT/metal oxides formulations get a HB classification in the UL94 test because of serious melting and dripping and the LOI value is roughly the same than PBT and does not significantly increase. In terms of LOI, Al_2O_3, Sb_2O_3 and Fe_2O_3 in PBT do not alter significantly the LOI value that remains constant in the range between 21.5-22.0%. Only TiO_2 seems to deteriorate the fire flammability properties of PBT, decreasing the LOI value up to 19.0% (Fig. 37). Combination of PBT with different amounts of AlPi both increase the LOI value of PBT and the UL94 classification.

The combination of metal oxides and AlPi gives the best results in relation with UL94 test but an antagonistic effect in LOI investigation. The advantage for passing the UL 94 by a combination of flame inhibition and charring has been reported before.[102] All the PBT/AlPi/metal oxide formulations pass the UL94 test with a V-0 classification meaning that the combination of metal oxides and AlPi overcome the problems relating to melt dripping and the extinguishing time during the test.

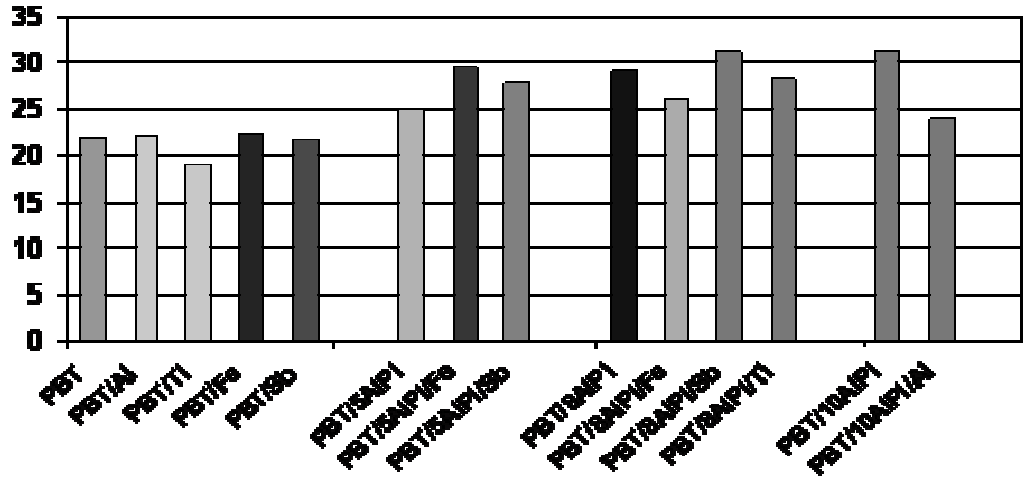

Fig. 37 Comparison of LOI results among all the investigated formulations.

In comparison to PBT/5AlPi formulations, the addition of both Fe_2O_3 and Sb_2O_3 increase the LOI value and this effect is more pronounced with Fe_2O_3. In PBT/8AlPi formulations, only PBT/8AlPi/Sb shows an improvement of the LOI value, while with the other nanoparticles the LOI tends to decrease with a worsening of the fire resistance properties. The same effect is found in PBT/10AlPi/Al, where the addition of nanometric Al_2O_3 does not help improving the LOI value of PBT/10AlPi but only the Ul94 ranking.

Based on the Van Keveler[28] equation, there's a clear correlation between the LOI value and the char yield. In Fig. 38 the LOI results are plotted against the char yield found in TG experiments. Based on the position of the points in the plot it is possible to evaluate the mechanism at the base of the fire retardant action. The upper line is the limit for a

complete gas phase action. All the formulations containing only PBT and AlPi are on this line. For the materials standing on the lower line, a solid phase mechanism must be formulated. All the metal oxides in PBT/ metal oxides formulations show this kind of mechanism. For all the materials standing between these two limits, a combination of both mechanisms can be postulated.

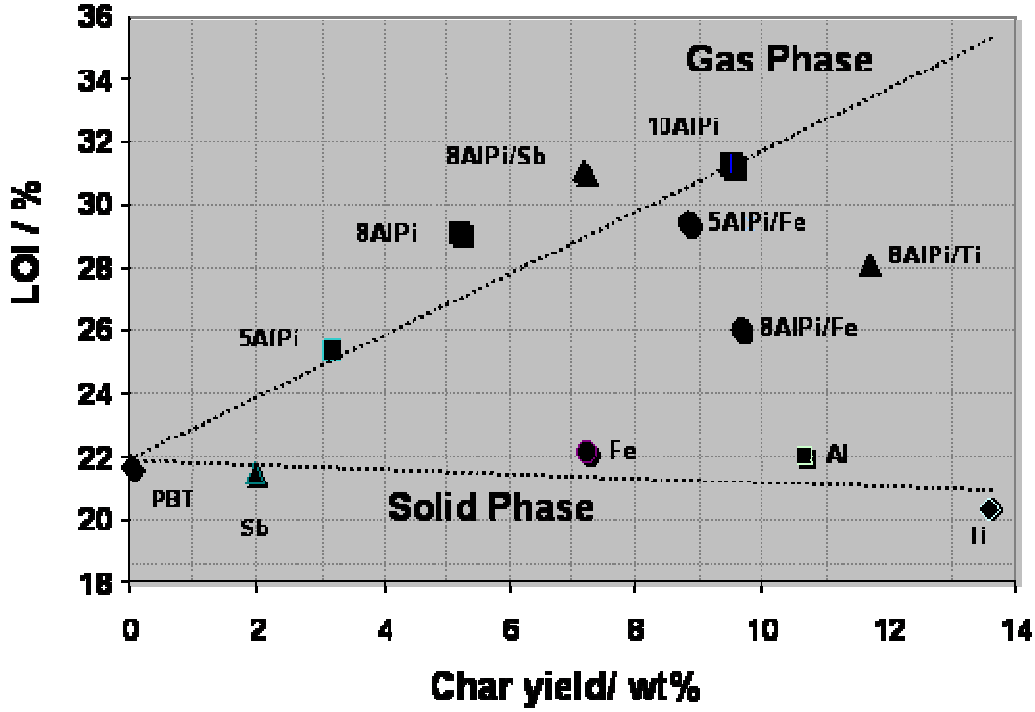

Fig. 38 Char yield *vs* LOI for all the formulations: individuation of the flame retardant mechanism.

4.6. Fire Behaviour: forced flaming combustion

Cone calorimeter test with an external heat flux of 50 KWm^{-2} was performed. Under forced flaming combustion, all materials burned homogeneously. The heat release rate (HRR) and total heat evolved (THE) were discussed. The residue amount was collected at flame-out. The THE/ total mass loss (THE/TML) was discussed for the analysis of the dominant flame retardancy mechanism in forced-flaming combustion: a significant reduction in THE/TML indicates flame inhibition, whereas fuel dilution

results in a moderate reduction in THE/TML. Both CO production and smoke (total smoke release, TSR) resulting from incomplete combustion and were evaluated to determine the fire hazards in forced-flaming conditions. Generally rough correlation between the LOI or UL94 performance and PHRR is expected since the reaction to small flame in UL 94 and LOI is controlled by a critical HRR or flame spread resulting in extinction. To explain this lack of correlation an alternative index was proposed, of total heat released at 60 s after ignition, divided by the t_{ign} (THR60s/ t_{ign}). Similar to PHRR/t_{ign} and FIGRA, this index attempts to cover the two most important parameters controlling flame spread: the HRR of the burning part and 1/t_{ign} of the material in the direction of flame propagation. In contrast to PHRR/t_{ign} and FIGRA, the index THR60s/t_{ign} emphasizes the HRR at the beginning of burning as responsible for flame spread rather than the maximum HRR. The HRR curve in PBT (Table 11) was characterized by a sharp peak after ignition with a peak HRR (PHRR) of 1404 KWm^{-2}. The THE (THE = THR at flame-out) is 74MJm^{-2}. No residue was collected for PBT.

4.6.1. PBT/AlPi formulations

In general, the bigger the amount of flame retardant in PBT, the bigger is the decreasing of the PHHR and THE and the bigger is the amount of residue collected at the end of the test. Only the reduction of PHHR is not following the increasing amount of flame retardant therefore the decreasing order is PBT/8AlPi > PBT/5AlPi > PBT/10AlPi. In all the AlPi formulations a small broad shoulder appeared at the beginning of the HRR. This shoulder is more pronounced and shifted to lower time (30 s) in comparison to PBT in PBT/10AlPi while PBT/8AlPi and PBT/5AlPi, both show a shoulder at about 55 s.

For the analysis of the flame retardant mechanism the THR/TML was determined: a reduction of this value clearly indicates flame inhibition or fuel dilution. This parameter is decreasing in the order PBT (2.1 $MJm^{-2}g^{-2}$) > PBT/10AlPi (1.6 $MJm^{-2}g^{-2}$) = PBT/5AlPi > PBT/8AlPi (1.5 $MJm^{-2}g^{2}$).

Table 11 Cone calorimeter results for PBT/AlPi formulations (irradiance 50 KW m^{-2}). Error based on maximal deviation of averaged values.

	Cone Calorimeter 50 KWm^{-2}						
	PHRR	**THE**	**Residue**	**THE/TML**	**CO yield**	**TSR**	**THR^{60s}/t_{ign}**
	KWm^{-2}	MJm^{-2}	wt%	$mJm^{-2}\ g^{-1}$	Kg/ Kg	m^2m^{-2}	$KWm^{-2}s^{-1}$
Error	± 50	± 2	± 0.5	± 0.1	± 0.002	± 50	± 2
PBT	1404	74	/	2.1	0.0589	1359	16
PBT/5AlPi	1172	53	3.6	1.6	0.1242	2328	12
PBT/8AlPi	1009	50	5.6	1.5	0.1071	2495	10
PBT/10AlPi	1291	63	6.8	1.6	0.1056	2584	7

Both smoke and CO production, resulting from incomplete combustion, were evaluated for the determination of the fire hazards. A strong increase in the CO release is evident in all the formulations containing the flame retardant, supporting the idea that P acts as a radical trapping in the gas phase suppressing the total oxidation processes.[103] Except for PBT, the pattern of RCOR does not correspond to the pattern of HRR. The RCOR for all the PBT/AlPi formulations exhibits two maximum, the first one corresponds to the HRR and therefore to the burning of the polymer (100 s), while the second one is attributed to the burning of the Al-phosphate char (125 s). In PBT/10AlPi the RCOR curve is shifted at lower time, so the first peak corresponding to the burning of the polymer is located at about 75 s and the combustion of the char occurs already at about 85 s. A general increase in the TSR is observed and is correlated to the increase amount of flame retardant. An increase of 42% in the TSR is found in PBT/5AlPi, 46% in PBT/8AlPi and 48% in PBT/10AlPi (in comparison to plain PBT). For the correlation between the flammability results and cone, the first stages of the burning are taken into account. The ratio between the average THR in the first stage of burning (from ignition to ignition + 60s, THR^{60s}) and the t_{ign} is considered an indicator of flame spread. The lowest value of this ratio means the higher barrier to flame propagation. The evaluation of this ratio among all the formulations (Table 11) perfectly correlates with the LOI and UL94 results.

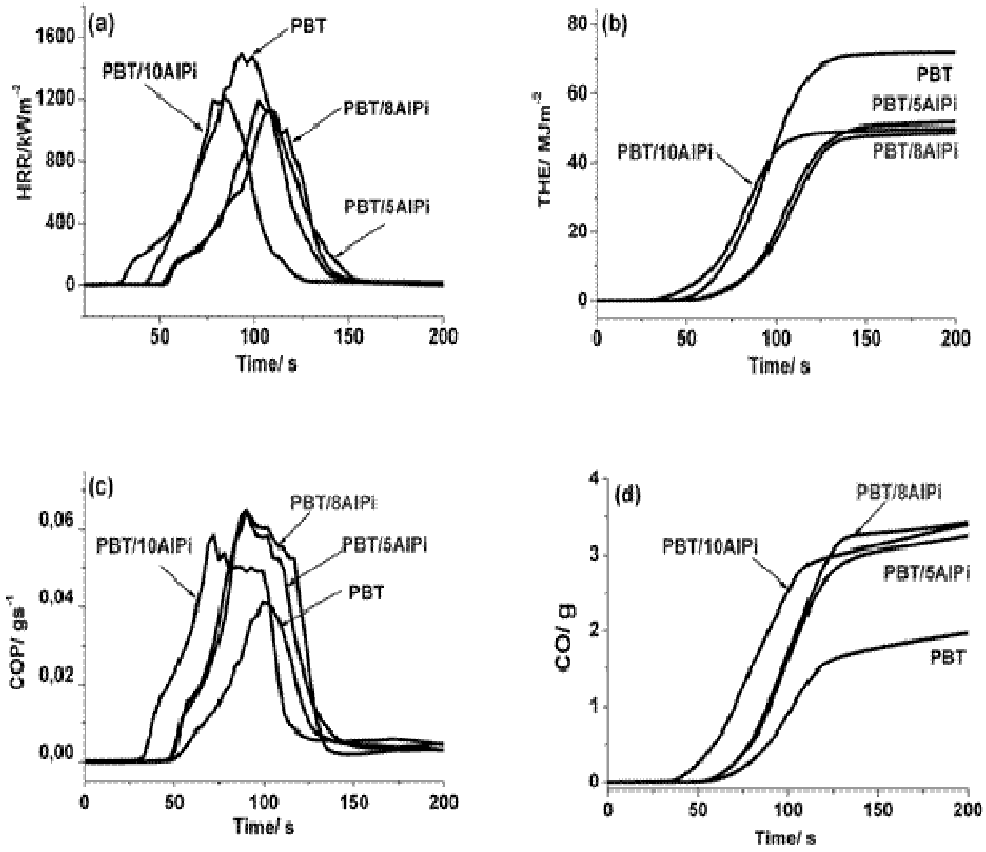

Fig. 39 (a) HRR, (b) THE, (c) CO production rate and (d) CO production of all of the AlPi formulations at 50 KWm^{-2}.

4.6.2. PBT/AlPi/TiO_2 formulations

The comparison of cone calorimeter test results for TiO_2 formulations are summarized in Table 12 and illustrated in Fig. 40. For PBT the HRR is characterized by an intensive peak with a maximum of 1404 KWm^{-2} and a THE by about 74 MJm^{-2}. When 8 wt% of AlPi is added in PBT/8AlPi, a reduction of about 30% is observed together with a shift of the PHHR at about 125 s. The presence of TiO_2 in PBT/Ti reduced the HRR of PBT. The PHRR is reduced of about 20% while a larger decrease of about 30% is observed in the THE. The combination of both AlPi and TiO_2 in PBT/8AlPi/Ti shows an antagonistic effect on both the THE and the HRR. Both additives have a positive effect in reducing these values but only when they are not blended together. Significant is the increase in the residue amount left after combustion. 2 wt% of TiO_2 in PBT/Ti gives rise to a 7 wt%

of residue. Once again, the combination of both additives in PBT/8AlPi/Ti shows an antagonistic effect on the residue collected at the end of cone test. No reduction of THE/TML is showed in PBT/Ti formulation. The increase of CO and smoke is ordered according to PBT/8AlPi> PBT/8AlPi/Ti> PBT/Ti> PBT. The order of sample correlates with the flame inhibition action of phosphorous. In PBT/8AlPi, the phosphorous acts mainly in the gas phase, whereas the gas-phase activity of PBT/8AlPi/Ti is reduced. The addition of TiO_2 in PBT/Ti slightly decreases the total carbon monoxide release, indicating a better ventilated combustion process due to the presence of a barrier former.

Table 12 Cone calorimeter results for TiO_2 formulations (irradiance 50 KW m^{-2}). Error based on maximal deviation of averaged values.

	Cone Calorimeter 50 KWm^{-2}						
	PHRR	**THE**	**Residue**	**THE/TML**	**CO yield**	**TSR**	**THR^{60s}/t$_{ign}$**
		MJm^{-}	wt%	mJm^{-2} g^{-1}	Kg/ Kg	m^{2}m^{-2}	KWm^{-2}s^{-1}
Error	± 50	± 2	± 0.5	± 0.1	± 0.002	± 50	± 2
PBT	1404	74	/	2.1	0.0589	1359	16
PBT/8AlPi	1009	50	5.6	1.5	0.1071	2495	10
PBT/Ti	1138	73	7.0	2.0	0.0562	1459	17
PBT/8AlPi/Ti	1162	54	9.0	1.5	0.1050	2152	10

Correlation between the flammability results and cone in PBT/AlPi/Ti is less evident. The differences in the PHHR are not as significant as to explain the UL94 results. For this reason the THR^{60s}/ t$_{ign}$ is taken into account. In this case the same reduction of this ratio is found for PBT/8AlPi and PBT/8AlPi/Ti meaning that they show the same barrier to flame propagation.

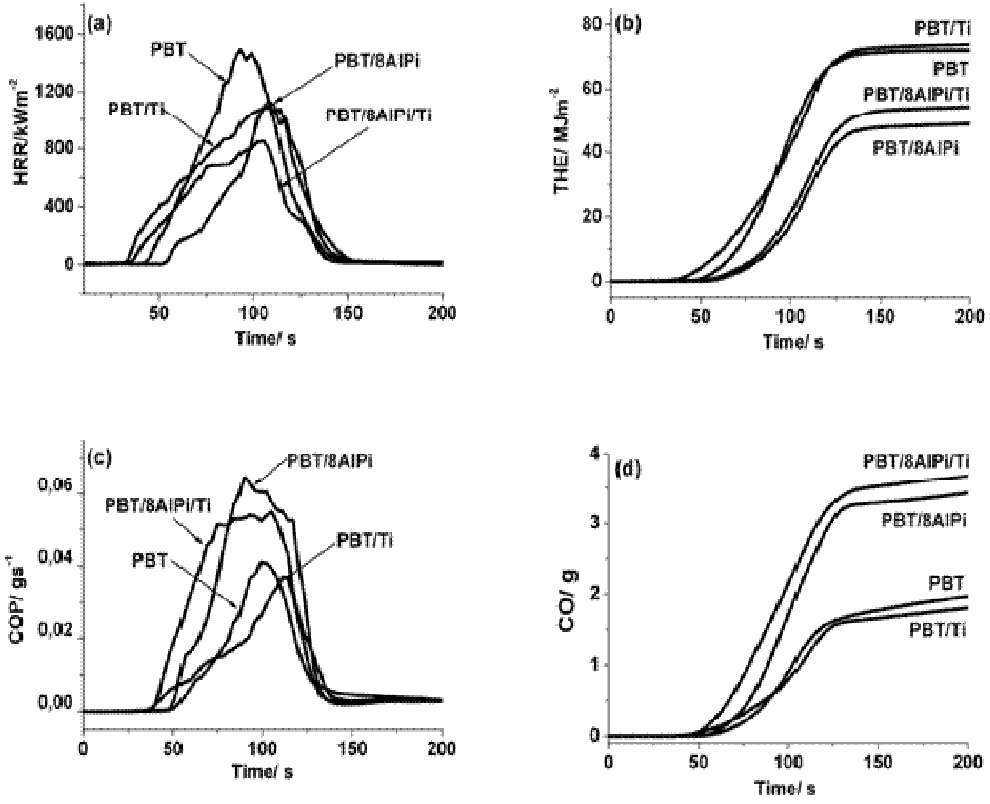

Fig. 40 (a) HRR, (b) THE, (c) CO production rate and (d) CO production of all of the TiO_2 formulations at 50 KWm^{-2}.

4.6.3. PBT/AlPi/ Al_2O_3 formulations

Al_2O_3 does not seem to have an effect in both HRR and THE in comparison to PBT. A slight increase of the PHRR of about 13 % is found in PBT/Al while the THE remains the same. The combination of both additives in PBT/10AlPi/Al shows a decrease in the PHHR in comparison to PBT but not in comparison to PBT/10AlPi. The addition of Al_2O_3 does not help in further reducing the PHRR. A positive effect of Al_2O_3 in PBT/Al but especially in PBT/10AlPi/Al is the shift if the time to ignition to later time. With PBT/10AlPi/Al the PHRR is located at about 125 s, about 50 s more than PBT/10AlPi. Also with Al_2O_3 particles an additional amount of residue is collected at the end of combustion. In PBT/Al an additional amount of 5.1 wt% is found but this positive effect is not found in PBT/10AlPi/Al, where the residue is only 8.1 wt%. The slight systematic reduction of THE/TML in the order PBT> PBT/Al> PBT/10AlPi >PBT/10AlPi/Al is caused by fuel

dilution due to the release of non-combustible pyrolysis products. For PBT/10AlPi/Al, the THE/TML was clearly reduced compared to PBT.

Table 13 Cone calorimeter results for Al_2O_3 formulations (irradiance 50 KW m^{-2}). Error based on maximal deviation of averaged values.

Cone Calorimeter 50 KWm^{-2}							
	PHRR	**THE**	**Residue**	**THE/TML**	**COyield**	**TSR**	**THR^{60s}/t_{ign}**
Error	KWm^{-2} ± 50	MJm^{-} ± 2	wt% ± 0.5	$mJm^{-2}\ g^{-1}$ ± 0.1	Kg/ Kg ± 0.002	m^2m^{-} ± 50	$KWm^{-2}s^{-1}$ ± 2
PBT	1404	74	/	2.1	0.0589	1359	16
PBT/10AlPi	1291	63	6.8	1.6	0.1154	2584	7
PBT/Al	1604	76	5.1	2.0	0.0640	1279	17
PBT/10AlPi/Al	1306	59	8.1	1.5	0.1013	1959	11

A clear increase in the CO production in comparison to plain PBT is observed in all the formulations containing AlPi. The addition of Al_2O_3 in PBT slightly increases the CO yield while it promotes the reduction of CO yield in combination with AlPi in PBT/10AlPi/Al. The TSR among all the formulations follows the same trend. A strong increase in the TSR is caused by a suppressed total oxidation process and indicates a radical trapping mechanism. As only a reduction in the TSR is found for PBT/Al, an alternative mechanism must be postulated involving a barrier former mechanism. The order in PHRR did not correlate with LOI or UL 94 performance. This is a remarkable result, because generally, at least rough correlations are expected since the reaction to small flame in UL 94 and LOI is controlled by a critical HRR or flame spread resulting in extinction. In addition, the high PHRR values observed between 1306 and 1291 KWm^{-2} are clearly atypical for materials showing V-1 or V-0 classification in UL 94 and LOI values of 29.4 and 31.3 %, respectively. It is proposed that the PHRR occurring at the end of the burning may be somewhat misleading with respect to the assessment of the flammability behaviour of the investigated materials. The index THR^{60s}/t_{ign} emphasizes the HRR at the

beginning of burning as responsible for flame spread rather than the maximum HRR. The THR^{60s}/t_{ign} showed the order: PBT/10AlPi ≤ PBT/10AlPi/Al ≤ PBT < PBT/Al. Thus there is a very good correlation with LOI and a reasonable one with the materials' UL 94 performance.

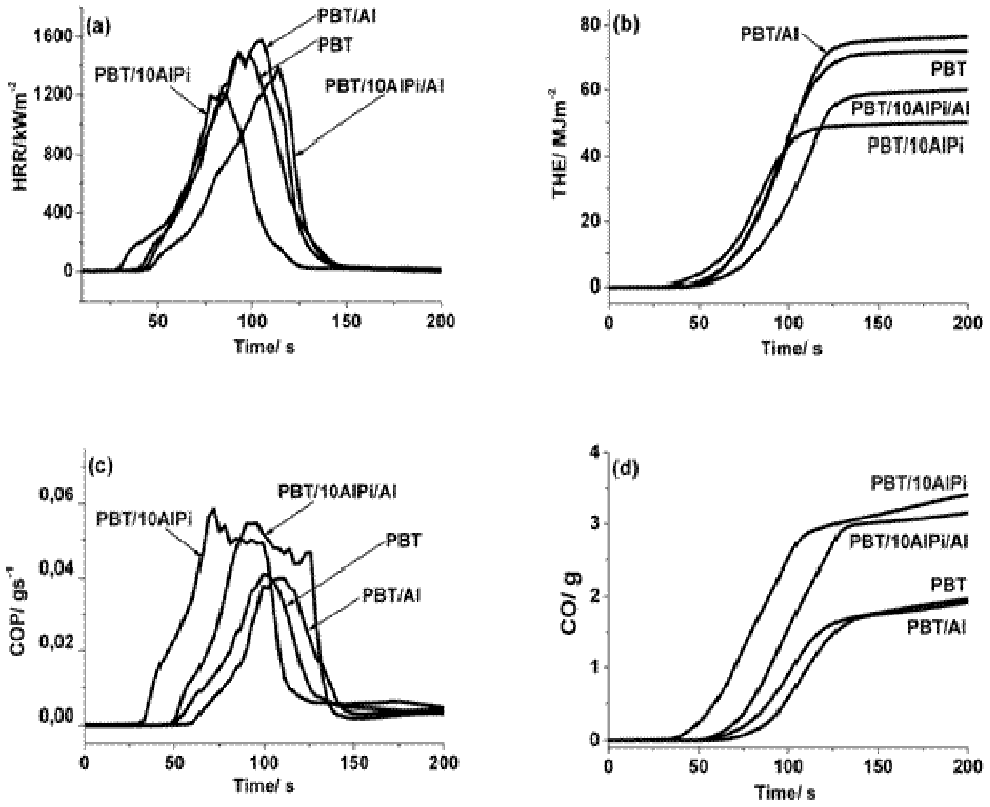

Fig. 41 (a) HRR, (b) THE, (c) CO production rate and (d) CO production of all of the Al_2O_3 formulations at 50 KWm^{-2}.

4.6.4. PBT/AlPi/ Fe_2O_3 formulations

The cone results for the two different groups of Fe_2O_3-fomulations are summarized in Table 14. The cone results correlating to the 5 wt%-AlPi system are shown in Fig. 42. The addition of Fe_20_3 in PBT/Fe leads to a 23% reduction of PHHR and 10% reduction of THE. The addition of Fe_2O_3 in PBT/5AlPi/Fe further decreases the THE to 46 MJm^{-2} in comparison to PBT/5AlPi but increases again the PHHR to 1242 KWm^{-2}. Fe_2O_3 helps increasing the residue amount of 5.3% in comparison to PBT. The residue collected for PBT/5AlPi/Fe is 7.3 wt%, higher than PBT/Fe and PBT/5AlPi but clearly less than expected, basing the calculation on the sum of the

residues collected by each additive alone. The reduction in the THE/TML follows the order PBT> PBT/Fe >PBT/5AlPi/Fe> PBT/5AlPi. As shown in Fig. 42, a clear reduction of the CO production is observed in PBT/Fe while in all the formulation containing AlPi, the amount of CO and smoke is higher than PBT. The index THR^{60s}/t_{ign} showed the order PBT/5AlPi ≤ PBT/Fe ≤ PBT < PBT/5AlPi/Fe. Taking into consideration the second group of Fe_2O_3 formulations, with a higher amount of AlPi, surprisingly, PBT/8AlPi/Fe gets the best result in terms of the PHHR, reduced of about 66% in comparison to PBT. As shown in Fig. 43 also the shape of the curve of HHR is clearly different in comparison to all the other formulations. PBT/8AlPi/Fe shows the typical shape of a charring material. The formation of a char layer that insulates the underlying material is postulated. The cross-linking reactions in the presence of Fe_2O_3 proceed through a Friedel Craft mechanism. Rapid char formation follows the cross-linking reaction. This lower sample temperature results in a lower mass loss rate and thus a lower HRR.

Table 14 Cone calorimeter results for Fe_2O_3 formulations (irradiance 50 KW m^{-2}). Error based on maximal deviation of averaged values.

	Cone Calorimeter 50 KWm^{-2}						
	PHRR	**THE**	**Residue**	**THE/TML**	**COyield**	**TSR**	**THR^{60s}/t_{ign}**
	KWm^{-2}	MJm^{-}	wt%	mJm^{-2} g^{-1}	Kg/ Kg	m^{2}m^{-}	KWm^{-2}s^{-1}
Error	± 50	± 2	± 0.5	± 0.1	± 0.002	± 50	± 2
PBT	1404	74	/	2.1	0.0589	1359	16
PBT/Fe	1093	67	5.3	1.9	0.0473	1464	15
PBT/5AlPi	1172	53	3.6	1.6	0.1242	2328	12
PBT/5AlPi/Fe	1242	46	7.3	1.8	0.0874	1603	21
PBT/8AlPi	1009	50	5.6	1.5	0.1071	2495	10
PBT/8AlPi/Fe	630	56	10.9	1.6	0.0841	2432	11

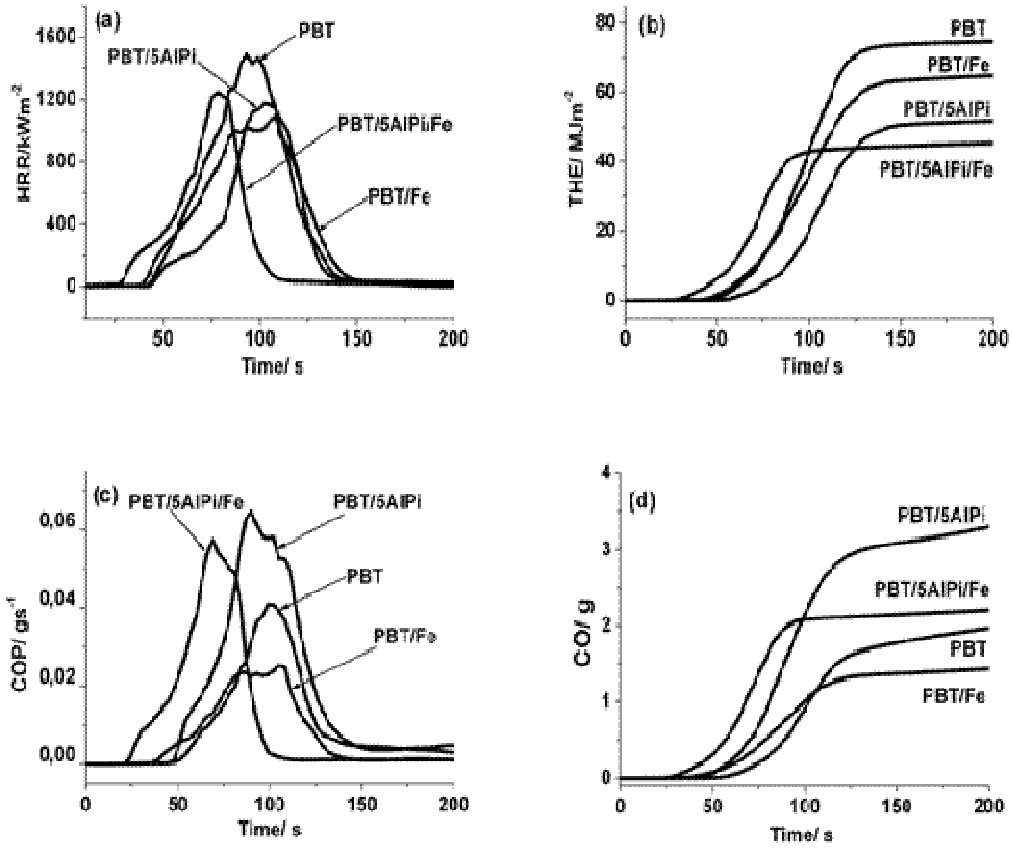

Fig. 42 (a) HRR, (b) THE, (c) CO production rate and (d) CO production of all of the Fe_2O_3 formulations at 50 KWm^{-2}.

The reduction in the THE does not follow the same order than the PHHR. In fact PBT/8AlPi/Fe, that shows the best result in terms HRR, is not the best in term of THE. The reduction in the ratio THE/TML is ordered PBT >PBT/Fe >PBT/8AlPi/Fe> PBT/8AlPi and indicates a reduction of the flame inhibition related to the phosphorous. Both CO quantity and smoke are increased increasing the amount of flame retardant, indicating a radical trapping mechanism. The ratio THR^{60s}/t_{ign} is strongly decreased in PBT/8AlPi and PBT/8AlPi/Fe (in comparison to PBT).

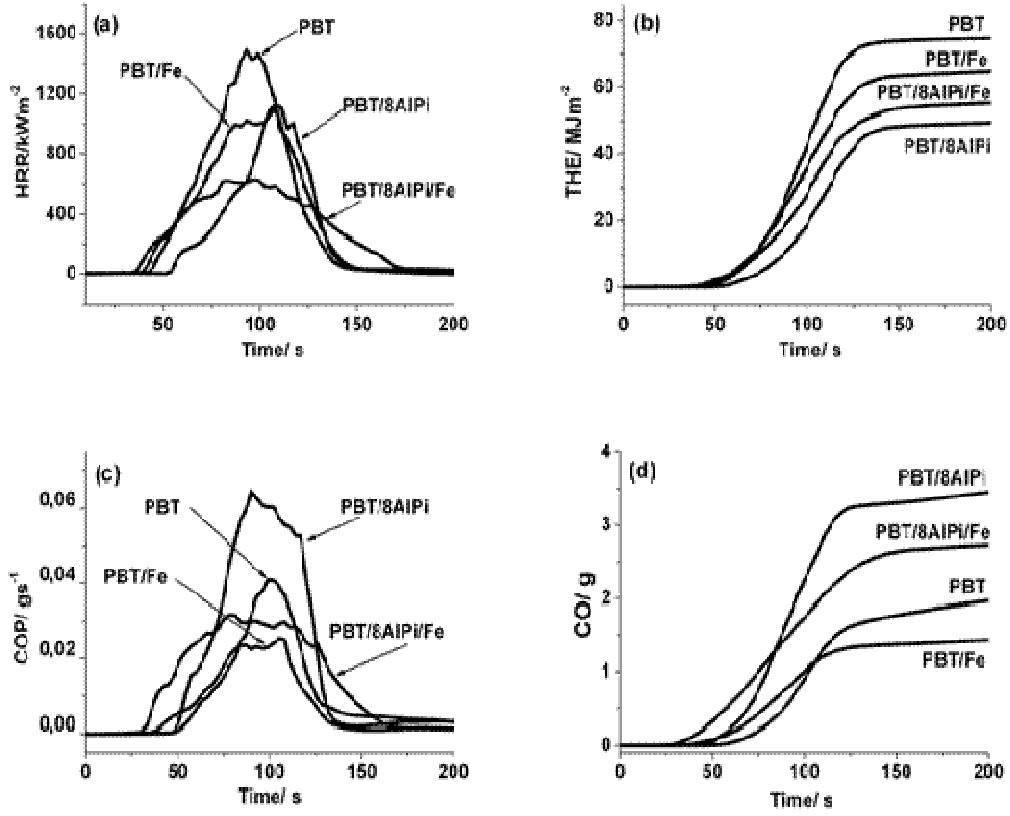

Fig. 43 (a) HRR, (b) THE, (c) CO production rate and (d) CO production of all of the Fe_2O_3 formulations at 50 KWm^{-2}.

4.6.5. PBT/AlPi/ Sb_2O_3 formulations

The results of all the Sb_2O_3 formulations are shown in Fig. 44 and Fig. 45. Sb_2O_3 in PBT/Sb does not lead to any significant decrease in the PHHR. Also, the shape of the HRR curve is very close to the one of PBT, with a sharp, high peak located at about 1437 KWm^{-2}. In comparison to PBT/8AlPi and PBT/5AlPi, the inclusion of Sb_2O_3 increases in both cases. The PHHR and the THE shows the best results for PBT/8AlPi/Sb and PBT/5AlPi/Sb, with a value of 44 and 42 MJm^{-2} respectively. Among all the other nanoparticles of metal oxides, Sb_2O_3 seems to be the less effective in increasing the residue amount. The amount of char found at the end of combustion corresponds roughly to the initial loading of additive. Apart from PBT and PBT/Sb, all the other formulations show the same value of THE/TML indicating the same flame inhibition effect, depending on the amount of AlPi.

Table 15 Cone calorimeter results for Sb_2O_3 formulations (irradiance 50 KW m^{-2}). Error based on maximal deviation of averaged values.

Cone Calorimeter 50 KWm^{-2}							
	PHRR	**THE**	**Residue**	**THE/TML**	**CO yield**	**TSR**	**THR^{60s}/t$_{ign}$**
	KWm^{-2}	MJm^{-}	wt%	mJm^{-2} g^{-1}	Kg/ Kg	m^{2}m^{-2}	KWm^{-2}s^{-1}
Error	± 50	± 2	± 0.5	± 0.1	± 0.002	± 50	± 2
PBT	1404	74	/	2.1	0.0589	1359	16
PBT/Sb	1437	67	2.4	1.9	0.0555	1538	14
PBT/5AlPi	1172	53	3.6	1.6	0.1242	2328	12
PBT/5AlPi/Sb	1281	42	4.8	1.6	0.1001	1574	15
PBT/8AlPi	1009	50	5.6	1.5	0.1071	2495	10
PBT/8AlPi/Sb	1216	44	5.6	1.5	0.0998	1792	13

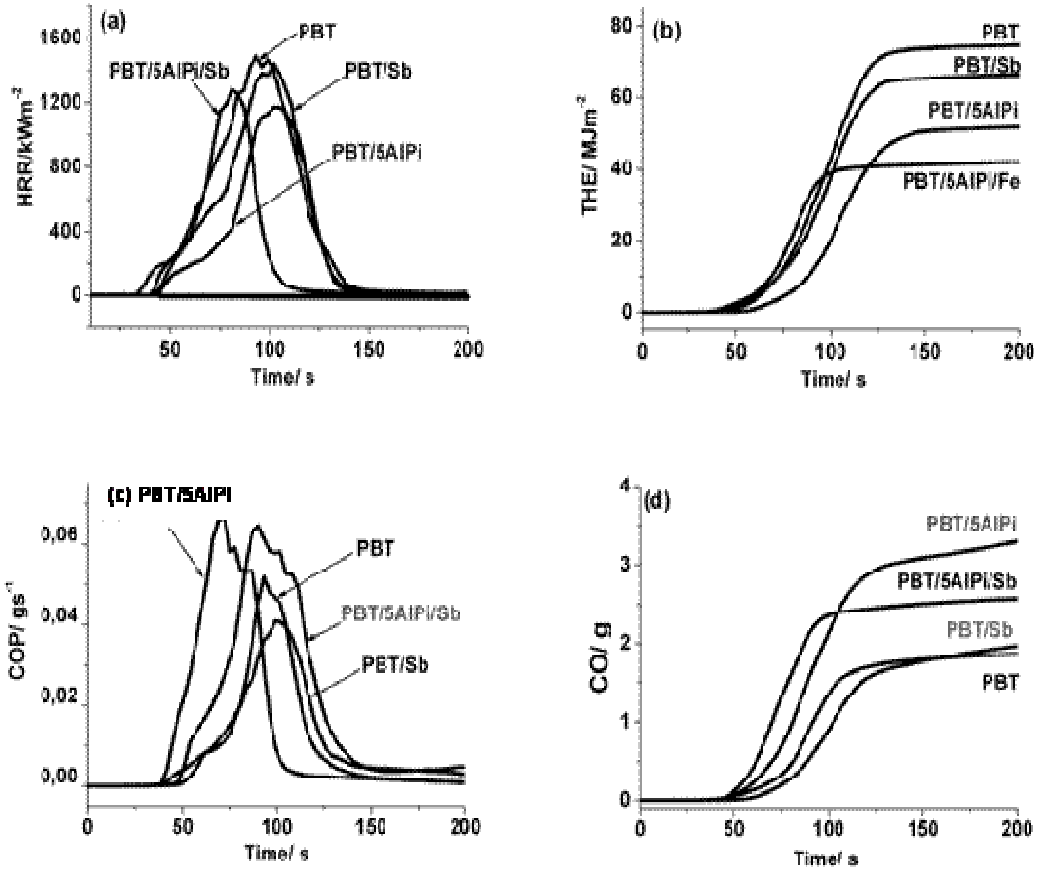

Fig. 44 (a) HRR, (b) THE, (c) CO production rate and (d) CO production of all of the Sb_2O_3 formulations at 50 KWm^{-2}.

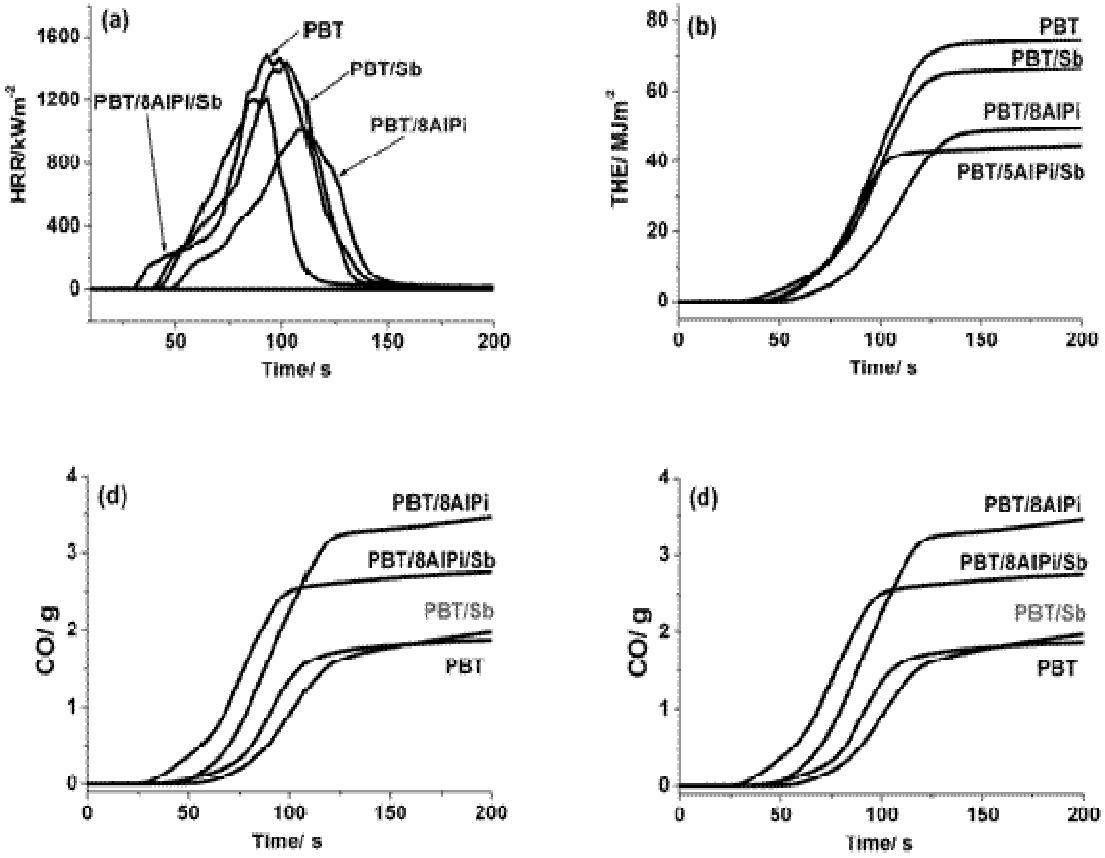

Fig. 45 (a) HRR, (b) THE, (c) CO production rate and (d) CO production of all of the Sb_2O_3 formulations at 50 KWm^{-2}.

The CO yield increases (in comparison to PBT) in all the formulations containing AlPi. Only in PBT/Sb, the quantity of CO is reduced. The TSR significantly increases in PBT/8AlPi and PBT/5AlPi, while the combination with Sb_2O_3 reduces the smoke production in comparison to the same amount of flame retardant. The THR^{60s}/t_{ign} is ordered PBT/8AlPi ≤ PBT/5AlPi ≤ PBT/8AlPi/Sb < PBT/Sb ≤ PBT/5AlPi/Sb ≤ PBT.

4.6.6. Fire behaviour: residue analysis

In order to understand the improved flame retardancy in moderate fires, the residues obtained at the end of cone test were homogenised and analysed by means of ATR-FTIR. The amount of residue measured using external heat flux of 50 KWm^{-2} increases in the order: PBT/Me-Oxide >PBT/AlPi/Me-oxide > PBT/AlPi. Me-oxides nanoparticles have a positive effect in improving the amount of residue but this synergistic effect is

suppressed in combination with AlPi. In all the PBT/AlPi formulations, the residue collected corresponds roughly at the initial loading of flame retardant.

All the formulations containing AlPi showed similar spectra where aluminium phosphate signals were observed as a broad band around 1115 and 720 cm^{-1} (Fig. 46). The spectra of pure AlPi burned in air up to 900 °C was taken as reference spectra (Fig. 46 left).The changed intensity of these signals is based on a reduced aluminium phosphate formation or a changed relative rate of various aluminium phosphates (ortho, pyro and polyphosphate). When the sample decomposes very quickly, as happened in cone calorimeter experiments, the formation of Al-phosphates competes with the vaporization of AlPi. Hence, phosphorous action in the gas phase was decreased (see THE/TML in cone results tables). When AlPi decomposes, the resulting phosphinate ion can induce the carbon char formation of the polymer. As already shown in all PBT/AlPi/Me-oxide formulations, an increased amount of char was found. In Fig. 47 the pictures of cone calorimeter experiments are shown. The interpretation of some synergistic effects of the Me-oxide combinations on fire behaviour of PBT (in comparison with only AlPi or Me-oxides) can be developed by considering that each kind of component could play a different role in relation to the flame behaviour of PBT. Considering the first stages of degradation of PBT, the specific role of AlPi seems well identified since, in the presence of this component, a gas phase action is found due to the phosphorous activity. In the latter stages of PBT decomposition, part of the phosphorous induces char formation in the solid phase. As shown in Fig.47 the residue appears not homogeneous but full of cracks. The high flame retardant action in the gas phase reduces significantly the amount of phosphorous that can undergo charring. In addition, the departure of the organic part of AlPi only leaves inorganic phosphate in the residue. The incorporation of oxide nanoparticles in PBT leaves an amount of residue that is clearly higher than the initial loading content. Me-oxides in PBT promote charring processes through cross-linking reactions of the polymer. The surface of PBT/Ti, PBT/Al and PBT/Fe appears to be more

homogeneous and crack-free. In PBT/Sb, the amount of residue is negligible to discuss about char forming process.

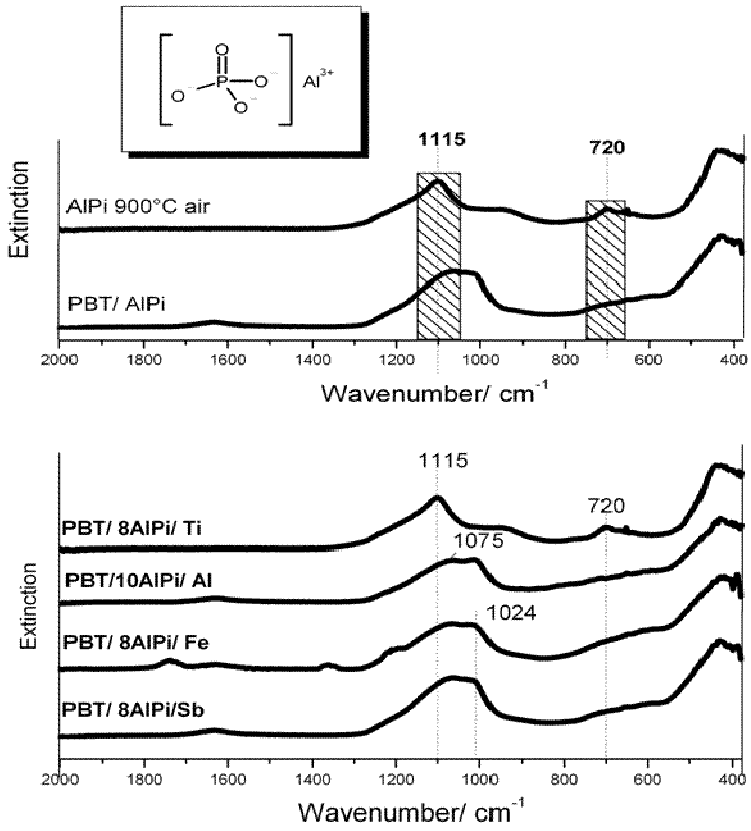

Fig. 46 ATR-FTIR of residue obtained in the cone calorimeter after combustion at 50 KWm^{-2}.

This behaviour could be explained by:

(1) The higher thermal stability of these oxides that act as a "heat sink" which can limit the thermal conduction inside the material and thereby the kinetics of degradation;

(2) Limitation of gas emission due to an increase in viscosity of the melt in the presence of metal oxide;

(3) Enhanced wetting of mineral compounds by the molten polymer at the highest temperature combined with the convection forces arising from temperature gradients existing in the sample, could lead to the particles migration towards the radiated surface.

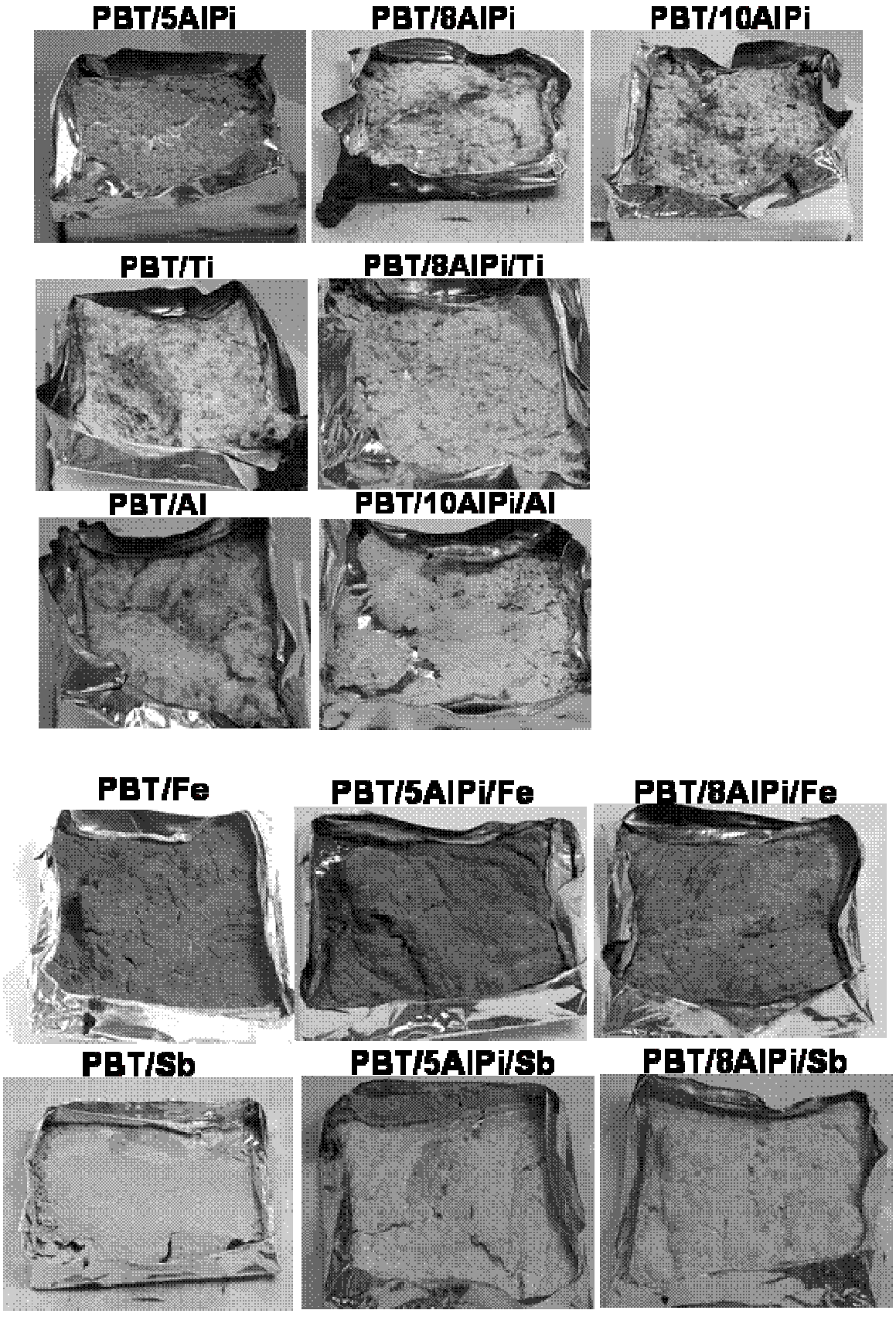

Fig. 47 Photos of the residue collected after cone calorimeter tests.

4.6.7. Fire behaviour conclusions

A positive interaction is found between metal oxides nanoparticles in PBT. In the formulations containing only metal oxides, no significant effect is found: the THR is very close to PBT, sometimes slightly higher. As expected, the reduction in the HRR for the ternary formulations results in a corresponding reduction in the THR.

The residues obtained in the cone calorimeter were analysed by means of ATR-FTIR. No residue was collected for PBT while all the other formulations left different percentages of a white porous residue. Combination of AlPi in PBT increases the residue amount mainly consisting of inorganic Al-orthophosphate. The characteristic signals are detected at 1110 and 715 cm^{-1}. In all the P-formulations it was possible to observe these peaks although the different shapes: this different behaviour was due to a change of the relative rate of various aluminium phosphates (orthophosphate, pyrophosphate and polyphosphate). PBT and nanoparticles combine beneficially with regard to the residue amount (7 wt% for TiO_2, about 5 wt% for Al_2O_3 and Fe_2O_3 and 2.4 wt% for Sb_2O_3), consisting of polyaromatic carbonaceous char.[104] An antagonism effect is found with the incorporation of both AlPi and metal oxides in PBT/8AlPi/Ti, PBT/10AlPi/Al, PBT/8AlPi/Fe-Sb, PBT/5AlPi/Fe-Sb: the residue amount is less than expected and consists only of Al-phosphate.

Correlations between flammability results (UL94, LOI) and forced flaming combustion are discussed. AlPi combines beneficially in PBT/AlPi with respects to UL94 test, LOI and cone calorimeter. A strong gas phase action is assumed according to THR/TML value, in comparison to PBT.

Metal oxides combined into PBT give the best results regarding the residue amount: both TG and cone experiments agree with each other on a strong synergism between metal particles and PBT. The cone test supports the idea that the metal oxide interacts with the polymer creating a more stable cross-linked char that decomposes after the phosphinate´s one.

4.7. Rheological properties

As already highlighted in the introduction of this work, it is well established that thermoplastic polyesters have poor fire resistance and caution has to be applied especially in fields such as transport where safety against accidental burning phenomena must be assured.

In light of this latter consideration, a lot of research work has been dedicated to improve the fire resistance of polyester based compounds. Phosphorous based compounds can be used as FR additives for these materials but normally, to achieve satisfactory results, a relevant amount of the same has to be added (around 20% by weight). Experimental work carried out on these systems has demonstrated that high amounts of FR additive are required. On one side this assures a safe use of polymer based materials on a large scale, on the other hand, it may compromise its processability by increasing the bulk viscosity or it may increase the smoke emission.

Recently, nanostructured polymer formulations have shown promising perspectives in terms of fire performances acting with different mechanisms. In particular, barrier (char) formation, nanoparticle network and the increase of melt viscosity are recognised as the main general fire retardancy mechanisms of polymer nanocomposites. Technical difficulties in this arise from the need to have a good distribution of the nanoscale filler within the polymer matrix in order to achieve satisfactory results. This target is usually difficult to approach, mainly because of high viscosity of the matrix at operative conditions and/or intrinsic chemical features of the host nanofiller that prefer to cluster rather than distribute within the surrounding of the neighbourhood matrix.

The aim of this chapter is to investigate effects of nanoparticle additions on the rheological behaviour of ternary formulations that are based on poly(butylene terephthalate) and that containing a relatively low amount of a traditional P-based fire retardant.

4.7.1. Steady shear results

In Figs 48-51 the ratio between the shear viscosity of the materials and the shear viscosity of the reference system coded as PBT* (η*) is reported as a function of the shear rate for different formulations.

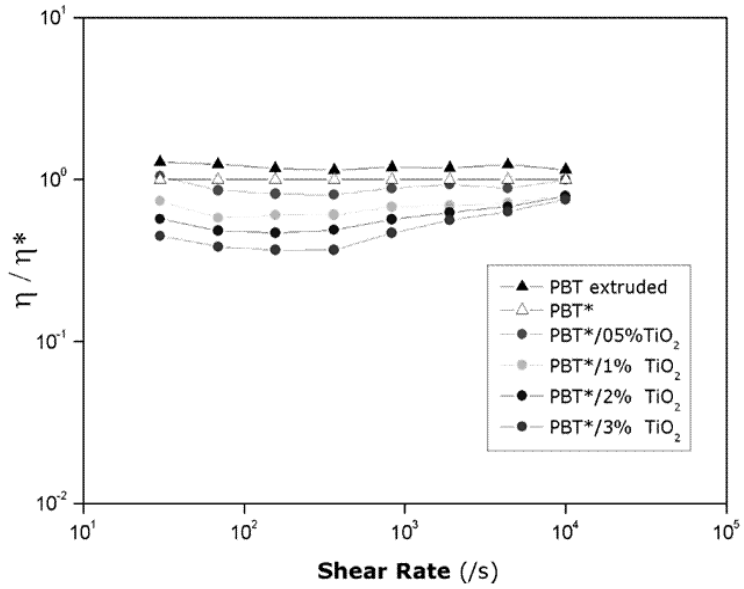

Fig. 48 Relative viscosity of TiO_2 based compounds as a function of the shear rate.

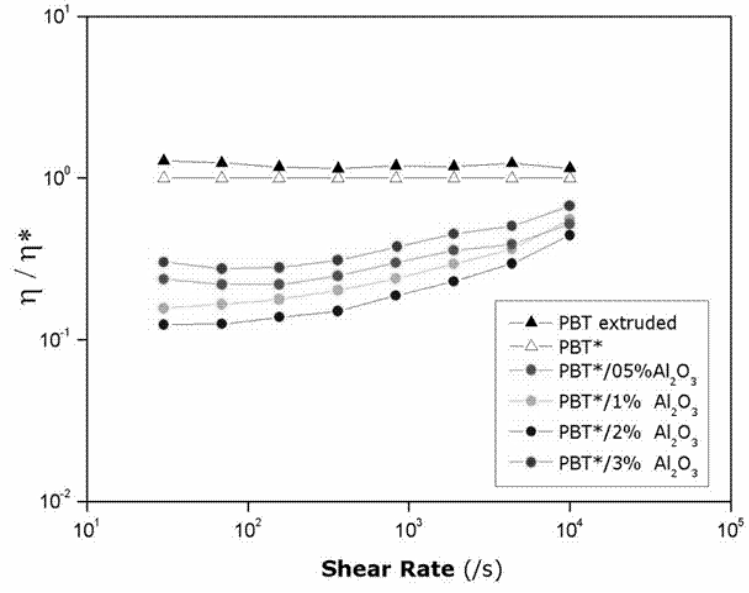

Fig. 49 Relative viscosity of Al_2O_3 based compounds as a function of the shear rate.

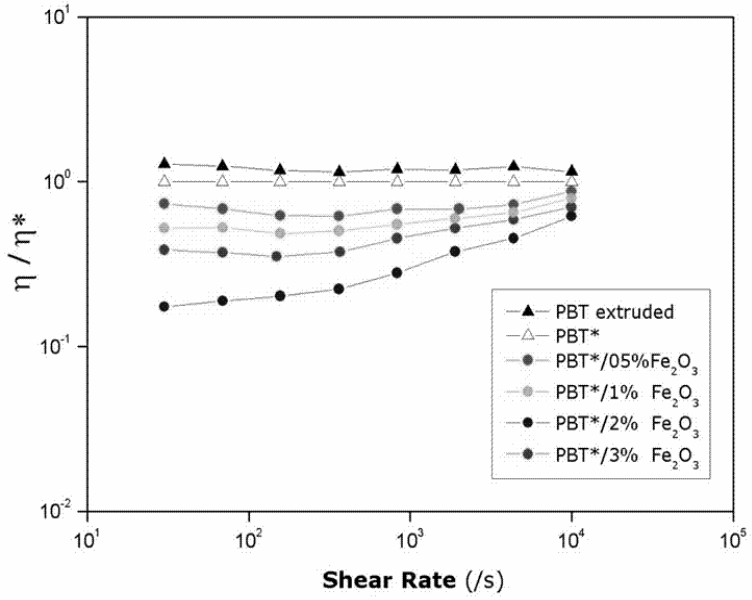

Fig. 50 Relative viscosity of Fe_2O_3 based compounds as a function of the shear rate.

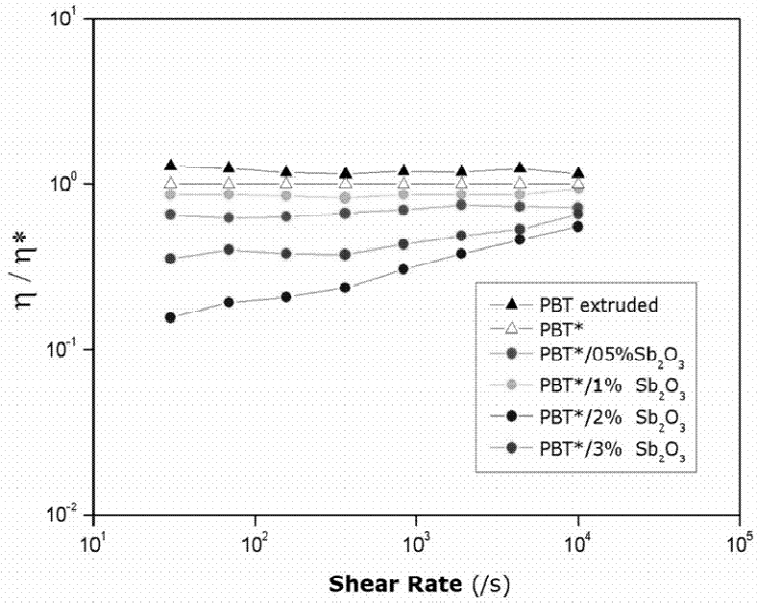

Fig. 51 Relative viscosity of Sb_2O_3 based compounds as a function of the shear rate.

In all cases, a reduction of the shear viscosity is observed for nanocomposites formulations with respect to the reference system. The effect is particularly marked at low shear rates and it seems to show a non monotonic trend with the nanoparticles content.

4.7.2. Rotational measurements data

Regarding dynamic oscillatory measurements, it is well established for systems including lamellar clays or carbon nanotubes that increasing the filler content, a transition from liquid to solid like viscoelastic behaviour typically occurs. The effect is explained by the restrainement of the long range motion of polymer chains including nanoparticles and to a weakening of the G'-frequency dependence. In other words, the nanocomposite formulations reach a rheological percolation at which the nanoparticle interactions dominate over polymer chain interactions and the magnitude of the G' plateau is known to correlate with the density of connections in the network. This behaviour is confirmed for pseudo-spheric nanoparticles.

As shown in Fig. 52-53 for titanium oxide and alumina, the low frequency slope of G' curves significantly decrease as clearly shown in the tables.

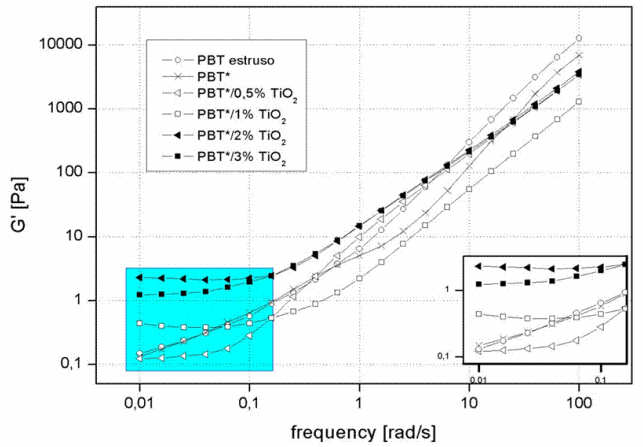

Materials	Slope for ω<0.1 rad/s
Extruded PBT	0.78
PBT *	0.72
PBT*/05%TiO_2	0.91
PBT*/1%TiO_2	0.25
PBT*/2%TiO_2	0.10
PBT*/3%TiO_2	0.30

Fig. 52 G' vs frequency for TiO_2 in combination with PBT.

Going through the elaboration of collected data, it is known from the literature that the bulk stiffness of the composites, i.e. the ratio between the storage modulus of the nanocomposite formulation and the storage modulus of the reference matrix, varies phenomenologically with the mass loading according to a power law were the rheological percolation threshold ϕc and the critical exponent υ are dependent on the oscillatory shear frequency.

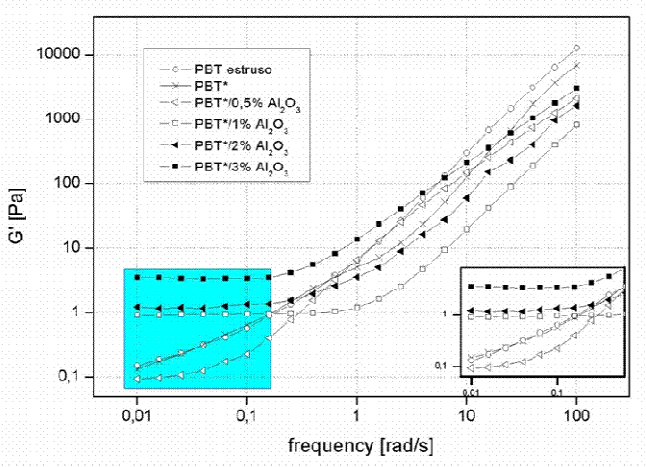

Materials	Slope for ω<0.1 rad/s
Extruded PBT	0.78
PBT *	0.72
PBT*/0,5% Al_2O_3	0.56
PBT*/1% Al_2O_3	0.03
PBT*/2% Al_2O_3	0.09
PBT*/3% Al_2O_3	0.02

Fig. 53 G' vs frequency for Al_2O_3 in combination with PBT.

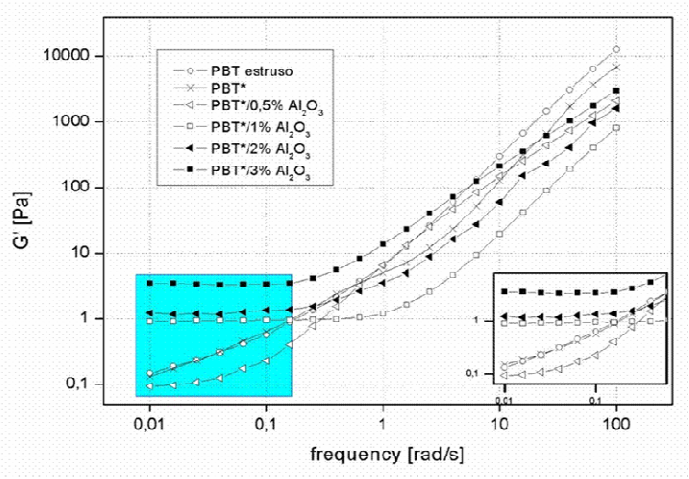

Materials	Slope for ω<0.1 rad/s
Extruded PBT	0.78
PBT *	0.72
PBT*/05%Fe_2O_3	0.14
PBT*/1%Fe_2O_3	0.09
PBT*/2%Fe_2O_3	0.10
PBT*/3%Fe_2O_3	0.19

Fig. 54 G' vs frequency for Fe_2O_3 in combination with PBT.

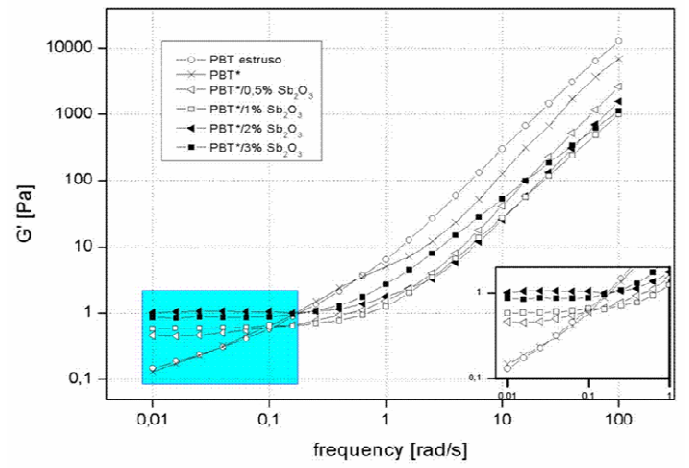

Material	Slope for ω<0.1 rad/s
Extruded PBT	0.78
PBT *	0.72
PBT*/0.5%Sb_2O_3	0.18
PBT*/1%Sb_2O_3	0.17
PBT*/2%Sbb_2O_5	0.15
PBT*/3%Sb_2O_3	0.13

Fig. 55 G' vs frequency for Sb_2O_3 in combination with PBT.

Determining all the rheological percolation threshold at the frequency of 0.025 for all nanostructured materials it is possible to quantifying by a simple best fitting procedure the value of the critical exponent.

$$G'/G'^* \propto [(\phi-\phi c)/\phi c)]\ \upsilon$$

where ϕc and υ are dependent on the oscillatory shear frequency.[105] The results are presented in the following plots.

TiO_2 inclusions- ϕc~1.00%

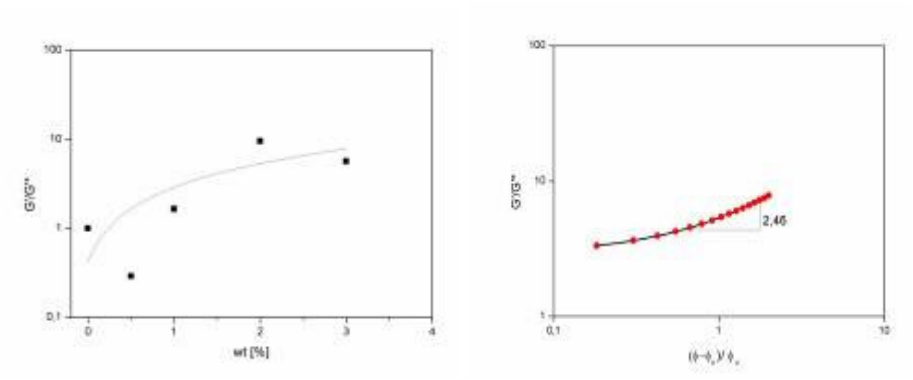

Al_2O_3 inclusions- ϕc~1.00%

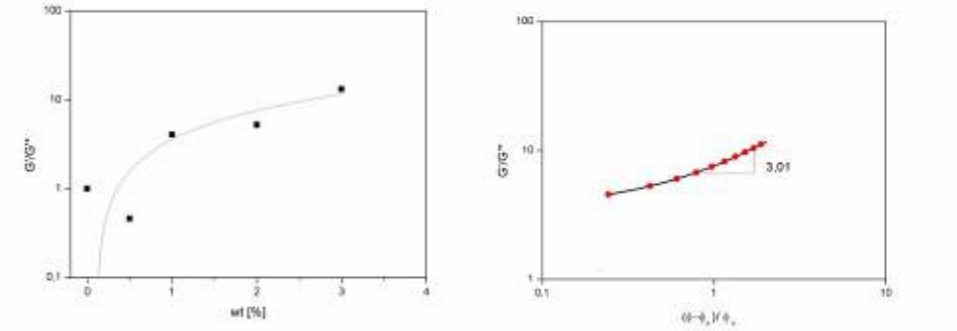

Fe_2O_3 inclusions- ϕc~0.50%

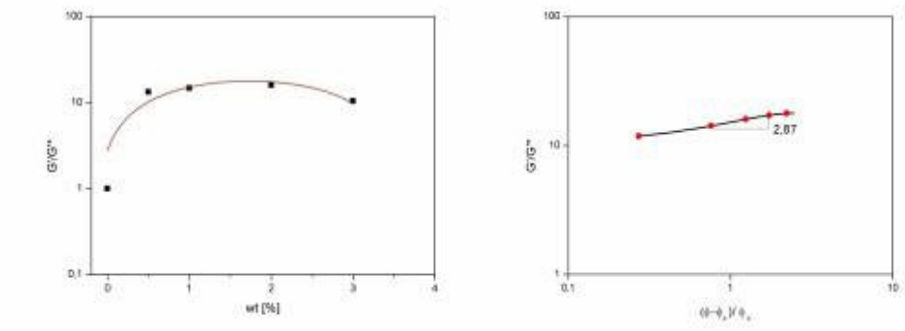

Sb_2O_3 inclusions-- ϕc~0.50%

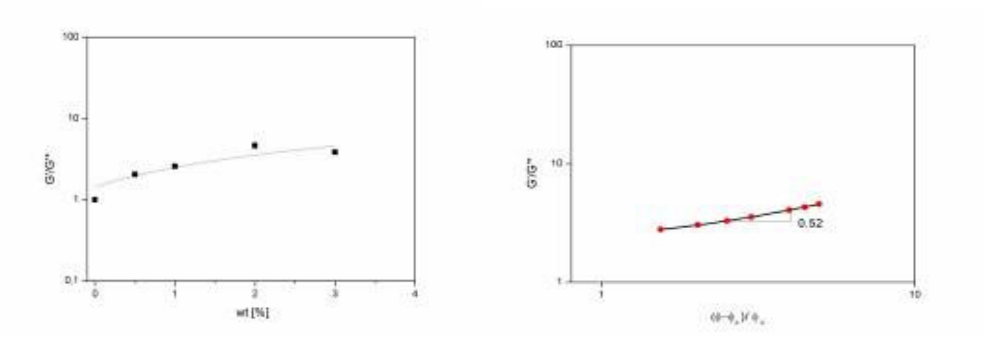

Summarising, percolation parameters are collected in Table 16.

Table 16 Percolation parameters

Nanofiller	**Rheological percolation threshold (ϕ - wt %)**	**Critical exponent (υ) ***
TiO_2	1.00	2.46
Al_2O_3	1.00	3.01
Fe_2O_3	0.50	2.87
Sb_2O_3	0.50	0.52

The critical exponent (*) is a measure of the percolation rate; for example, systems containing alumina percolate less rapidly than the ones with iron oxide nanoparticles. According to the percolation theory, it represents the dimensionality of the system.

Regarding the complex viscosity, different materials containing titanium oxide and alumina, are reported. It is clear that for contents of nanoparticles higher than the rheological percolation threshold (equal to 1.00 wt% for both cases) at low frequencies the complex viscosity positively deviates from the viscosity of the reference matrix PBT*, mirroring the increase in G'. In particular, at low frequencies (< 0.1 rad/s), for $\phi \leq \phi c$ the complex viscosity of the nanocomposite is lower or at least equal to the one

of the reference matrix but for $\phi > \phi c$ the complex viscosity reverses its trend beginning to rise.

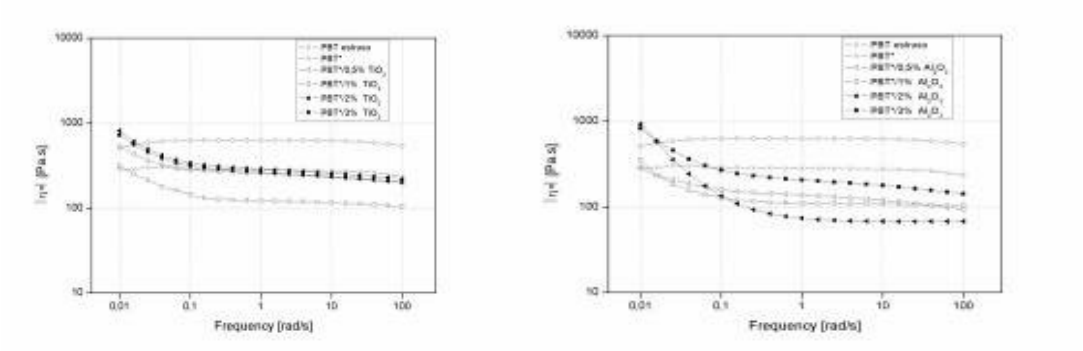

The same can be said for systems containing iron oxide and antimony oxide nanoparticles.

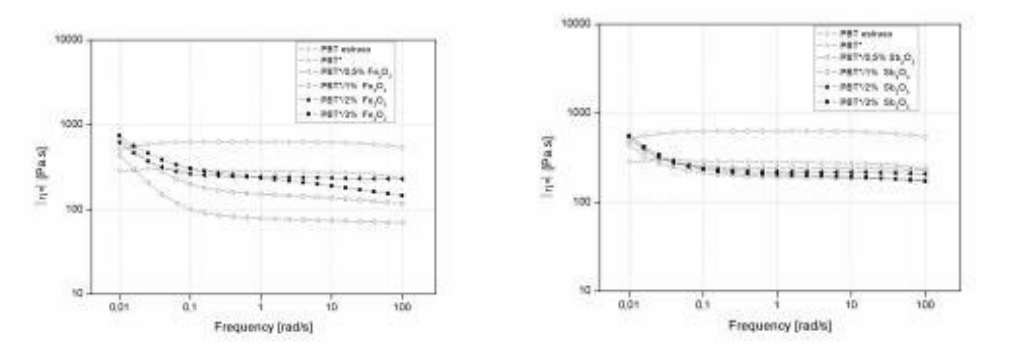

Thus, it is possible to assume that, besides the technique used to measure the viscosity, a key factor is represented by the nanofiller content. In details, for contents lower or at least equal to the rheological percolation threshold, a reduction of the nanocomposite viscosity with respect to the reference matrix is monitored. On the contrary, an increase of both steady shear viscosity and complex viscosity is shown for mass content of filler higher than the rheological percolation and this effect is evident especially at low frequencies.

In other words, considering that a notable aspect of nanocomposites is the size of the average interparticle half gap approximated by the relation:

$$\frac{h}{a} = \left(\frac{\phi_m}{\phi} \right)^{1/3} - 1$$

where a is the mean radius of the included nanoparticles, ϕ_m is the maximun random packing volume fraction (~ 0.638) and ϕ is the content in volume fractions of the nanosized phase. Given the radius of gyration of the matrix:

$$R_g = \frac{1}{6}\left\langle \overline{R}^2 \right\rangle^{1/2} = \frac{a}{6} N^{1/2}$$

normally defined as the Root Mean Square (RMS) distance of the collection of atoms from their common centre of gravity and used to describe the dimensions of a polymer chain, evaluated by light scattering measurements on PBT previously dissolved in an appropriate solvent, it has been demonstrated that the viscosity ratio of the nanoparticle blend with respect to the reference matrix (denoted as PBT* in our case) is a complicated function of the Rg/h ratio.

This behaviour is in line with considerations of Mac Kay et al.[106] according to whom the contents of nanofiller are higher than the percolation threshold, for which it is possible that the interparticle gap may become less than the radius of gyration of the polymer matrix and, as a consequence, that confinement effects occur giving raise to a sharp increase of the viscosity of the polymer melt: micro-rheological effects prevail on macro-rheological ones and an opposite trend may be verified.

When R_g/h is less than 1, no confinement occurs and the viscosity increase sharply with the nanofiller content while, when R_g/h is greater than 1, confinement is responsible of an abrupt decrease in viscosity. Thus, assuming $R_g^* > R_g$, an upward shift of the trends is expected and,

consequently, it results that the confinement effects (i.e. viscosity decreases) prevail on the confinement ones (viscosity increases).

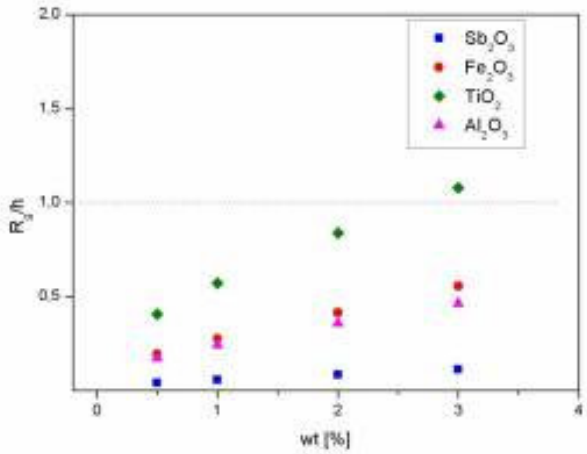

As a conclusion, besides the low contents of nanosized filler viscosity of nanocomposite materials, evaluated both in shear and in oscillatory way, appears to be relevantly influenced.

The entity of these effects, variable with the nanofillers content, results in a preliminary reduction of the viscosity for concentrations less than or equal to the percolation threshold and a subsequent increase of the same rheological parameter for higher contents especially in circumstances where it is likely to assume that the average inter-particle distance could be higher than the radius of gyration of the reference matrix.

CONCLUSION

In this work the flame retardancy mechanisms in halogen-free PBT were investigated for AlPi in combination with different kinds of nanodispersed nanometric metal oxides. Decomposition behaviour was analysed by thermogravimetry, evolved gas analysis and residue analysis. Fire behaviour has been analysed by flammability tests, cone calorimeter measurements, and the chemical analysis of residue.

Adding AlPi in PBT improves the fire resistance in the cone calorimeter test and in UL 94, and increases the LOI value, thanks to a predominant gas-phase action, as confirmed by thermal analysis and cone calorimeter results. AlPi also induces the formation of char consisting of phosphinate-terephthalate salts that decompose to phosphates at higher temperatures.

Small percentages of nanodispersed metal oxides in PBT do not improve UL 94 classification or the LOI. Moreover, the influence on the performance is restricted under forced-flaming conditions in the cone calorimeter. However, interactions between the metal ion and the decomposing PBT promote the formation of some stable carbonaceous char.

When the AlPi is combined with metal oxide nanoparticles, the fire performance of PBT improves; in particular a V-0 classification is achieved using only between 10-5 wt % of AlPi and small percentages of nanoparticles. Thus, the same V-0 ranking is achieved that is usually reported only for higher percentages of AlPi (20 wt %). The combination of efficient flame inhibition due to the release of phosphorus and a solid-phase action by the metal oxide is postulated. Nevertheless, flame inhibition remains the predominant mechanism.

This work has shown the effectiveness of certain inorganic additives. A good dispersion of small percentages of nanometric mineral fillers into PBT seems to be promising in terms of better fire retardant performance, allowing the reduction of the higher levels of flame retardant additive normally required to achieve a good fire classification in terms of UL 94, LOI and cone calorimeter.

ACKNOWLEDGMENTS

E' difficile in poche righe ricordare tutte le persone che, a vario titolo, hanno contribuito alla realizzazione di questa tesi. Innanzitutto desidero ringraziare il prof. Domenico Acierno per aver creduto nelle mie capacità e per avermi offerto la possibilità di compiere questo percorso formativo. Ing. Pietro Russo per essere stato sempre presente, per la sua disponibilità e per avermi seguito durante lo svolgimento del lavoro.

Un ringraziamento al BAM Bundesanstalt für Materialforschung und prüfung di Berlino, in modo particolare a Mr Schartel per aver mostrato fiducia e interesse nel mio lavoro e nelle mie idee, e per avermi accolto come all'interno del gruppo. Ulrike Braun, per tutti i consigli, i suggerimenti e per i lunghi pomeriggi spesi cercando di decifrare spettri IR. Mr. Bahr, per aver sopportato con me interminabili giornate di fronte al cono calorimetro, nella speranza della riproducibiltà dei risultati. A tutti i colleghi/amici del BAM, Eliza, Mei, Henrik, Florian, Birgit, per avermi accettato, non solo come parte del gruppo ma anche come amica, per l'aiuto reciproco e per il tempo trascorso insieme.

Un grazie anche a tutti i colleghi/amici del DIMP che mi sono stati vicini durante questi tre lunghi anni, aiutandomi a “sopportare” e superare le difficoltà quotidiane. Massimo L. che, nonostante continui a dire che se ne va, è rimasto fino all’ultimo, aiutandomi con estrusioni/grafici/reologia. Grazie soprattutto per avermi avvertito che il melt flow index era a 200°C. Paola per avermi fatto capire che non tutti sono come sembrano (vedi Ischia) Guglielmo per essersi improvvisato psicoterapeuta nel momento del bisogno. Francesca per gli indimenticabili caffè.

Un grazie anche a Paola Desidery, per la gentilezza e il calore con cui ci ha sempre trattato nonostante le domande, i dubbi e il certificati con cui l’abbiamo tempestata.

Infine, un rigraziamento particolare alla mia famiglia, ai miei genitori e a mio fratello, per essermi stati sempre vicini seppure lontani, e a Befy e Rocco per avermi accolto come una figlia, sopportandomi per 8 lunghi anni.

REFERENCES

[1] Samperi F, Puglisi C, Alicata R, Montaudo G. Polym Degrad Stab 2004; 83:11.

[2] Loma Kin SM, Zai Kov GE. Ecological aspects of polymer flame retardancy. Utrecht: VSP; 1999.

[3] Takeda K, Nanasawa A, Ta Kayama S. In: Proceedings of the International Symposium by Fire Retardant Chemicals Association (FRCA), San Francisco, CA, January 1–10, 1997.

[4] Nelson GL. The future of fire retarded materials: applications and regulations FRCA 1994,135.

[5] Bourbigot S, Bras ML, Leewendal R, Shen K K, Schubert D. Polym Degrad Stab 1999; 64: 419.

[6] Gilman JW, Kashiwagi T. SAMPE J 1997; 44: 40.

[7] Schartel B, Bartholmai M, Knoll U. Polym Degrad Stab 2005; 88(3):540.

[8] Schartel B, Knoll U, Hartwig A, Pütz D. Polym Adv Technol 2006;17(4):281.

[9] Lewin M. Polym Adv Technol 2001;12(3-4):215.

[10] Lewin M, Endo M. Polym Adv Techn 2003;14(1):3.

[11] Yoshio Ka T, Handa T, Grause G, Lei Z, Inomata H, Mizoguchi T. J Anal Appl Pyrol 2005;73(1):139.

[12] Weil ED, Patel NG. Polym Degrad Stab 2003; 82(2):291.

[13] Schartel B, Hull TR. Fire Mater 2007; 31(5):327.

[14] Kuljanin J, Marinovic-Cincovic M, Zec S, Comor MI, Nedelj Kovic JM. J Mater Sci Lett 2003; 22: 235.

[15] Weil ED, Patel NG. Polym Degrad Stab 2003;82:291.

[16] Laachachi A, Cochez M, Ferriol M, Leroy E, Lopez-Cuesta JM. MaterLett 2005; 59: 36.

[17] Kodolov VI. Fire retardants for polymeric materials. Moscow: Khimiya, 1980.

[18] Endo M, Lewin M. In Advances in Flame Retardancy of Polymeric Materials, Lewin M (ed.) BCC: 1993; 4: 171.

[19] Weil ED. In Flame Retardancy of Polymeric Materials, Kuryla WC, Papa AJ (eds). De K Ker: New Yor K, 1975; vol. 3: 185.

[20] G. Pal, H. Macs Kasy, Plastics: Their behaviour in fires, Elsevier, New Yor K, 1991.

[21] G. Pal, H. Macs Kasy, Plastics: Their behaviour in fires, Elsevier, New Yor K, 1991.

[22] A. T Kac, J. Polym. Chem. Ed. 1981; 19: 1475.

[23] Calcraft and Maries A.M. Calcraft, K. Maries, Plast. Polym. 1974; 42: 247.

[24] Troitzsch J. International Plastics Flammability Handboo K, 2nd ed., Oxford University Press, New Yor K, 1990, 52–53.

[25] A.R. Horroc Ks, D. Price, Fire Retardant Materials, CRC Press, Boston, 2001.

[26] Weil ED, Zhu W, Patel N, Mu Khopadhyay SM. Degrad Stab 1996; 54(2–3):125.

[27] Suebsaeng T, Wil Kie C. J Polym Sci, 1984; 22, 945.

[28] Van Krevelen D W, Polymers, 1975; 16(8): 615.

[29] Balabanovich AI, Levichi K GF, Wil Kie C, In Le Bras M, Camino G, Bourbigout S, DeLobel R, eds. London, Royal Chemical Society, 236-251.

[30] Suebsaeg T, Wil Kie CA, Carter J, Brown CE. J Polym Sci Polym Let, 1984; 22: 625.

[31] Kuryla W. eds. De K Ker, 1975; 185. Revised and updated in Fire Retardancy of Polymeric Materials, Grand A. and Wil Kie C, M. De K Ker Inc., 2000; Additivity, Synergism and Antagonism in Flame Retardancy, in Flame Retardancy of Polymeric Materials.

[32] Nyden MR, Forney GP, Brown JE, Macromolecules 1992; 25: 1658.

[33] Chandrasiri JA, Wil Kie CA. Polym Degrad Stab, 1994; 45: 97.

[34] Oya A, Marsh H, J Mat Sci 1982; 17: 309.

[35] Wang W, Thomas KM, Poultney RM, Willmers RR, Carbon 1995; 33(1): 1525.

[36] Kammerec K, Na Kanzo, Carbon 1974; 29 (2): 251.

[37] Weil ED, Meeting FR goals using polymer additive system. In Pearce EM ed. Improved fire and smo Ke resistant materials for commercial aircraft interiors. Washington DC, Natliona Academy Press, 1995: 129.

[38] Bo Kros JC, Price RJ, Carbon 1966; 4: 441.

[39] Acheson EG, US Patents 558323 (1996).

[40] Se Kiguch Y, Shafizadeh F. J app K Polym Sci, 1984; 29: 1267.

[41] Weil ED. Phosphorus-based flame retardants. In Engel R, ed. Handboo K of organophoshorus chemistry, New Yor K: Marcel De K Ker 1992; 683-738.

[42] Granzow A. Acc Chem Res, 1978; 11: 177.

[43] Nelson GL. The future of fire retarded materials: applications and regulations FRCA 1994, 135

[44] E.D. Weil, Encyclopedia of Polymer Science and Technology, 11, Wiley Interscience, New Yor K, 1986.

[45] A.M. Aronson, Phosphorous Chemistry, in: ACS Symposium, 486, 1992.

[46] G. Camino, Polym. Degrad. Stab. 1984; 12: 213.

[47] V. Babusho K, W. Tsang, Combust. Flame 2000; 124: 488.

[48] Hastie, Bonnel, NBS research report NBSIR 80-2169, National Bureau of Standards, Gaithersburg, MD, 1980.

[49] Davis J, Huggard M, Vinyl J. Addit. Technol. 1996; 2: 69.

[50] Piechota H. Kunststoffrundschau 1965; 12: 191.

[51] Granzow A, ACC. Chem. Res. 1978; 11: 177.

[52] Peters EN, in: W.C. Kuryla, A.J. Papa (Eds.), Flame Retardancy of Polymeric Materials, vol. 5, De K Ker, New Yor K, 1979.

[53] Braun U, Schartel B. Fire retardancy mechanisms of red phosphorus in thermoplastics, in: Proceeding of the Additives 2003 Conference, San Francisco, CA, 2003.

[54] Levchi K SV, Weil D. Polym. Int. 2005; 54: 11.

[55] Pawlows Ki KH, Schartel B. Polym. Int. 2007; 56: 1404.

[56] Pawlows Ki KH, Schartel B. in: M. Lewin (Ed.), Proceedings of the Conference on Recent Advances in Flame Retardancy of Polymeric Materials, 17, BCC, Norwal K, CT, 2006.

[57] Horn WE. in Fire Retardancy of Polymeric Materials, A.F. Grand and C.A. Wil Kie (eds.), Marcel De K Ker, New Yor K, 2000; 285.

[58] Hornsby PR. Int. Mater. Rev., 2001; 46:199.

[59] Gilman JW, Kashiwagi T, Lichtenhan JD, SAMPE Journal, 1997; 33:40.

[60] Gilman JW, Jac Kson CL, Morgan AB, Harris RH, Manias E, Giannelis EP, Wuthenow M. Hilton D, Phillips SH. Chemistry of Materials, 2000; 12:1866.

[61] Gilman JW. Applied Clay Science, 1999; 15: 31.

[62] Giannelis EP. Advanced Materials, 1996; 8: 29.

[63] Lewin, Endo, Polym. Advan. Technol., 2003; 14: 3.

[64] Laachachi A, Cochez M, Ferriol M, Lopez-Cuesta JM, Leroy E. Mater. Lett. 2005; 59:36.

[65] Lewin M, Sello SB. In Flame Retardant Polymeric Materials, Lewin M, Atlas SM, Pearce EM (eds). Plenum Press: New Yor K, 1975; vol. 1, 19.

[66] Horace K H, Grabner R, Polym. Degrad. Stab. 1996; 54: 205.

[67] Lyons JW. The Chemistry and Uses of Fire Retardants, R.E. Krieger Pub. Comp., 1987.

[68] Levchi K, Selevich, Camino, Costa, J.Fire sci, 1995, 13, 43-58., (Levchi K, Selevich, Camino, Costa, Fire Mater. 1996, 20, 183-190) and Lewin.(Lewin, Endo, Polym.Adv. technol, 2003, 14: 3.

[69] Fisher EG, Extrusion of Plastics, Newnes- Butterworths: London, 1-14, 1976.

[70] Babraus Kas V. J Fire Mat, 1984; 8: 81.

[71] Schartel B, Hull TR, Fire Mater. 2007; 31:327–354

[72] A. I. Leonov. On the rheology of filled polymers. J. Rheology, 1990; 34:1039.

[73] C. W. Macos Ko. Rheology Principles, Measurements and Applications. VCH Publishers, USA, 1993.

[74] Ganesan V, Pryamitsyn V, Surve M. Narayanan B. J.Chem.Phys. 2006: 124, 221.

[75] Kashiwagi T. Proc Combust Inst, 1994; 28:1423.

[76] Botelho G, Queiros A, Gijsman P. Polym Degrad Stab 2001;73(3):431-435.

[77] E. Gallo, U. Braun, B. Schartel, P. Russo, D. Acierno Pol Degr Stab, 2009; 94(8):1245.

[78] Braun U, Knoll U, Neubert D, Schartel B. In: Schartel B, editor. Advances in the Flame Retardancy of Polymeric Materials: Current Perspectives presented at the FRPM´05 2007, 35.

[79] Arii T, Masuda Y. J Anal Appl Pyrol 2004; 71(2):525.

[80] Braun U, Schartel B, Fichera MA, Jäger C. Polym Degrad Stab 2007; 92(8),1528.

[81] Brown CE, Jones MB, Kovacic P, J Polym Lett Ed, 1980; 18, 653.

[82] Braun U, Schartel B. Macromol Mater Egin 2008;293(3):206-217.

[83] Braun U, Bahr H, Sturm H, Schartel B. Poly Adv Technol 2008;19(6):680.

[84] Rivaton A, Gardette JL. Die Angew Ma Kromol Chem 1998; 261:173.

[85] Bothelho G, Queiros A, Liberal S, Gijsman P. Polym Degrad Stab 2001; 74:39.

[86] Lu SY, Hamerton I. Prog Polym Sci 2002;27:1661.

[87] Catala JM, Brossas J. Prog Org Coatings 1993; 22(1–4):69.

[88] Vijaya Kumar CT, Ponnusamy E, Bala Krishnan T, Kothandaraman H. J. Polym. Sci., Polym. Chem. 1982; 20: 2715.

[89] Lum RM. J. Polym. Sci., Polym. Chem. 1979; 17: 203.

[90] Nearly DI. J. Polym. Sci., Part A-1 1971; 9: 2063.

[91] Spanniger PA. J. Polym. Sci., Polym. Chem. 1974; 12: 709

[92] Sato H, Kondo K, Tsuge S,Ohtani H,Sato N. Polym.Degrad. Stab. 1998; 62: 41.

[93] Balabanovich AI, Engelmann J. Polym. Degrad. Stab. 2003; 79: 85.

[94] Balabanovich AI, Zevaco TA, Schnabel W. Macromol Mater Eng 2004;289(2):181.

[95] Thomas LC. Interpretation of the Ir spectra of organophosphorus compounds. London: Heyden, 1974.

[96] Braun U, Schartel B, Fichera MA, Jäger C. Polym Degrad Stab 2007;92(8),1528.

[97] Weil ED, Hirschler MM, Patel NG, Said MM, Sha Kir S. Fire Mater 1992; 16(4):159.

[98] Casu A, Camino G, Giorgi MD, Flath D, Laudi A, Morone V. Fire Mater 1998; 22(1):7.

[99] Laoutid F, Ferry L, Lopez-Cuesta JM, Crespy A, Fire Mater. 2006; 30:343–358

[100] Balabanovich AI, Levchi K GF, Levchi K SV, Engelmann J. J Fire Sci 2002; 20(1):71.

[101] Weil ED. Synergists, adjuvants, and antagonists in flame-retardant systems. In: Grand AF, Wil Kie C, editors. Fire retardancy of polymeric materials, New Yor K Basel: Marcel De K Ker, 2000: 115.

[102] Braun U, Bahr H, Sturm H, Schartel B. Poly Adv Technol 2008;19(6):680.

[103] Yeh JT, Hsieh SH, Cheng YC, Yang MJ, Chen KN. Polym Degrad Stab 1998; 61(3): 399.

[104] Weil ED. Synergists, adjuvants, and antagonists in flame-retardant systems. In: Grand AF, Wil Kie C, editors. Fire retardancy of polymeric materials, New Yor K Basel: Marcel De K Ker, 2000: 115.

[105] Munson-McGee S.H., Phys. Rev. B 1991; 43 (4): 3331.

[106] Mac Key. Macromolecules 2005; 38: 8000.